Ana Carolina Correia da Silva Pádua

Master in Biomedical Engineering

Design and assembly of an opto-electronic device for artificial olfaction

Thesis submitted in partial fulfillment
of the requirements for the degree of
Molecular Biosciences

Adviser: Ana Cecília Afonso Roque,
Associate Professor,
School of Science and Technology of NOVA University Lisbon

Co-advisor: Hugo Filipe Silveira Gamboa, Assistant Professor,
School of Science and Technology of NOVA University Lisbon

Examination Committee:

Chairperson: Professor Ana Isabel Nobre Martins Aguiar de Oliveira Ricardo

Rapporteurs: Professor João Pedro Estrela Conde
Professor Ana Luísa Nobre Fred

Members: Professor Ana Cecília Afonso Roque
Researcher Filipe Cruz Gomes Soares
Researcher Susana Isabel Conde Jesus Palma

FACULDADE DE CIÊNCIAS E TECNOLOGIA
UNIVERSIDADE NOVA DE LISBOA

November, 2019

Design and assembly of an opto-electronic device for artificial olfaction

This document was created using the (pdf)LaTeX processor, based in the "novathesis" template[1], developed at the Dep. Informática of FCT-NOVA [2].
[1] https://github.com/joaomlourenco/novathesis [2] http://www.di.fct.unl.pt

Acknowledgements

First, I would like to thank my supervisor, Professor Ana Cecília Roque, for her strong support and for her enthusiasm for embracing the challenges of this project. Prof. Cecília offered me a dedicated and continuous guidance, always making sure I was on track and following the objectives of the project. Furthermore, Prof. Cecilia has been on my side in the development of innovative and well-structured ideas for this project.

My co-supervisor, professor Hugo Gamboa was also an excellent mentor for this project, who thaught me important concepts and methods in the fields of instrumentation, programming and machine learning. The knowledge that Prof. Hugo transferred me contributed to boost my skills in important areas for this project. I consider that Prof. Hugo instructed me with the right tools to tackle the challenges of this Ph.D. project, and his vision about he future of the project was essential.

In the panel of mentors, it's a pleasure to include also Professor Jonas Gruber, who received me in such a welcoming way in his laboratory, in Brasil, for two months. Professor Jonas was an extremely collaborative teacher, contributing with his wide and deep knowledge in a variety of fields for this project, ranging from the materials until electronics.

Also, I would like to thank my colleagues from the Biomolecular Engineering and LIBPhys groups for their collaborative spirit and for the good environment, especially Susana Palma for contributing with valuable insights for this project, and also Rita Oliveira, Gonçalo Santos, Claudia Alves, Daniel Osório and João Rodrigues. Moreover, thank you to my colleagues from the MolBioS program for the union and friendship. Also, I am thankful to ITQB and my Ph.D. program for this opportunity, and to FCT for funding.

Thanks to my friends for their support, namely: Pedro Correia, Elias Chalhoub, Rafaela Matos, Catarina Almeida, Ricardo Eleutério, Pedro Ferreira, Guilherme Coutinho, Alexandre Costa, David Barbosa, Margarida Felix and Filipa Ferreira. And, of course, to the best person I could have on my side, the love of my life: Francisco Simões.

Finally, I want to thank to my fantastic family: my sister for always being there for me; my cousins and uncles, for making our family so strong and united; our little stars, grandmother Isilda, grandfather Manuel, and my godfather, for your love and education; and my mother, my father, my grandmother and my godmother: Thank you for always being the first to believe in me, for the education your provided me and for encouraging me to pursue my dreams!

"Alone we can do so little, together we can do so much." – Helen Keller

Abstract

Volatile Organic Compounds (VOCs) patterns have been associated to diseases, food quality, and safety issues. Sophisticated analytical techniques, such as gas chromatography coupled to mass spectrometry are the most widely used for VOCs identification. However, they require specialised operation, time-consuming sample preparation, and high operating costs. Other devices for sensing VOCs, named electronic noses (e-noses), have been developed in the past decades. These are easier to operate, faster, and low-cost.

This work is about the design and evolution of an e-nose based on opto-electronic sensors, which possess innovative sensing materials. Three optical-devices, one electrical-device, and a common data acquisition system were designed and assembled. A proof of concept was performed with the first optical e-nose. The second was mainly used for reproducibility tests, and to study the impact of the sensing film's production technique on the capacity for VOCs classification. Features extraction and selection was performed, and diverse machine learning algorithms were explored for classification. Moreover, the sensing films' stability was assessed by evaluation of their morphological changes before and after cyclical exposure to specific VOCs.

The analysis time, the signal-to-noise ratio, and the stability were some of the parameters improved comparing the initial prototype with the final one. The proof of concept showed that it is possible to distinguish 13 pure VOCs with 100 % accuracy applying Principal Component Analysis and Support Vector Machines. The reproducibility tests performed with the second prototype allowed to study the sensing films' stability along the time, leading to the conclusion that the responses were affected by ambient conditions or by the sensors' lifetime. Two methods were applied for sensing films' production and both revealed to be adequate, since the estimated accuracy was higher than 96 % for Decision Tree, Naïve Bayes and Multinominal Logistic Regression. Overall, we achieved a miniaturised, accurate and easy-to-use system, well-characterised, that can be explored towards diverse applications, such as medical research, food industry, and security.

Keywords: Electronic nose, Gas sensing, Volatile Organic Compounds, Machine Learning.

Resumo

Padrões de compostos orgânicos voláteis têm vindo a ser associados a doenças, qualidade alimentar e segurança. A sua identificação é geralmente feita com recurso a análises como cromatografia de gás associada a espectrometria de massa. No entanto, estas ténicas requerem morosa preparação de amostras, pessoal especializado e têm elevado custo de operação. Os narizes electrónicos (e-noses) são dispositivos mais simples que têm vindo a ser desenvolvidos nas últimas décadas para detecção de voláteis. São fáceis de manusear, rápidos e de baixo custo. Este trabalho reporta o projeto e evolução de um e-nose baseado em sensores optoelectrónicos, que possuem materiais sensitivos inovadores.

Três versões de dispositivos ópticos, um eléctico, e também um sistema de aquisição de dados escalável foram desenhados e construídos. Uma prova de conceito foi realizada com a primeira versão de e-nose. A segunda foi principalmente usada para testes de reprodutibilidade, e para estudos do impacto das técnicas de produção de filmes sensitivos a voláteis na capacidade de classificação dos mesmos. Foram extraídas e selecionadas várias características de sinais, e diversos algoritmos de aprendizagem automática foram explorados. Além disso, a estabilidade dos filmes foi aferida por avaliação das suas alterações morfológicas antes e depois da exposição cíclica a voláteis.

O tempo requerido para análise, a razão sinal-ruído e a estabilidade dos sistemas foram alguns dos aspetos melhorados comparando o primeiro protótipo com o final. A prova de conceito demonstrou que por *Principal Component Analysis* e *Support Vector Machines* foi possível distinguir 13 voláteis puros com taxa de 100 % de acerto. Os testes de reprodutibilidade feitos com o e-nose v2 permitiram estudar a estabilidade dos filmes ao longo do tempo, concluindo-se que estes são afectados por condições ambiente ou pelo tempo útil dos filmes. Dois métodos estudados para produção de filmes são adequados, uma vez que a estimativa de taxa de acerto de voláteis foi superior a 96 % para ambos usando *Decision Tree*, *Naïve Bayes* e *Multinominal Logistic Regression*.

Alcançámos um e-nose pequeno, fácil de usar e com elevada taxa de acerto, que pode ser explorado para diversas aplicações, incluindo medicina, alimentação e segurança.

Palavras-chave: Nariz electrónico, Detecção de gás, Compostos orgânicos voláteis, Aprendizagem automática.

Contents

List of Figures

List of Tables

Acronyms

AC Alternating Current.

AUC Area Under Curve.

BSG Bovine Skin Gelatin.

CV Coefficient of Variability.

DC Direct Current.

DT Decision Tree.

ENIG Electroless Nickel Immersion Gold.

e-noses electronic noses.

EPDM Ethylene Propylene Diene Terpolymer.

FC Film Coating.

GA Glutaraldehyde.

GC Gas Chromatography.

HASL Hot Air Solder Leveling.

ID Inner Diameter.

IL Ionic Liquid.

k-NN k-Nearest Neighbours.

LC Liquid Crystal.

LDR Light Dependent Resistor.

LED Light-Emitting Diode.

MLR Multinomial Logistic Regression.

MOS Metal Oxide Semiconductors.

MOSFET Metal-Oxide-Semiconductor Field-Effect Transistor.

MS Mass Spectrometry.

NAS Network Attached Storage.

NB Naïve Bayes.

OD Outer Diameter.

PCA Principal Component Analysis.

PCB Printed Circuit Board.

PLA Polylactic Acid.

ppb parts per billion.

ppm parts per million.

PTFE Polytetrafluoroethylene.

QCM Quartz Crystal Microbalance.

RFE Recursive Feature Elimination.

SAW Surface Acoustic Wave.

SC Spin Coating.

SMT Surface-Mount Technology.

SSH Secure Shell.

SVM Support Vector Machines.

VOCs Volatile Organic Compounds.

Chapter 1

Introduction

1.1 Motivation for odour detection

Odours are composed by sets of Volatile Organic Compounds (VOCs), which can be used as targets to detect food spoilage [1], explosives [2], environmental quality and safety [3], and even certain diseases when found in biological samples [4]. It is known that Hippocrates (400 BC), considered the father of medicine, used smell to help in disease diagnosis, considering characteristic odours from patients' breath and urine [5].

Early contamination and defects in food can be assessed by detecting VOCs produced by bacteria and/or fungal metabolism [6]. The VOCs associated with flavours and smells can be used to inspect food quality and safety, including freshness of fish and meat quality. [1]. In addition, some VOCs are used to identify ageing of milk or milk collected from cows affected by mastic disease. Moreover, they can also be used to distinguish high-quality from low-quality products (e.g. coffee beans and wine [7]). For public safety and welfare, VOCs might be used to detect explosive materials [8]. In cosmetics, they can help in the development of perfumes. And, in air and water quality control, VOCs can be useful for pollution detection, or identification of hazardous gases [9, 10]. Furthermore, some diseases such as diabetes [11], cancer [12] and bacterial infections [13] have been reported to change the normal VOCs profile in the headspace of breath, blood, urine and faeces. For example, in cancerous cells, the metabolic pathways are expressed to a different extent compared to normal cells, which may cause a change in the VOCs profile. Due to the change in the pH of the cancer cells and the surrounding medium, the acid/base equilibrium of some VOCs is affected. Another example is the case of bacteria, that release VOCs as part of their metabolic activity. Different bacteria species and strains are associated with different patterns of VOCs [14].

1.2 Conventional methods for odour detection

For off-line or indirect analysis of samples, Gas Chromatography (GC) combined with Mass Spectrometry (MS) - GC MS - is considered the gold standard [15]. In GC, the sample components are separated and then detected sequentially due to their different chemical and physical properties (namely size, volatility and hydrophobicity). Then, the individual components present in the analysed sample are identified by MS. The GC MS technique presents high reproducibility, sensitivity and robustness [16].

Real-time analysis is possible with selected ion flow tube mass spectrometry [17], proton transfer reaction mass spectrometry [18] or ion-molecule reaction mass spectrometry [19]. In these techniques, the sample is presented to the instrument and then reacts with a precursor ion. The analysis is more prone to error than GC MS since the deduction of the compound that originated certain ions is more complex. Laser-based spectroscopic techniques, and ion mobility spectrometry [20] have also been used for direct analysis. Ion mobility spectrometry is relatively inexpensive and is based on the behaviour of the sample components when an electric field is applied. This technique can detect VOCs normally in the range of pg/L to ng/L, in 8 minutes total analysis time.

The price paid to get detailed volatile fingerprint limits the widespread of these techniques for routine applications. The VOCs analysis is time-consuming, laborious and requires specialised personnel and laboratories. Hence, these sophisticated technologies are used especially for identification of VOCs in laboratory environment. When the aim is to apply a simple or fast point-of-care device for regular decisions, a better approach consists in the use of portable and user-friendly instruments, such as gas sensors and e-noses [16].

1.3 Electronic noses

In 1964, reactions of odorants with electrodes of a multisensor system were first reported by Wilkens and Hatman [21]. Later, in 1965, an e-nose based on thermal modulation of contact potential was reported by Dravnieks and Trotter [22]. Only after almost 20 years, Persaud and Dodd created an array of gas sensors as odour transducers [23], and Kaneyasu et al. proposed an integrated sensor with a microcomputer [24]. Since then, many devices have been optimised and developed to be applied in a variety of fields, such as environmental monitoring, military, food and beverage applications, and healthcare [25].

Conventionally, the concepts of e-nose and gas sensor differ. Gas sensors are simple instruments to detect specific compounds. For example, they are useful to detect gas leaks or evaluate single gas concentration. Nevertheless, many applications are associated with high variability of compounds thus requiring a more complex approach [10].

Differently from gas sensors, e-noses do not provide information about the individual compounds responsible for the odour. Instead, they detect and recognise the whole gas

mixture using non-specific sensors [26]. Besides having an array of sensors, the concept of e-nose includes a suitable post-processing unit for data analysis and pattern recognition [1].

This process is similar to what happens in the human olfactory system when an odour is detected by the nose [27]. Figure 1.1 illustrates the process of olfaction, which starts when we sniff VOCs and other molecules associated with odours into our nose. They flow through the nasal cavities, and some reach the olfactory epithelium, which contains olfactory sensory neurons that define action potentials up their own axons, until the olfactory bulb, which then transmits the signal to the brain that helps us taking decisions.

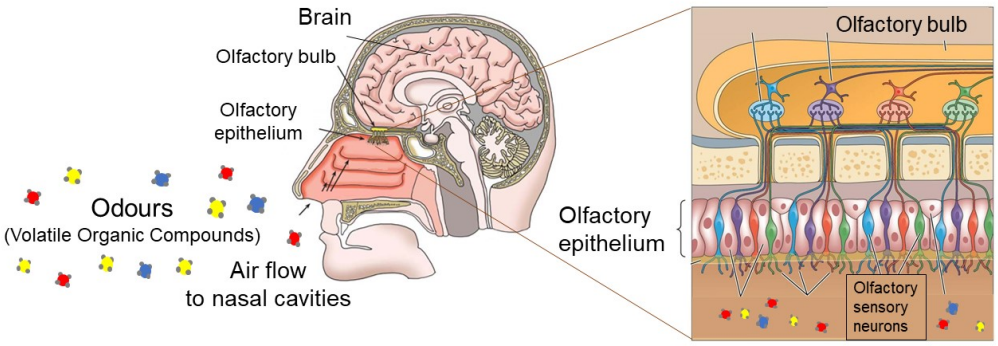

Figure 1.1: Schematic of human olfactory system. Images adapted from [28] and [29].

Infact, a typical e-nose is composed of:

- a delivery system: which directs the air towards the sensor array. This resembles the role of the nasal cavity, the flow created by the respiratory system, and the natural odorant delivery structures;
- a detection chamber with a sensor array: where the VOCs interact with the sensing materials. It works in a similar way to the olfactory epithelium, which has olfactory receptor cells that bind to the odours;
- a signal processing unit, like the olfactory bulb: that processes the molecular signal obtained from olfactory receptor cells and transmits it to the olfactory cortex;
- a pattern recognition system: for odours prediction similarly to the brain function.

Figure 1.2 illustrates the interaction of an analyte with an array of sensing materials, which results in characteristic material responses (i.e. changes in materials' properties) that are converted into signals (e.g. electrical signals) by the signal-transducing unit. The

resultant signals act as a "fingerprint" of the analyte, from which features are extracted by the signal processing unit and interpreted by pattern recognition methods for analyte classification [30].

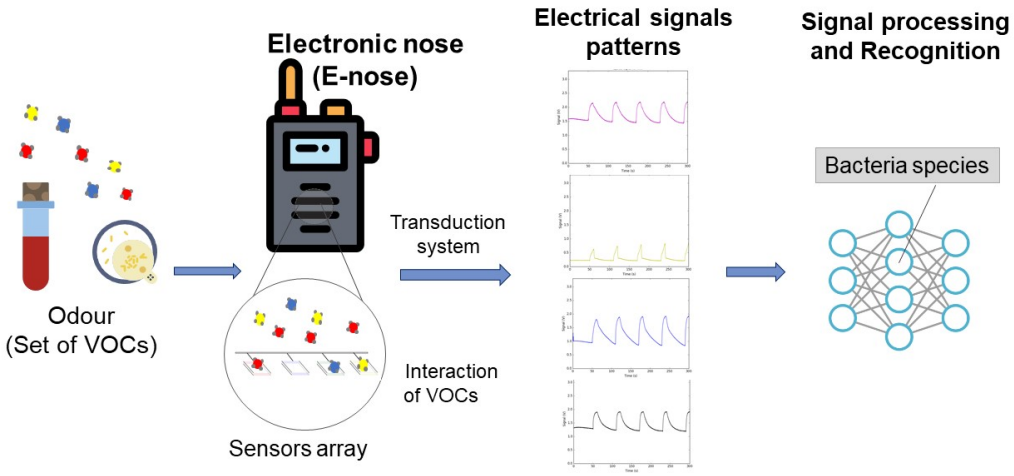

Figure 1.2: Schematic of e-nose working steps. Icons made by Icon Pond and Freepik from flaticon.com

1.3.1 Delivery system

The delivery system is responsible for transferring the gas sample to the detection chamber in a reproducible manner. The gas sample can be directly introduced in the detection chamber, an approach known as *static sampling*, or pumping the headspace from the sample chamber to the detection chamber, known as *dynamic sampling* [31].

For the first electronic nose systems, the gas samples (at constant temperature) were manually transferred from the sample chamber to the detection chamber using a glass syringe pressed manually. Although simple and inexpensive, this procedure was labour intensive and had poor reproducibility [9].

An automated system can reduce the variability in the sample delivery, pumping or purging the headspace into the detection chamber [9]. These systems are typically composed of tubing, pumps, and related units. Various automated systems have been developed depending on the e-nose application. The type of sample that will be analysed conditions the system apparatus.

To implement the gas transfer from the sample chamber to the detection system, pumps and micro-pumps [32, 33] have been applied to create a gradient of pressure, generating compressed air with constant flow rate. Mass flow controllers have been used to dilute the sampling gas in the carrier gas (e.g. Nitrogen), controlling the mixed gas concentration [34, 35]. Additionally, flowmeters can be used to measure the flow rate [33].

Solenoid valves can control the sampling and purging in an automated sequence [32, 33]. Check-valves and humidity and temperature sensors [34] have also been included in

delivery systems of e-noses.

The sample chamber should be made of non-reactive and inert materials [6]. For example, glass sample chambers [33] have been reported as appropriate. The chamber configuration should be adjusted to the sample size. Depending on the application, a heater might be applied to increase the concentration of VOCs inside the chamber [6].

It is also important to select adequate materials for tubes and fittings involved in gas delivery. For example, silicon, Polytetrafluoroethylene (PTFE) [33, 36], and polyvinyl chloride tubings [37] are appropriate. Other suitable materials for gas sampling and storage are stainless steel and polyvinyl fluoride [38].

1.3.2 Detection chamber

Inside the detection chamber, the VOCs interact with the sensors array, altering their chemical and physical properties. These variations are then converted into electrical signals which are sent to a data processing system. The number and type of sensors that compose the array should be set according to the application. One of the most important characteristics is the partial selectivity of each sensor of the array for the VOCs of interest. Furthermore, desirable attributes for the sensors' response are: reproducibility, reversibility, fastness, and stability [10]. The sensors' lifetime is relevant as well. If the sensors require a heating process to work properly, then the heating system should be activated the necessary time prior to the experiments in order to stabilise them [6].

1.3.2.1 Sensors array

The sensors that compose the array change their properties, due to the interaction with the odour molecules present in the gas flow. The most common sensing materials developed towards gas sensing are Metal Oxide Semiconductors (MOS), conducting and composite polymers, and other novel materials. Examples of transducing technologies that have been explored are chemo-resistive, Surface Acoustic Wave (SAW), Quartz Crystal Microbalance (QCM), optical transducers and Metal-Oxide-Semiconductor Field-Effect Transistor (MOSFET) [39].

Table 1.1 summarises the advantages and disadvantages of the most common types of sensors applied in e-noses [39–41].

Metal-Oxide Sensors

MOS operation is based on a change in conductance of the oxide when interaction with the odour molecules of the gas occurs. MOS sensors are one of the most investigated gas sensors due to their low-cost, flexibility in production, large number of applications, fast response, and low maintenance required [39, 42]. Since they generally present large surface areas for analyte adsorption, they can detect very low concentrations of VOCs in the range of parts per billion (ppb) [39]. This sensors' category has two main types: n-type (such as zinc oxide, tin dioxide, titanium dioxide or iron(III) oxide) and p-type (e.g. nickel oxide and cobalt oxide) [39]. The metal oxide films can be deposited over

Table 1.1: Advantages and disadvantages of several types of sensors possible to use in the e-nose sensors array. Adapted from [39–41].

Sensor type	Advantages	Disadvantages
Metal-Oxide Sensors	Small size Fast response Inexpensive production	Sensitive to H High power consumption High T operation
Conducting polymers	Sensitive Inexpensive Easy to produce Room T operation	Lack specificity Limited sensor life Sensitive to H Limited reproducibility
Piezoelectric sensors	High sensitivity Short response time Low power consumption	Poor reproducibility Difficult to replace sensors T&H dependent
Optical sensors	Versatile Very fast response Room T operation	Shorter lifetime Increased production cost More complex than others

T = Temperature H = Humidity

different types of substrates, mainly ceramic or silicon [39]. Usually, the electrode design consists in an interdigitated structure. The operation of MOS as gas sensors requires high temperatures (commonly 300-450 ºC) [42]. MOSFET sensors change the threshold voltage when the gate material interacts with certain gases [40].

Conducting polymers

Conducting polymers are commonly used as chemo-resistors, but they have also been applied in field effect transistors and as semi-selective coatings for piezoelectric crystals. They are easy to produce through chemical or electrochemical processes [41], and their typical sensitivity ranges between 10 to 100 parts per million (ppm) [40]. Moreover, some of these sensors can identify odours at sensitivities below 1 ppm, specially when the interaction occurs with redox active or acid-base active analytes [41]. Inert organic analytes are usually detected at several ppm.

Conducting polymers include polyaniline, polypyrrole, polythiophene [41], poly(p-phenylene vinylene)s [43] and poly-p-xylylene derivatives bearing conjugated side-chains [44] or doped with porphyrins [45], which change their electric conductivity due to the interaction of the gas analyte with the polymeric structure.

The main drawback of conducting-polymer sensors is the limited reproducibility. They often present high variability among different batches, because it is difficult and time-consuming to electro-polymerize the active material. Additionally, their responses can drift over time, and they are susceptible to humidity. Moreover, some VOCs might penetrate through the polymer, which contributes to increase the time needed for sensors' recovery. [40]

Piezoelectric sensors

Two types of piezoelectric sensors are frequently reported for gas sensing: the SAW

sensors and the QCM. Their working principle is based on changes in the mass of the piezoelectric sensor coating, due to VOCs absorption, thus altering their resonant frequency. [10] The detection limit is normally in the range of ppm, but varies depending on the analyte [41].

Optical sensors

There is a wide range of optical sensors and a variety of techniques that might be applied to collect intensity and wavelength information related to changes in the electromagnetic spectrum. Photodiodes, cameras, and other electronic components can detect these changes [39]. There are colourimetric and fluorescence sensors which have nanoporous pigments [46] or dyes [47] as sensing materials. Liquid crystal-based films or composites change their optical properties, due to changes in the Liquid Crystal (LC) alignment upon analyte interaction [48]. Other optical sensing materials change absorbance, reflectance or refractive index.

Their detection limits have been reported in the range of ppm [40]. Some optical sensors allow less than 10 s for sampling and analysis. However, their transduction systems are more complex than other sensor types, which increases their cost. Besides that, these sensors can present lower lifetime due to photobleaching [40].

1.3.3 Data processing and pattern recognition system

The changes that occur in the sensors array are typically converted to electrical signals by the transduction system. Each sensor reacts to the presence of the odour in a different way, depending on its own sensibility and specificity. The electrical signals that result from the variance of the sensor properties (such as conductance, voltage and capacity) generate characteristic patterns for the molecules detected, also called the odours "fingerprint".

The acquired data is further analysed and processed. Finally, a recognition step is performed. The recognition part includes methods for features extraction and selection, as well as machine learning algorithms [30].

1.3.3.1 Features extraction and selection

A set of features is extracted and selected from the signals obtained. Yan et al. (2015) reviewed many feature extraction methods, including features extraction from the original response curves, curve fitting parameters and transform domains. In conclusion, the authors stated that the best method depends on the situation. Nevertheless, some advice was given: for steady-state features, normalisation models are the best option; and transient features, such as derivatives and integrals of original response curves, have more information than steady-state features [30]. Moreover, Principal Component Analysis (PCA) can be used for dimensionality reduction. It has been employed to reduce the number of features extracted from the signals [50, 51].

1.3.3.2 Machine learning algorithms

After features score and selection, advanced computational techniques can be applied. Examples of linear classification methods are linear discriminant analysis, functional discriminant analysis, partial least square discriminant analysis and cluster analysis; and examples of non-linear models are fuzzy logic and Artificial Neural Networks [49].

Machine learning algorithms are commonly used for odours recognition [52–54], and are also employed for concentration prediction [55].

Some articles reported the use of Support Vector Machines (SVM) for data acquired by e-noses, namely in classification problems e.g. to evaluate the quality of olive oil [51], to recognise fruit odours [56], and to discriminate alcoholic and non-alcoholic beers [50]. SVM was also applied to address regression problems, such as prediction of formaldehyde concentration [55].

Machine learning algorithms are becoming very important for medical data analysis. For instance, Decision Tree (DT) is a transparent and easily interpretable method, presenting a high potential for diagnostic model building. [57].

The best classification results for e-noses have been reported with SVM for MOS sensor arrays [50], and neural networks and the large margin nearest neighbours for SAW sensors array [100]. However, when discrimination can be done with a simple method, the usage of more complex approaches is not needed [50].

Ordukaya *et al.* (2017) [51] compared the performances of different machine learning algorithms for olive oil classification by an e-nose (*Cyranose 320*®): Naïve Bayes (NB), k-Nearest Neighbours (k-NN), Linear Discriminant Analysis, DT, Artificial Neural Networks, and SVM using two different approaches: with dimensional reduction and without data reduction. The best success rate was found with NB classifier after data reduction from 32 features to 8 features based on PCA.

The work of Cho *et al.* (2011) [101] showed that DT models have excellent results for classification and provide easily interpretable tree structure for e-nose data. The DT approach was reported as a promising pattern recognition method with accuracy rates above 97 % using several features extracted from signals acquired by an e-nose based on MOS sensors. The training of the DT was also faster compared to multilayer perceptron and fuzzy adaptive resonance theory classifiers.

Esfahani *et al.* (2018) [102] developed a research where e-noses based on MOS sensors (*FOX 400*, *Alpha M.O.S*, *France*) and Field-Asymmetric Ion Mobility Spectrometry (*FAIMS*, *Owlstone Lonestar*) were used to distinguish healthy from diabetic patients based on urinary samples. High prediction accuracy was achieved by combining PCA with a sparse Logistic Regression and a Gaussian process classifier. Another study used Logistic Regression to classify data collected by an e-nose to identify correctly biofilm-producing versus non biofilm-producing bacteria species with accuracy ranging from 72.2 % to 100 %, depending on the organism and methodology.

1.4 Applications for e-noses and gas sensors

More than 50 % of the gas sensors and e-noses commercially available are applied in the environmental sector, or in safety (both industrial and domestic safety) - see Figure 1.3. There are gas sensors and e-noses able to monitor air quality (e.g. at home, industries, or weather stations), gas leakages, or to detect fire. Many of these products add value in the protection of personnel from hazardous gases in the environment since they run continuously and at low costs [10].

Although the medical sector is one of the most demanding sectors, it has been highly explored for VOCs detection (Figure 1.3). Several commercial gas sensors and e-noses are being used in medical research. Food and beverage, and product quality assurance are important sectors as well. Many gas sensors and e-noses are used to guarantee the quality of the atmosphere of food packages, or to guarantee the gold-standard quality of certain brands.

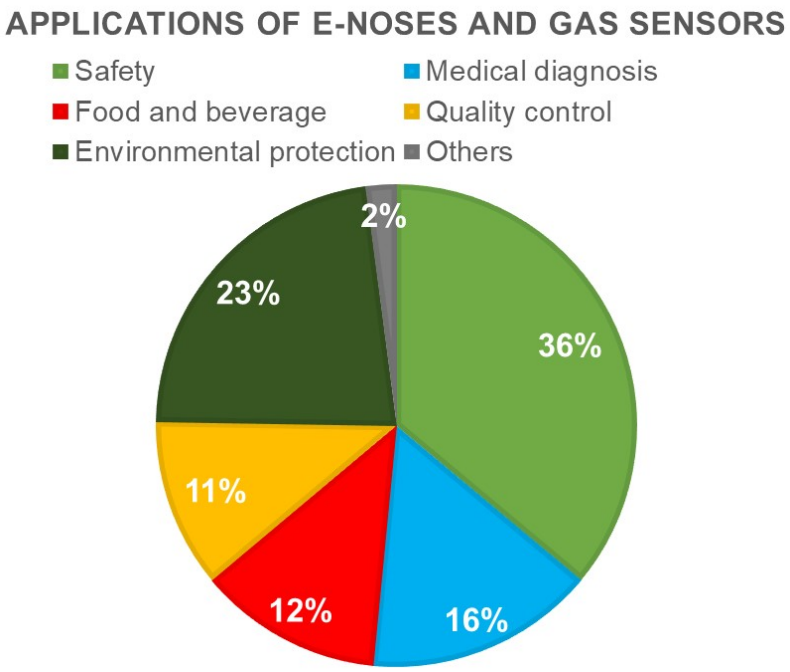

Figure 1.3: Applications of commercial e-noses and gas sensors. "Safety" includes: industrial safety (aviation, automotive, aerospatiale, military, naval, petrochemical and chemical industries), domestic safety, personal safety, fire and gas safety, road safety (e.g. detection of marijuana and alcohol on driver's breath). "Quality control" includes: pulp and paper, pet food, plastics, packaging materials, pharmaceutical industry, industrial quality control (fermentation and bioreactor gas analysis) and cosmetics. "Others" include: detection of cannabis plants, detection of toxic or chemical warfare gases, monitoring cabin-air quality in aeroplanes, and other customisable applications.

The response times for both e-noses and gas sensors usually range from seconds up to 20 minutes. In general, their sensitivity is in the range of ppm or ppb, and the prices vary from around 100 euros up to 15 000 euros.

Currently, there are several companies commercialising e-noses. The commercial

e-noses´ sensing materials are usually based on metal-oxide sensors, carbon filaments/-nanotubes or conducting polymers. Some e-noses´ companies such as *Sensigent* (USA) [58], *Alpha M.O.S.* (France) [59], *Sacmi* (Italy) [60] and *AIRSENSE Analytics* (Germany) [61]; and research centres like *NASA* (USA) [62] and *CSIRO* (Australia) [63]) present devices suitable for a wide range of applications. Others, develop devices specifically to be applied in certain areas. For instance, *The eNose company* (Netherlands) [64] and *Breathtec Biomedical Inc* (Israel) [65]) are mainly focused on applications for medical research; and *Peres* [66] (Switzerland) offers a specific product to evaluate food quality.

In general, e-noses' size varies a lot: some are desktop size (e.g. *Heracles Neo*, *Aetholab*, *EOS Ambiente and Aroma*), a few are laptop size (e.g. *PEN*), while others hand-size (e.g. *Cyranose 320*, *My Food Sniffer*, *Aeonose*).

Typically, the machine learning algorithms used are: (Artificial Neural Networks [67], k-NN, K-means, canonical correlation analysis, confirmatory data analysis, SVM, automatic baseline correction, and multivariate statistical analysis (euclid, correlation, mahalanobis, Linear Discriminant Analysis, PCA, and Partial Least Squares).

1.4.1 Versatile e-noses

Sensigent (USA) developed one of the most versatile e-noses in the market – *Cyranose®320*. Such versatility is possible due to the use of customisable sensor modules (including chemically-modified single-wall carbon nanotubes, metal nanoparticles, and conductive composites). Pilot studies indicate its potential as a point-of-care device that can probably be applied in several different areas. The device captures the VOCs from the sample of interest using an internal air pump. Once inside, they interact with the sensors and then many machine learning algorithms can be used for odours recognition. The detection limit is in the range of ppm to ppb. The price of the device is around 8,000 dollars [68].

Previously, *Alpha M.O.S.* (France) also developed several products for applications in different areas (medical diagnosis, cosmetics, environmental protection, food quality, among others). This company created machines based on traditional methodologies, such as *Heracles* based on ultra-fast GC, and *AirSense* based on gas ion mobility spectrometry; and *FOX* and *GEMINI* with an array of MOS sensors. Additionally, these devices could be easily adapted to numerous sampling options. Currently, this company is focused on a single e-nose - *Heracles Neo* - applied for quality assurance in food and beverage industries.

Besides medical applications, *The eNose company* also produces personalised products (e.g. for detection of cannabis plants, detection of toxic or chemical warfare gases, monitoring cabin-air quality in aeroplanes) based on customisable MOS sensors. All of them benefit from the absence of need of post-manufacturing calibration. Many prototypes and proofs of concept were already conducted.

*Cybernose®*is a device on the frontier between research and commercialisation. It is being explored towards many different applications: in food and beverage for taste and

aroma quality assurance, and for ingredients' authenticity verification; in safety, based on detection of toxins or contaminants; in public security; in disease detection; and in air quality for detection and management of greenhouse gases, and for monitoring indoor air quality.

1.4.2 E-noses for food and beverage quality control

For food quality checking, the company *Peres* created an easy-to-hold device - *My Food Sniffer*, which detects food spoilage in meat, poultry, or fish. The sensor array includes, at least, two sensors adapted to record changes in the VOCs concentration. The detection module can be connected with smartphones through a user-friendly application. For pattern recognition, it uses algorithms in synchronisation with a cloud database. The devices' price is 130 euros.

1.4.3 E-noses for air quality control

Sacmi develops products for environmental protection, namely for automatic and continuous outdoor monitoring of odorous emissions - *EOS Ambiente* and *EOS Portable*; and for quality control of products, and industrial processes (including the agro-industrial sector, food industry, and packaging) – *EOS Aroma*. These products have a data acquisition rate of 1 Hz.

JPL Electronic Nose was designed to help reduce risks associated with space flights, to protect crew member who can possibly be exposed to toxic or dangerous chemicals. Many air quality problems have already occurred on the International Space Station and Space Shuttle. This e-nose can help in the identification of dangerous chemicals, reducing health and safety risks to the crew member [62].

1.4.4 E-noses for medical applications

The application of e-noses in the medical diagnosis sector is one of the most difficult areas to explore commercially, due to the strict regulation and rigorous studies required for being validated. Nevertheless, some companies are exploring this sector and several studies [69–72] show promising results regarding the application of e-noses in this field.

The eNose company, *Osmetech Ltd* (formerly *AromaScan* – UK) and *Breathtec Biomedical Inc* are some of the few companies interested in e-nose technology for medical research.

Osmetech Ltd received US Food and Drug Administration (FDA) approval for detecting urinary tract infections and bacterial vaginitis (using vaginal acetic acid as a marker) [68].

Breathtec Biomedical Inc is interested in early screening of diseases, such as lung and breast cancers, infectious diseases, diabetes, and liver disease. This company is focused on developing a low-cost, non-invasive, portable and hand-held device for detection of biomarkers in the breath, to be used by clinician's in the office, clinic or hospital setting, or by agents screening for infectious diseases at national border entry points (e.g. airports).

The eNose company developed a device for bacterial detection and identification - *Aetholab*™. Bacteria need to be collected from blood samples, and cultured in a special medium at $35 - 37\,°C$. A study showed that this e-nose could identify *Klebsiella*, and distinguish between 'gram+' and 'gram-' bacteria. This company also developed another device – *Aeonose*™ - for detecting tuberculosis, asthma, and throat cancer in exhaled breath.

Clinical trials and pilot studies on detecting tuberculosis; asthma, throat, and breath cancer; and veterinary Metritis have started, in 2014, using this device. The device consists of three different micro-hotplate metal oxide sensors. The interaction of VOCs at the surface of the sensors can generate oxidation and reduction (redox) reactions, that result in changes in the conductivity of the sensors. Exhaled air is guided over the sensors at a constant flow, ensured by a small pump. The combination of sensors and Tenax tubes allows the detection, even at low VOCs concentration, because the tube is heated. The sensors are exposed to a sinusoidal temperature cycle between 280 °C and 340 °C. Then, the sensors are regenerated using a filtered environmental air passage. A recent study [73] indicates that this e-nose can help to diagnose prostate cancer patients, through the VOCs present in exhaled breath. Another study reports the use of this e-nose as a valid diagnostic tool for differentiating between head and neck carcinoma and lung carcinoma [69]. Also, a pilot study [74] shows its accuracy in diagnosing bacterial and viral infections in acute chronic obstructive pulmonary disease.

1.4.5 Gas sensors

Nowadays, numerous gas sensors are available in the market. Their sensing unit might be based on:

- Chemical reactions and consequent changes in conductivity (e.g. MOS);
- Spectroscopy;
- Optical principles;
- Electrochemical cells;
- Hybrid methods, which combine several techniques (e.g. GC with SAW; or catalytic oxidation, photo-ionization and MOS).

The configuration of such devices varies depending on the technology they are based on. Some gas sensors, which are based on MOS technology, are very compact and miniaturised (the size of an electronic component), and detect specific gases (e.g. products from *ams* [75] and *Figaro USA, Inc* [76]), whereas others are very robust and desktop size (e.g. products from *RoboScientific Ltd* [77]).

The company *ams* commercialises several gas sensors based on MOS for air quality monitoring. Some can be applied in smartphones, wearables or smart home devices. The

sensors detect one or more specific VOCs (e.g. alcohols, aldehydes, ketones, organic acids, amines, and aliphatic and aromatic hydrocarbons) and gases (such as carbon monoxide). The prices range from 14 000 to 25 000 dollars.

Figaro USA, Inc also commercialises several gas sensors based on MOS for industrial and domestic safety, that can detect alcohols or other solvent vapours. Other gas sensors (e.g. from *Alphasense* (UK) [78]) detect hydrogen sulfide, sulfur dioxide and carbon monoxide, in order to ensure personal safety. Gas sensors from *Alphasense* benefit from stable baselines and low humidity sensitivity.

Gas sensors based on spectrometry can be used for identification of unknown solid and liquid substances, mostly narcotics, and explosives (*AIRSENSE Analytics* [61], Model: *Liquids and Solids identifier*), or for chemical warfare agents and selected toxic industrial chemicals (*Environics* [79], Model: *ChemPro100i*), industrial gases, and VOCs (*Owlstone*, Model: *Lonestar VOC analyser*).

Gas sensors based on optical principles include infra-red sensors, LC sensors and fluorescent light sensors. E.g. *Cirius* infrared gas sensors from *Clairair Ltd* (UK) [80] can be used for detecting carbon dioxide or hydrocarbons. Gas sensors from *Draeger* [81] can detect flammable gases and vapours, and others from *Dr Foedisch* [82] (Model: SGA16) are able to identify carbon dioxide or hydrocarbons, or for monitorisation of hydrogen sulfide exposure.

Platypus Chemical Sensors™from *Platypus Technologies* [83] change colour due to interaction with toxic gases. These sensors have advanced surface nanomaterials that selectively bind to target compounds. The colour change is caused by molecular reorganisation of the LC film. This colour change can be read directly from the sensor, or it can be integrated into an electronic circuit to provide immediate and accurate detection of toxic gases. The *Platypus dosimeter*™, also from *Platypus Technologies* detects hydrogen sulfide more sensitively and with higher specificity than do electrochemical monitors.

Another optical sensing system is *GreenLight ®930* from *Mocon* [84]. This works by optical fluorescence and employs a unique oxygen sensor with high sensitivity. The sensor can be used to get information about microbial load because aerobic microbial samples deplete oxygen as they grow and respire.

Electrochemical sensors are used in gas sensors for oxygen monitoring (*Honeywell Analytics*, Model: Neotox XL Oxygen Analyser) [85], or to detect specific gases like carbon monoxide (*Figaro USA Inc*) [86], nitrogen trifluoride, fluorinated and chlorinated hydrocarbons (*Draeger*).

Some gas sensors combine different techniques to give a response: *Electronic Sensor Technology* created the product *zNose* [87], which combines GC with SAW. This technology includes a crystal microbalance that utilises an uncoated quartz crystal for maximum sensitivity and minimal recovery times. Other hybrid gas sensors use a combination of different detectors, based on infra-red sensors, electrochemical cells, catalytic beads, photoionization detectors, photometer technologies, among others.

1.5 Background

A new class of gas sensing materials was recently created by our research group, with interesting properties to be applied in artificial olfaction [88]. These materials possess versatility and have unique stimuli-responsive characteristics, altering their optical and electrical properties while interacting with VOCs [88]. They are composed of LC droplets self-assembled in the presence of Ionic Liquid (IL), dispersed inside a biopolymer matrix.

ILs have been reported as very promising in the development of electrochemical gas sensors, since they present negligible vapour pressure, ionic conductivity and high thermal, chemical and electrochemical stability [89]. Moreover, they exist in diverse strucutural and functional forms, which is important in the generation of selective gas sensing materials [88].

LCs are characterised by fluidity, yet the molecules within them possess some sort of structural order in their arrangement. The anisotropy of LCs, makes them attractive for sensing applications [90]. Indeed, the changes in their orientation due to external stimuli can be easily detected by a variety of optical sensors [91]. They are considered valuable in gas sensing, due to fast response, versatility and reversibility.

The LCs and ILs are prone to self-assembly in the presence of water [88]. The droplets' composition confers them potential for selectivity. LCs can be modified and tuned in order to make them more sensitive to specific compounds [92]. Since both ILs and LCs are fluids, the gelation is induced by polymers that offer a better mechanical strength to the sensing gels.

Our research group is exploring the application of these sensing gels, especially in healthcare, to identify the bacteria species which cause infections, and possibly specific strains resistant to certain antibiotics.

In order to achieve this long-term goal, there have been three complementary projects being developed in our research group. The first steps towards the use of the sensing gels for gas sensing required the development of a first prototype (reported in section 2.1) to transduce the optical and electrical responses into digital signals. This Ph.D. project started from the necessity to design and assemble improved versions of this prototype that could be easily scalable to enable running several future experiments. In parallel with this Ph.D. project, some researchers have been dedicated to exploring the composition of the sensing materials and their potential for VOCs sensing and selectivity. Others have been focusing on identifying the most relevant VOCs associated with diseases, while I have been committed with the development of the device prototypes.

1.6 Objectives

The aim of this Ph.D. project is to explore the application of a new type of sensing material developed by our research group [88], using e-noses. If distinct VOCs have different dynamics of interaction with the sensing gels, this will result in optical and

electrical signals having different features. After processing and analysing those signals, this brings the possibility for VOCs detection and identification, applying a simple and fast method. The final goal is to achieve an accurate, miniaturized and potentially scalable device that could run the analysis automatically.

1.7 Structure of the dissertation

As Figure 1.4 shows, this dissertation is composed of five chapters.

The first one is the introduction already presented, where the motivation for this work was explained, conventional methods for odours detection were reviewed, the concept of e-nose was introduced as well as the applications for e-noses and gas sensors. Finally, the objectives were stated.

The process for the design and assembly of the first autonomous e-nose prototype is described in the Chapter 2. First, the working principle of the sensors used in the device is explained, and the architecture and results obtained with the previous prototype assembled are discussed. Then, the new prototype - e-nose v1 - is presented and the studies performed for the proof of concept are indicated. In the context of the proof of concept, the sensors were calibrated and several machine learning algorithms were explored. In the conclusions subchapter, the advantages and limitations of this prototype are presented.

The second version implemented - e-nose v2 - is described the next chapter. As introduction for this chapter, the e-nose v1 and several classification models are revised. Then, the objectives for the second version of e-nose are indicated. In the results and conclusion subsection, four studies performed with this prototype are presented. Two of them related to the optical responses: reproducibility tests and study on the impact of the sensing films' spreading method in the classification accuracy by the e-nose. And other two related to the electrical responses: preliminary electrical signals and their optimization, and study on how different electrodes' finishing surfaces are affected by corrosion. In the end, the achievements and conclusions acquired due to the use of this e-nose are summarised, and the drawbacks and ideas for the future prototype version are presented.

The next chapter presents the third e-nose version - e-nose v3. In the introduction, there is a review of the previous e-nose versions implemented (e-nose v1 and e-nose v2). After that, the objectives established for e-nose v3 are indicated. The materials and methods subchapter provides information about the hardware and software implemented for this device, including a scalable and easy-to-use data acquisition system. Then, the results of several studies performed using this e-nose version are discussed, namely in that concerns to: exploring different sensing films' compositions, studying the effect of humidity on the sensing films' response, studying the detection limits of the system for the optical sensors, and exploring different ionogels and functionalizations with particles.

Finally, the work developed is reviewed and future perspectives are given in the section of conclusions. A list of contributions and publications resultant from the work developed is also present in that chapter.

To finish, the resources used for this dissertation are referred in the bibliography, and extra-information is provided in the appendixes.

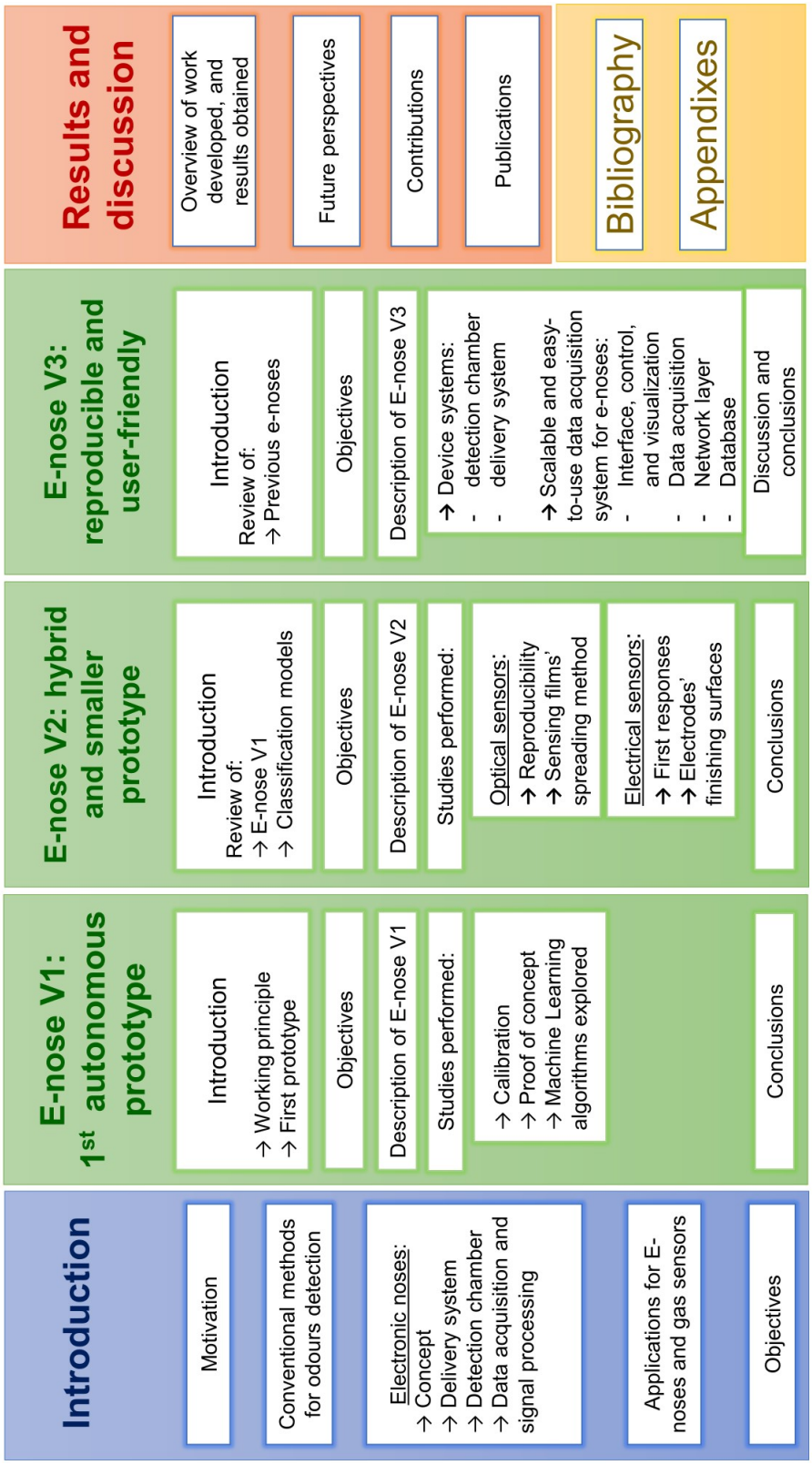

Figure 1.4: Diagram of the structure of the dissertation.

Chapter 2

Bringing autonomy to the first prototype: E-nose v1

In this chapter, as introduction (Section 2.1), the working principle of the optical sensing films is explained, previous work is revised, namely in what concerns to the sensing films' validation and assembly of the first prototype in the laboratory (e-nose v0). After e-nose v0 description, the problems identified in this first device version are presented and the objectives (Section 2.2) for the next e-nose are defined.

In materials and methods (Section 2.3), a description of the hardware and software used in the next device version (e-nose v1) is presented. Besides being an autonomous device, e-nose v1 became smaller and more stable than the previous prototype. Moreover, the methodologies applied for the optical sensors' calibration and for the experiment to do the proof of concept are explained. The following organic solvents were used in the proof of concept: hexane, heptane, toluene, xylene, carbon tetrachloride, chroloform, dichloromethane, diethylether, acetone, ethyl acetate, isopropanol, ethanol and methanol. Some have distinct functional groups (hydrocarbons, aromatic hydrocarbons, chlorinated, ether, ester, ketones, alcohols), whereas others belong to the same category (e.g. acetone and ethyl acetate are both ketones). This could be useful to test the e-nose capabilities to distinguish VOCs from different groups and within the same group. Moreover, diethylether, toluene, ethyl acetate and methanol have been identified in samples of pathogens associated to human infections [94].

The results obtained in the proof of concept are shown in Section 2.4, considering a single test or three tests performed.

Parts of this chapter were published in Pádua *et al.* (2018) in *Proceedings of the 11th International Joint Conference on Biomedical Engineering Systems and Technologies - Vol. 1.* [93] , and presented in *BIODEVICES 2018* conference in the oral presentation entitled *"Design and Evolution of an Opto-electronic Device for gas sensing"*.

To finish, in Section 2.5, e-nose v1 is revised and new perspectives for the next e-nose version are indicated.

2.1 Introduction

The gas sensing gels described in Section 2.2 alter their optical and electrical properties when in contact with VOCs. The optical changes can be seen by the way light propagates through nematic LCs, which typically produce a 90°shift in light polarisation. Thus, having the sensing films sandwiched between two crossed polarising filters, it is possible to observe changes in light polarisation, when in the presence or absence of VOCs. Therefore the sensors' array was assembled, having the following composition:

- a source of unpolarised light;
- the sensing films sandwiched between two crossed polarising filters;
- a light detector.

In the absence of VOCs (see Figure 2.1a), the unpolarised light emitted by the LED passes through the first polariser, which only allows the light waves polarised along the y-axis to cross it. Next, the light passes through the optical sensing film, which has nematic LC in its composition. Due to its anisotropy, part of the incident light becomes polarised along the x-axis. Therefore, it can then pass through the second polariser (which is crossed to the first one, and called analyser), and finally reaches the LDR.

When the VOCs are present (see Figure 2.1b), their interaction with the droplets dispersed inside the matrix, changes the LC configuration from radial to isotropic. Thus, the light waves polarised along the y-axis that could pass through the first polariser, even passing through the optical sensing film, maintain their polarisation, and so are blocked by the analyser. Hence, minimal light intensity reaches the LDR.

In 2013, Semeano *et al.* [88] developed the very first prototype of a transduction system to capture optical signals from the sensing films. Three sensing films with different compositions were exposed to 11 different organic solvents' vapours: carbon tetrachloride, dichloromethane, diethyl ether, dioxane, ethanol, ethyl acetate, heptane, hexane, methanol, toluene and xylene.

The optical sensors were exposed for 6 seconds to the VOCs placed in the headspace of the sample chamber (reservoir where the solvents are placed). This period was followed by 54 seconds of recovery, in which atmospheric air was used to clean the sensors chamber, removing the VOCs. Each test lasted 60 seconds and was repeated for 10 cycles.

Three signals were obtained for each solvent. The signals s were analysed cycle by cycle and the relative amplitude - Ra - of each cycle was calculated using the following equation 2.1:

$$Ra = \frac{max(s) - min(s)}{min(s)} \tag{2.1}$$

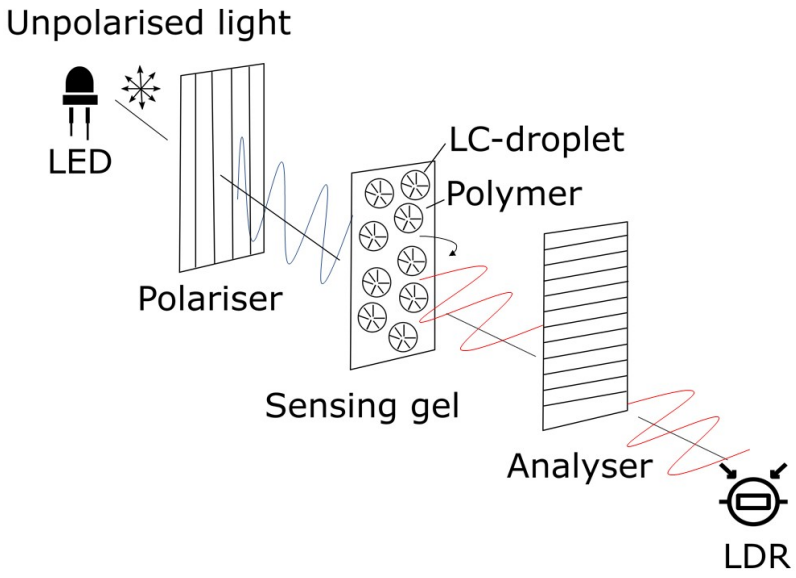

(a) In the absence of VOCs.

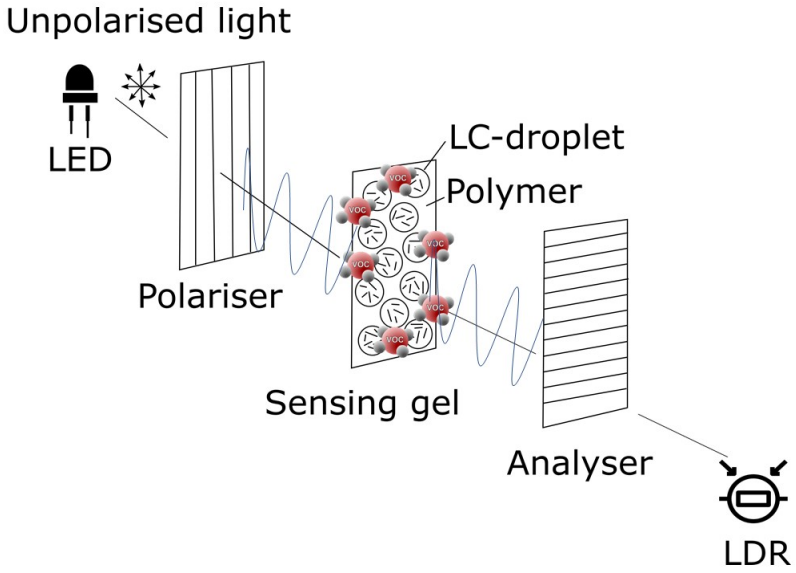

(b) In the presence of VOCs.

Figure 2.1: Illustration of light propagation through an optical sensor.

The *Ra*'s were used as input variables for PCA, performed by the commercial software *Statgraphics XV*.

The result of this proof of concept showed a clear separation of the different 11 solvents tested, applying PCA, where 97 % of the total variance was described by the first two principal components. Based on this result, Semeano *et al.* stated that this device had the ability to distinguish all the solvents tested, using only three sensing films with different compositions.

The first prototype developed by Semeano *et al.* was named e-nose v0. The schematic of the device assembled is shown in Figure 2.2.

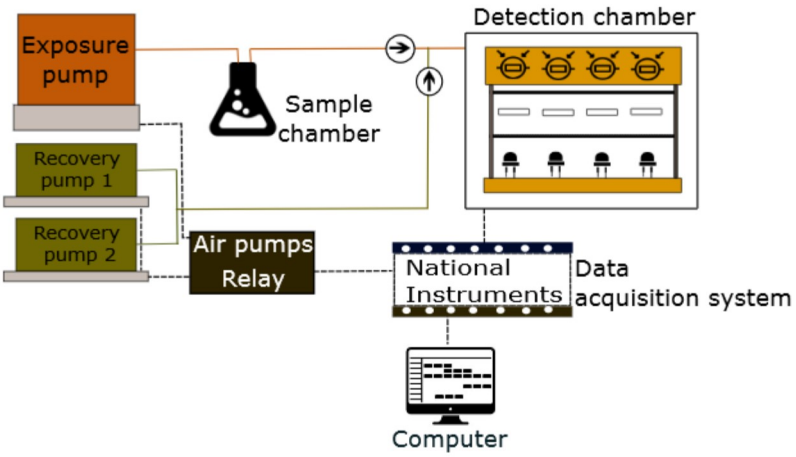

Figure 2.2: Schematic of the e-nose v0.

The e-nose v0 had three systems:

- A delivery system through which the gas sample contained in the headspace of the sample chamber (in the exposure periods) and the atmospheric air (in the recovery periods) were transferred to the detection chamber;
- A detection system inside which the gas interacted with the sensors' array;
- A transduction system that acquired and sent the signals obtained in the detection chamber to a computer.

The delivery system includes the air pumps (exposure and recovery pumps), the sample chamber, tubes and connectors, and two non-return valves to prevent backflow.

The exposure pump is a *Sera Precision 275R Plus*. This is responsible for carrying the VOCs from the sample chamber (where the chemical solution is placed) to the detection chamber. Therefore, it is ON in the exposure periods and OFF in the recovery periods.

The recovery system is composed of two air pumps *ELITE800*, which clean the detection chamber, making the atmospheric air circulate through the chamber, and removing

the VOCs. The "recovery pumps" operate alternately with the "exposure pump". These are ON in the recovery periods and OFF in the exposure periods. The recovery system cleans the detection chamber, making the atmospheric air circulate through it, and removing the VOCs.

The sample chamber used was an *Erlenmeyer* of 25 mL volume with a rubber cap crossed by two tubes: inlet and outlet illustrated in Figure 2.2. The area of the liquid-gas surface inside the sample chamber was changing for different volumes of solvent, due to its tapered configuration.

Non-return valves were used to prevent backflow in both exposure and recovery pipeline tracks. Some tubes were longer than necessary, which resulted in higher exposure and recovery times required for the experiments.

The detection chamber – Figure 2.3a - is the e-nose component where the VOCs interact with the sensing materials. It contains an array of four optical sensors able to detect those interactions. For each optical sensor, the unpolarised light emitted by the LED passes through a sensing film sandwiched between two crossed polarising filters (polariser and analyser), and finally reaches the LDR.

The LED and LDR boards were placed so that the LED and LDR components were aligned in front of each other. Screws and wooden sticks supported the two circuit boards, having two crossed polarising filters and the sensing films between them.

The LEDs board circuit - Figure 2.3b - consists of a set of LEDs connected in parallel to a 5 V energy source, having resistances in series to the LEDs.

The LDRs are components which decrease their resistance with increasing incident light intensity. This allows them to be used in light sensing circuits. The LDRs board circuit of e-nose v0 is shown in Figure 2.3c below. The resistance variations originate analogue signals, which are then converted into digital signals by the transduction system.

The data acquisition and control was based on a *National Instruments USB-6008* board, which acquired the data generated by the LDRs. This board alone costs more than 200 euros. The collected signals were sent to a computer and could be visualised in a *LabVIEW* interface.

Additionally, the exposure and recovery times were defined as *LabVIEW* inputs. The board used a 5 V to trigger the relay switch unit, which in turn determined the exposure and recovery pump states.

Finally, the main aspects of this device that needed to be improved were reported. The principal problems identified were the following:

- Regarding the electronic components, the LEDs and LDRs have some variations among them, which were inherent to their own production;
- Interference between optical sensors was observed in the signals' response;
- The detection chamber was difficult to handle;
- High noise levels were observed in the signals obtained.

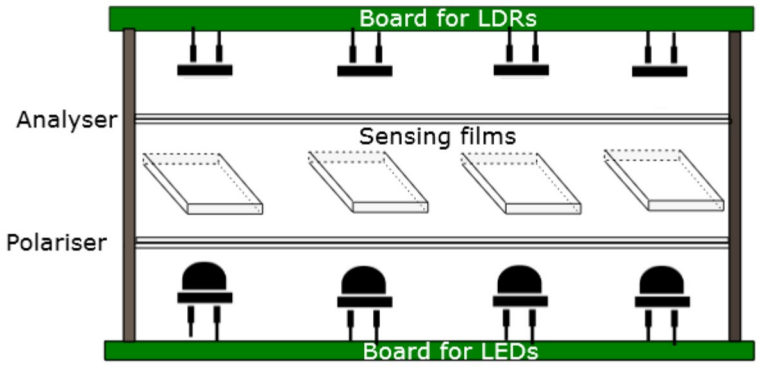

(a) Detection chamber.

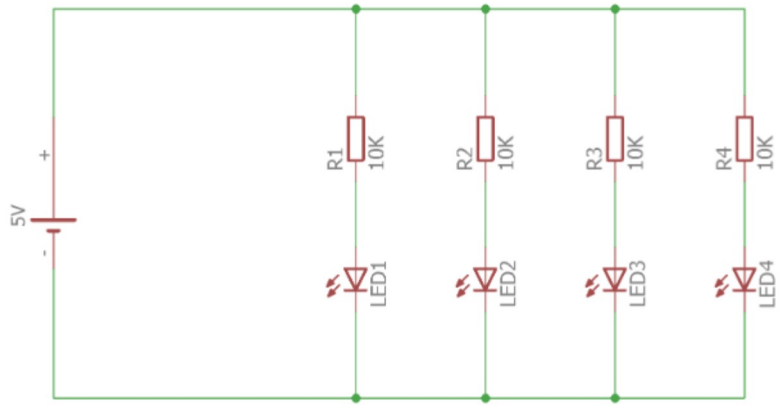

(b) Emission circuit.

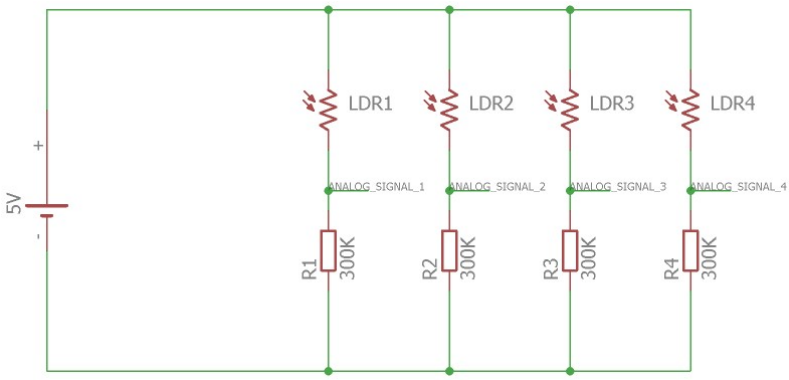

(c) Detection circuit.

Figure 2.3: Elements of the e-nose v0 detection system.

2.2 Objectives

The aim of assembling a new e-nose version was to make the device more reproducible and stable.

To compensate the differences among electronic components that compose different sensors in the array, for the next e-nose version, signals calibration was performed. Another goal for the next e-nose was to better isolate the optical pairs, because the LDRs of the optical pairs were not only receiving light from the LED in front, but also from the LEDs in the surroundings. Variations in the sensing films' exposed area to light also resulted in unstable responses, given that the sensing gels were not homogeneously spread over all the parts of the glass slides. A solution to solve this problem would be to confine the area of gel exposed, so that it could be more easily characterised.

The first prototype was also difficult to handle and it had air leaks in the tube connectors. Some tubes were longer than necessary. To solve this, a new detection chamber should be assembled, and new tubes and fitting-connectors should replace the existing ones.

In respect of the data acquisition and control system, in some situations, the noise was too high, inhibiting the observation of the sensor response. Besides, the hardware and software used were both expensive. We concluded that the construction of a cheaper and controllable data acquisition system could help in solving these problems.

2.3 Materials and methods

The schematic of the optical e-nose v1, which resulted from improvements made in e-nose v0, is represented in Figure 2.4a.

2.3.1 Delivery and recovery system e-nose v1

The sample chamber of e-nose v1 - Figure 2.4b - is a glass flask with 30 mL of volume. It has a cylindrical configuration, where the area of the liquid-gas surface is the same, independently of the volume used. The inlet and outlet glass tubes have 2 mm of Inner Diameter (ID) and 4 mm of Outer Diameter (OD). Its cover is screwed and made of plastic and can be easily opened and closed.

In the pipelines, new shorter tubes made of silicone (a biocompatible and transparent material) replaced the oldest ones. Having shorter tubes, less time is needed for the recovery and exposure periods. The silicone tubes (from the supplier *Deltalab*) were used to connect the various components of the system. Tubes with ID/OD = 4/6 mm were used all over the circuit. The silicone tubes used are translucent, non-toxic, have a high chemical and mechanical resistance, and can be used at temperatures from -50 °C to 200 °C.

The tube connectors were sold by *LaborSpirit's* supplier *Deltalab*. The types of connectors used were the following: T-connectors for 4-8 mm tubes; Y-connectors for 4-8 mm

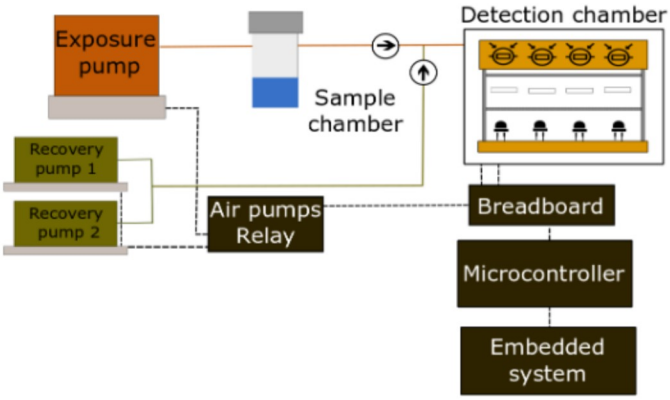

(a) Schematic of e-nose v1.

(b) Sample chamber of e-nose v1.

(c) Detection chamber of e-nose v1 (exterior view).

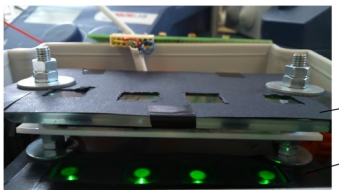

(d) Opaque layers inside the detection chamber.

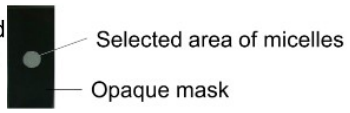

(e) Sensing films with opaque mask applied.

Figure 2.4: Components of e-nose v1.

pipes; and straight connectors for tubes with 4/5/6 mm of diameter. All these accessories are made of polypropylene and autoclavable.

2.3.2 Detection chamber of e-nose v1

A new detection chamber, easier to handle, was assembled for e-nose v1 - Figure 2.4c.

Inside the detection chamber, the interference between optical sensors was minimised. Each optical sensor is composed of a LED-LDR pair, and the LDR should only receive light from the LED in front, and not from the LEDs in the surroundings. Therefore, opaque mask's layers (see Figure 2.4d) were implemented to prevent the interference of dispersed light from neighbour LEDs.

Given that the sensing gels were not homogeneously spread over all the parts of the glass slides, opaque black masks – Figure 2.4e - were applied on the back of the glass slides. This delimitates the area of gel exposed, and allows better control of the optical sensing film.

2.3.3 Data acquisition and control system of e-nose v1

The data acquisition and control system previously implemented in e-nose v0 was not easy to scale-up, because the data acquisition system was expensive, and required cable connection to a computer. Thus, for e-nose v1, the data acquisition and control system was redesigned.

The new system uses a microcontroller *Arduino Uno* and an embedded system *Raspberry Pi 2 Model B*, that can be remotely controlled by a computer (using a cryptographic network protocol, Secure Shell (SSH)).

Since the data acquisition and control system was implemented using open-source hardware and software, it became much cheaper than the previous version. The new microcontroller plus the embedded system cost under 100 euros.

The signal to noise ratio was increased compared to e-nose v0 (see Figure 2.5).

2.3.4 Optical sensors' calibration of e-nose v1

The optical sensors were calibrated for each LED/LDR pair, according to the following equation:

$$Calibrated\ signal = \frac{(s - min)}{(max - min)} \tag{2.2}$$

Where s represents the signal values obtained. The value is given by the LDR, when a sensing film is sandwiched between two crossed polarising filters, in the absence - Figure 2.1a - or presence of VOCs - Figure 2.1b.

In the equation, min is the average of signal values obtained when two crossed polarising filters are placed between the LED and the LDR. Without placing the sensing gel in

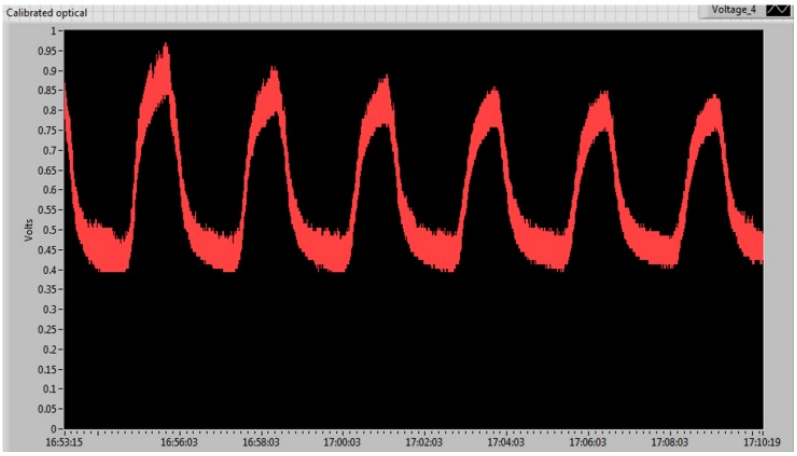

(a) Example of signal acquired with e-nose v0.

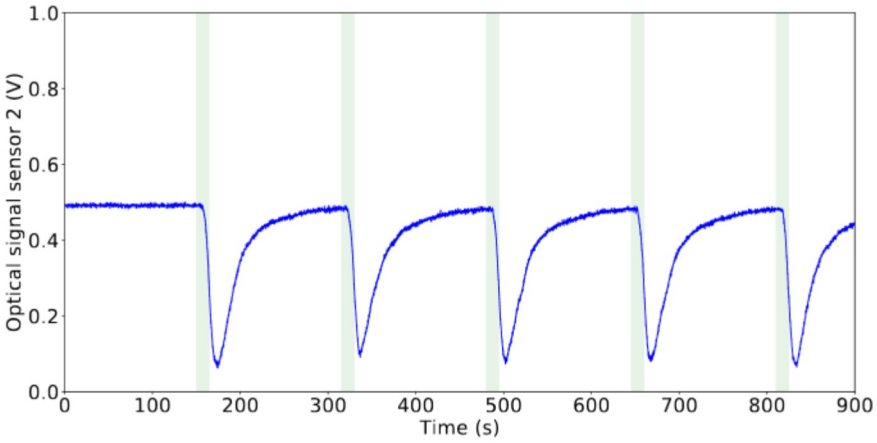

(b) Example of signal acquired with e-nose v1, given by sensing film B.

Figure 2.5: Example of non-filtered signals acquired from two different versions of e-noses for exposure to acetone.

the middle, the light intensity that reaches the LDR is minimal. The images of Figure 2.6a illustrate this process. Given the LDR response curve, due to receiving minimum light intensity the LDR resistance will be maximum. Consequently, according to the Ohm's law, the voltage drop at the LDR will be maximum. Yet, taking into account the LDR schematic shown in Figure 2.3c, the analogue output signal V_{out} (detected by the *Arduino*) is given by equation 2.3:

$$V_{out} = V_R = V_{Source} - V_{LDR} \tag{2.3}$$

Thus, if the voltage drop at the LDR is maximum, the output voltage will be minimum.

The value *max* is the average of signal values obtained when two parallel polarising filters are placed between the LED and the LDR (without sensing gel in the middle) - see Figure 2.6b. The light intensity that reaches the LDR is maximum. Therefore, its resistance will be minimum. Consequently, the voltage drop V_{LDR} will be minimum.

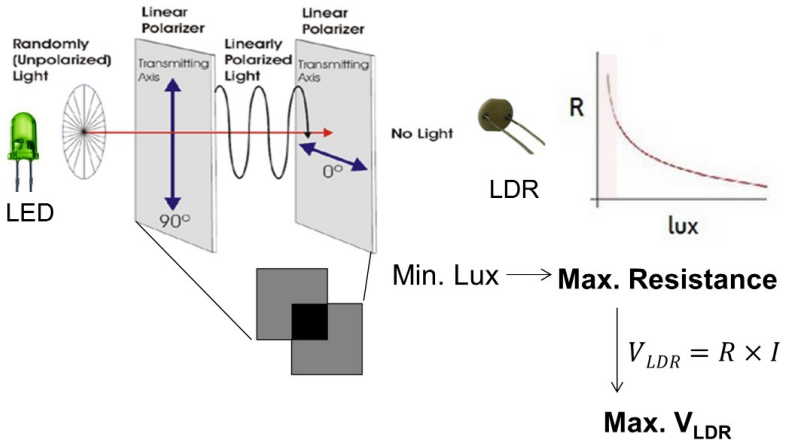

(a) Situation when minimum light intensity reaches the LDR with crossed polarisers.

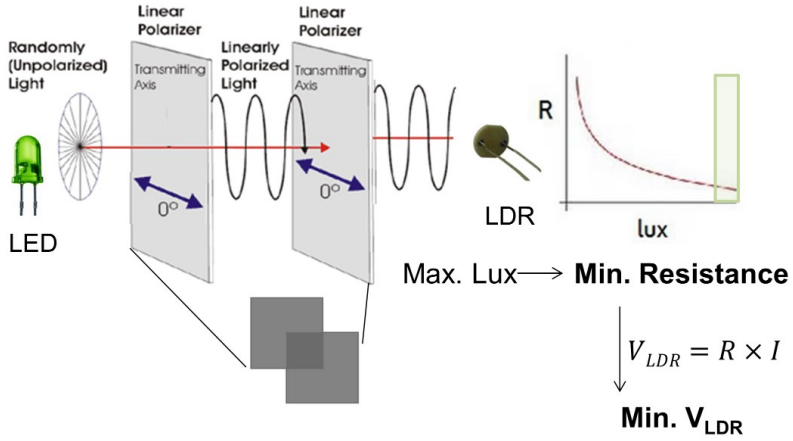

(b) Situation when maximum light intensity reaches the LDR with parallel polarisers.

Figure 2.6: Unpolarised light from the LED passing through the polarisers and reaching the LDR.

According to equation 2.3, if the voltage drop at the LDR is minimum, the output voltage will be maximum.

The calibration signals, from which the min and max are calculated, are obtained without placing any sensing film between the two polarising filters. The experiments are performed inside the detection chamber, with the LEDs ON. The e-nose only needs a single calibration, before the first experiment, and not at the beginning of each experiment. In case of devices replication, each e-nose unit requires its own calibration, and cannot use calibration values from other e-noses, because the rationale behind calibration is to compensate differences among the different LEDs and LDRs of the array, which are inherent to their production.

2.3.5 Proof of concept using e-nose v1

After having the e-nose assembled and several sensing films prepared, our goal was to evaluate if the e-nose v1 could distinguish different solvents.

Four optical sensors (A, B, C and D), with sensing films having different compositions, were used. The compositions of the sensing film's applied in the sensors' array are described in Table 2.1. The sensing films A, B and C were produced using the same conditions that Semeano *et al.* [88] used. The sensing film D was produced using similar conditions to the sensing film A, but applying a different ionic liquid.

Table 2.1: Sensing films' composition

Optical sensor	IL	LC	Polymer	Water
A	[BMIM][DCA]	5 CB	BSG + Dextran	MilliQ water
B	[BMIM][DCA]	5 CB	BSG + Sorbitol	MilliQ water
C	[Alocim][Cl]	5 CB	BSG + Dextran	MilliQ water
D	[BMIM][Cl]	5 CB	BSG + Dextran	MilliQ water

IL: Ionic Liquid; LC: Liquid Crystal; [BMIM][DCA]: 1-butyl-3-methylimidazolium dicyanamide; [BMIM][Cl]: 1-Butyl-3-methylimidazolium chloride; 5CB: 4-Cyano-4'-pentylbiphenyl; BSG: Bovine Skin Gelatin.

After the batch production, a drop of gel was deposited on each microscope glass slide (40 mm x 15 mm), and manually spread over it using a roll-on technique. A sensing film consists of a thin layer of sensing gel spread on a glass slide.

Three tests were conducted in the e-nose v1. Each test included 13 experiments, each one using a different organic solvent in the sample chamber: acetone, carbon tetrachloride, chloroform, dichloromethane, diethyl ether, isopropanol, ethanol, ethyl acetate, heptane, hexane, methanol, toluene and xylene.

The experiment conditions were also similar to the ones used by Semeano *et al.* [88]. The organic solvents were kept at 36 °C (in a thermostated water bath) during the experiments because it is close to the temperature of the human body. The room temperature was controlled setting the air conditioning of the room to 20 °C. The solvent quantity, the flow rate of the exposure and recovery pumps, the room temperature, and the sampling rate were kept the same for the different experiments. The exposure and recovery times were set to the minimum that allowed signal visualisation. The experiment conditions are explained below. The same experiment conditions were applied for the three tests.

Experiment conditions:

- **Sample quantity:** 5 mL
- **Sample temperature:** 36 °C
- **Exposure time:** 15 s

- **Recovery time**: 150 s
- **Total duration**: 15 min
- **Sampling rate**: 10 Hz

Four optical signals (A, B, C and D) were collected for each of the 13 solvents tested in the e-nose. The three tests performed in consecutive days intended to study the reproducibility of the results.

An example of a typical calibrated signal is shown in Figure 2.5b. A set of features was collected, for each cycle of the signals given by sensors A, B, C and D. Figure 2.7 illustrates the features extracted for a single cycle of a optical signal S_{OS}.

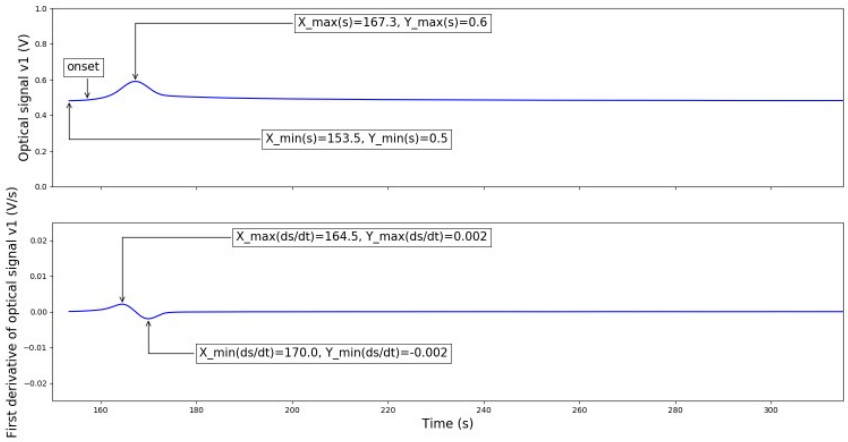

Figure 2.7: Illustration of features extracted from the signals.

The extracted features were the following:

- **Relative amplitude**(Ra)

$$Ra(S_{OS}) = \frac{max(S_{OS}) - min(S_{OS})}{min(S_{OS})} \tag{2.4}$$

S_{OS} is a signal obtained from the optical sensor OS = A, B, C or D.

- **Maximum of** S_{OS}:
  - X coordinate of $max(S_{OS})$
  - Y coordinate of $max(S_{OS})$
- **Minimum of** S_{OS}:
  - Y coordinate of $min(S_{OS})$

- **Maximum of the signal's first derivative**:
  - X coordinate of $max(\frac{d(S_{OS})}{dt})$
  - Y coordinate of $max(\frac{d(S_{OS})}{dt})$
- **Minimum of the signal's first derivative**:
  - Y coordinate of $min(\frac{d(S_{OS})}{dt})$
- **Onset**:
  - Time at which the signal achieves the double of the noise level since the exposure time started working.

The extracted features were ranked by impact on variance coverage. Then, the best features for solvents distinction were identified and PCA was used for VOCs distinction.

Additionally, four classification methods (NB, DT, k-NN, and SVM) were applied to evaluate their accuracy for VOCs prediction.

2.4 Results and discussion

The new e-nose assembled, e-nose v1, was firstly used for device calibration and then to perform a proof of concept.

For the proof of concept, three tests were performed under the same experiment conditions.

Considering the first test performed (test 1), it was observed that the interaction of the six sensing films in the sensors' array with different VOCs originates signals with different features. This is an indicator that the device might be useful for VOCs distinction and identification. For example, Figure 2.8 shows that the wave shape given by the optical sensor B is distinct for the different solvents used in test 1.

After features extraction and their ranking, the two more informative features for solvents distinction were identified: y coordinate of maximum of the signal given by the optical sensor B ($max(S_B)$) and y coordinate of the maximum of the first derivative of the signal B ($max(\frac{d(S_B)}{dt})$). Selecting the two best features, it is possible to identify a clear separation of all the 13 solvents (Figure 2.9), with 100 % of the total variance covered.

The results of the four classification methods applied for VOCs prediction are shown in Table 2.2. The leave-one-out cross validation was used for data sampling. For NB, the likelyhood of the features was assumed to be Gaussian, being the Gaussian NB algorithm applied in this case. In DT the number of leaves was explored from 2 (minimum) until 100 (maximum), and subsets samller than 5 were not split. For k-NN, the algorithm looked for the 5 nearest neighbours with k=5 and using the Euclidean distance as metric. In the case of SVM the Kernel applied was the Radial Basis Function, and the parameters

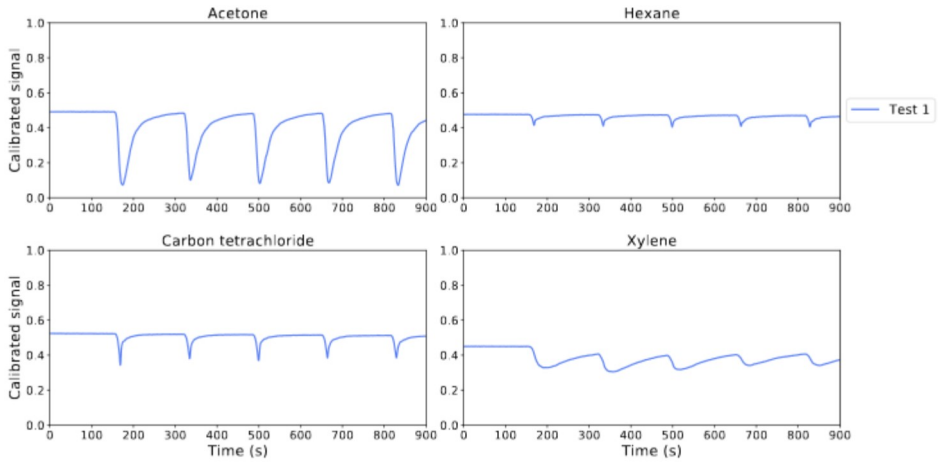

Figure 2.8: Signals given by optical sensor B for the experiments using acetone, hexane, carbon tetrachloride and xylene obtained with e-nose v1 in test 1.

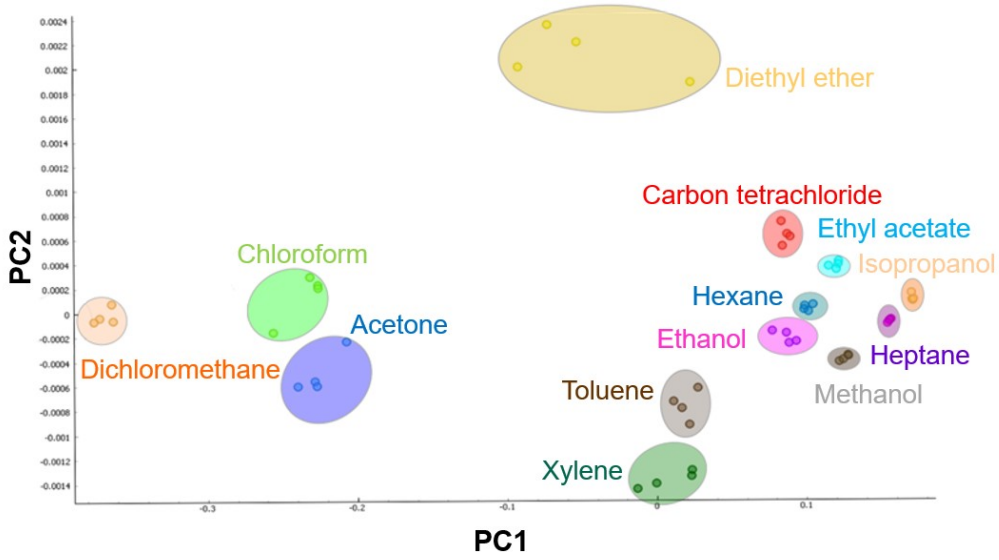

Figure 2.9: 2-D data visualisation using data from test 1.

Table 2.2: Evaluation parameters of the classification methods applied for test 1.

Method	AUC	F1	Precision	Recall
NB	0.625	0.321	0.401	0.308
DT	0.927	0.862	0.886	0.865
k-NN	0.792	0.587	0.593	0.615
SVM	1.00	1.00	1.00	1.00

used were: 1.00 for the Cost, 0.1 as Regression loss, and the opmimization was done with a numerical tolerance of 0.001 with an iteration limit of 100.

To evaluate the performance of the selected classifiers, Area Under Curve (AUC) ROC (Receiver Operating Curve) was used. AUC ranges from 0 to 1 and a random classifier presents an AUC of 0.5. A model whose predictions are 100 % wrong has an AUC of 0; one whose predictions are 100 % correct has an AUC of 1. For SVM the AUC was 1. AUC ranges in value from 0 to 1. This means that the SVM model was 100 % correct for the VOCs predictions.

The F_1 score is the harmonic average of the precision and recall, where an F_1 score reaches its best value at 1 (perfect precision and recall) and worst at 0. F_1 can be written according to equation 2.5. The precision (p) is given by equation 2.6, and the recall (r) is given by equation 2.7. SVM achieved the best score for F_1, recall and precision.

$$F_1 = \frac{2 \times p \times r}{p + r} \tag{2.5}$$

$$p = \frac{TP}{TP + FP}, \text{ ,where } TP = \text{True Positive}, \quad FP = \text{False Positive} \tag{2.6}$$

$$r = \frac{TP}{TP + FN}, \text{ where } TP = \text{True Positive}, \quad FN = \text{False Negative} \tag{2.7}$$

For test 2, the sensing films were removed from the sensor array and placed again. After this, the same procedure was repeated for test 3. Examples of optical signals obtained in the three tests for the experiments using acetone, hexane, carbon tetrachloride and xylene are shown in Figure 2.10.

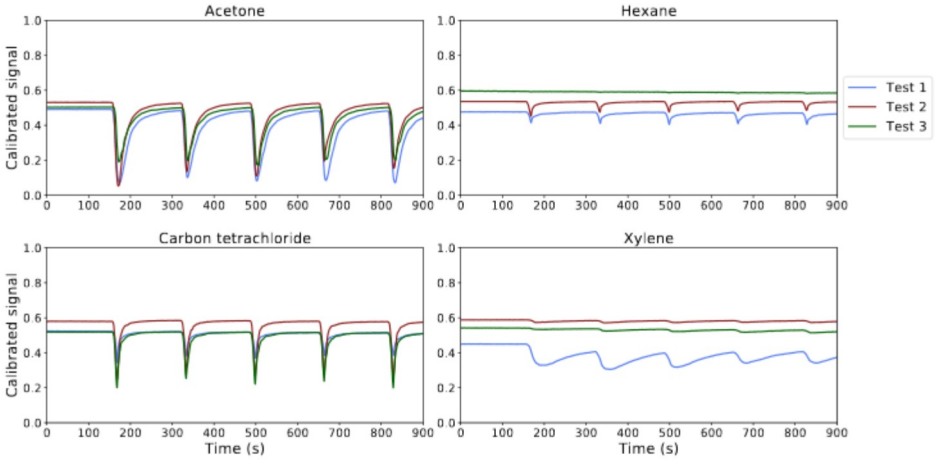

Figure 2.10: Optical signals obtained with sensor B in e-nose v1 for the experiments using acetone, hexane, carbon tetrachloride and xylene in tests 1, 2 and 3.

Observing the signals for each organic solvent, one can identify significant differences comparing test 1, test 2 and test 3 results. Thus, we can conclude that the results were not reproducible for different tests. Possible reasons for lack of reproducibility can be: the sensing films spreading method was not adequate; the device was not stable enough, because it was difficult to place the sensing films at the same position when they were removed and placed again in different days, and the PCB with the detection circuit had to be taken out and placed again for different tests.

PCA was also performed having as input the extracted features from signals obtained in test 1, test 2 and test 3. Selecting the best two features obtained for test 1, it was not possible to cluster the different solvents using PCA, as can be seen in Figure 2.11.

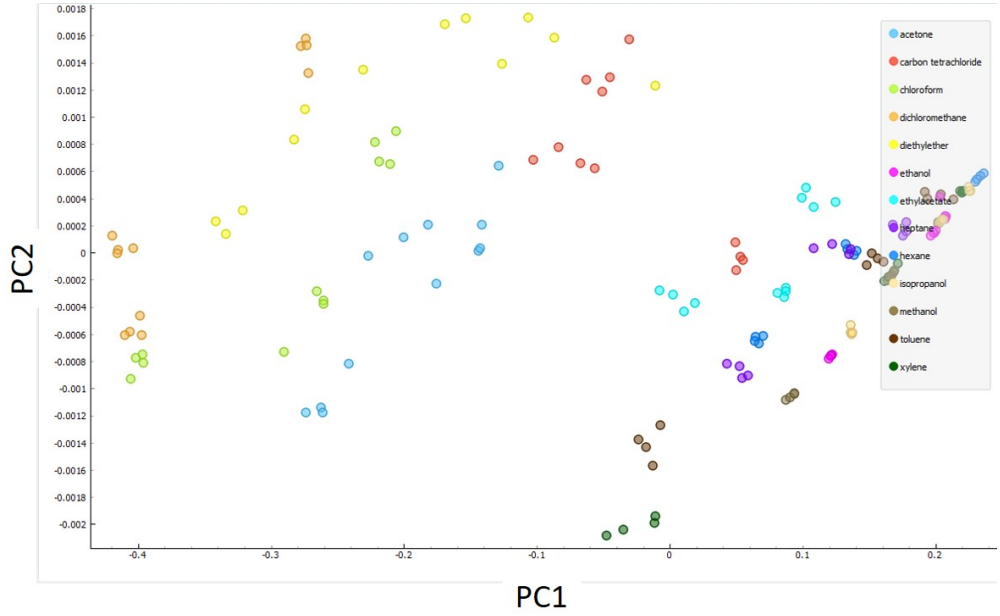

Figure 2.11: 2-D data visualisation using data from test 1, test 2 and test 3.

Again, four classification methods (NB, DT, k-NN, and SVM were applied for data from test 1, test 2 and test 3, and the evaluation parameters of each one were accessed - Table 2.3.

Table 2.3: Evaluation parameters of the classification methods applied for test 1, test 2 and test 3.

Method	AUC	F1	Precision	Recall
NB	0.608	0.271	0.317	0.276
DT	0.851	0.723	0.729	0.724
k-NN	0.76	0.543	0.564	0.558
SVM	0.74	0.527	0.527	0.519

In this case, the best classification results were found for DT. However, when using data from the three tests performed, none of the evaluation parameters of any classifier achieved the maximum rate of 1, which means that none of them was capable of

predicting all the VOCs correctly.

2.5 Conclusion

The e-nose v1 can measure four optical signals simultaneously. A method was developed for the signals calibration, and a stable data acquisition system was implemented. In general, the device is economic and easy-to-handle. The main advantages of the new data acquisition and control system based on *Arduino* and *Raspberry Pi* are:

- The inexpensive price, due to the use of open-source hardware and software;
- Faster mechanisms for data visualisation and data analysis;
- The system is easily scalable and autonomous;
- A better signal to noise ratio was achieved (see Figure 2.5).

A preliminary data analysis showed promising results regarding VOCs prediction and classification using data from a single test. However, for multiple tests, accurate classification was not achieved. Thus, the device should be first improved to be more stable and reproducible.

To reach our research purposes, which include testing many sensing films and VOCs in a fast and automated manner, the next project tasks should include a device optimisation. In terms of hardware, the next version of e-nose should be a miniaturised and hybrid device (with optical and electrical detection systems). In addition, the number of sensors working in parallel should be increased, to allow testing more sensing films during the same experiment. Moreover, the system should have a humidity and temperature sensor for room conditions' control, and an interface for real-time signals' visualisation should be implemented to easily detect eventual anomalies in the system. These further steps are essential to meet the final goal of creating an autonomous, accurate, stable and miniaturised device.

Chapter 3

Towards a hybrid and miniaturised prototype: E-nose v2

In this chapter, the main achievements obtained with e-nose v1 are reviewed and the limitations associated to this system are mentioned as well (Section 3.1). Then, the objectives (Section 3.2) for the next e-nose version, e-nose v2, are presented and the tests conducted in order to achieve stability and reproducibility are explained.

In materials and methods (Section 3.3), the design and assembly of e-nose v2 is reported, including a description of the three e-nose systems: delivery system, data acquisition and control system and detection system . E-nose v2 is an opto-electronic device, faster and easier to scale-up than e-nose v1. The methodologies applied for the experiments performed with this device are also presented .

Section 3.4 contains the results of the studies which intended to evaluate device's reproducibility (Section 3.4.1), accuracy (Section 3.4.2) and stability (Section 3.4.3) .

Finally, Section 3.5 gives an overview of e-nose v2, discussing the experiments performed with this device and analysing the results obtained. After the analysis of these results, the ideas and improvements discussed for the next e-nose version are presented.

This work was published in Pádua *et al.* (2018) in *Proceedings of the 11th International Joint Conference on Biomedical Engineering Systems and Technologies - Vol. 1.* [93] , and presented at *BIODEVICES 2018* conference in the oral presentation entitled *"Design and Evolution of an Opto-electronic Device for gas sensing"*.

Also, part of the work described in this section was published in Pádua *et al.* (2019) in *Proceedings of the 12th International Joint Conference on Biomedical Engineering Systems and Technologies - Vol. 1.* [95] , and presented at *BIODEVICES 2019* conference in the oral presentation entitled *"Impact of sensing films' spreading method on classification accuracy by electronic nose"*.

Reproducibility tests can be found in Hussain *et al.* (2019) in *Tunable Gas Sensing Gels by Cooperative Assembly* [88].

3.1 Introduction

The first prototype (named e-nose v1) became an autonomous unit, not needing to be physically connected to a computer. This was achieved due to the new data acquisition and control system that was implemented based on a microcontroller (*Arduino*) to convert the analogue data to digital data, and an embedded system (*Raspberry Pi*) to collect the data. This unit confers an advantage comparing with other e-noses described in the literature which require a computer connected to the e-nose data acquisition system for running the experiments [36].

The use of open-source hardware and software represents a benefit compared with other e-noses that use a *National Instruments* board / LabVIEW or MATLAB [8, 36, 96] (whose licenses are expensive). The programming language used in this project, python, is free. It has extensive support libraries and clean object-oriented designs that increase programmer's productivity.

From e-nose v0 to e-nose v1, a higher level of device stability was achieved due to the use of a more robust and easy-to-use detection chamber. Yet, there was still room for improvement regarding the detection chamber stability. Using e-nose v1, it was still difficult to change sensing films between experiments, due to its horizontal configuration with the sensing films sandwiched between two layers of PCBs. Additionally, the detection chamber was not hermetic, therefore flow losses were occurring during the experiments. Devices stability has a tremendous impact in reproducibility and scalability. Reproducibility has been mentioned as an important factor to take into account when designing and assembling biodevices [97, 98], in particular electronic noses [99]. Our more recent prototype, e-nose v1, had some issues regarding detection chamber stability because:

- It did not have fixed positions to insert the sensing films in the array;
- The horizontal configuration forced the removal of the upper PCB to insert the sensing films. This was not practical and contributed to generate instabilities in the system.

These facts were affecting device stability and consequently the reproducibility of the results was compromised. That is why, for the next e-nose version the main goal should be to improve the detection chamber for achieving reproducible and stable results.

From e-nose v0 to e-nose v1 the detection chamber volume was reduced in 40 %. However, it was still possible to decrease the chamber volume to a lower value. This would consequently enable to maximise the number of cycles obtained per minute.

The sensing gels change both optical and electrical properties while interacting with VOCs. However, e-nose v1's data acquisition system was only prepared to collect optical signals. The next version, e-nose v2 should be able to collect information about the two sensing films' working principles: optical and electrical.

3.2 Objectives

The new e-nose implemented should fulfil some requirements: it should be miniaturised, easier to handle and more stable. Better stability would be achieved if the device had specific slots to insert the sensing films, and flow losses were minimised. Moreover, it should enable less time needed for experiments, and to test more sensing films simultaneously.

Additionally, e-nose v2 should be hybrid, which means that it should enable the acquisition of both optical and electrical signals given by the sensing films.

After its assembly, the optical e-nose v2 would be used to perform reproducibility tests, and to test sensing films' stability for different compositions and spreading methods applied. We were also interested in exploring more machine learning approaches (especially in comparing the performance of simple algorithms such as Multinomial Logistic Regression (MLR), DT and NB).

Furthermore, we wanted to test the use of GA in the gels' composition as an attempt to improve the sensing gels' stability when these are exposed to VOCs. We decided to study three parameters associated with the optical structure of the gel - droplets' number, optically active area, and droplets' mean diameter - based on which we quantified the relative variations in the sensing films before and after exposure to the VOCs.

3.3 Materials and methods

3.3.1 Design and assembly of e-nose v2

Having these goals defined, the e-nose v2 was designed according to the schematic shown in Figure 3.1. In Figure 3.1 below, the detection chamber represents the optical detection chamber. This device is hybrid, since the optical detection chamber can be easily replaced by an electrical sensors chamber (see Section 3.3.1.3).

To make e-nose v2 compatible with our goals, a new optical detection chamber was designed and the first electrical detection chamber was created. The e-nose v1 delivery system was considered stable, as well as the data acquisition and control system. However, some aspects described in Section 3.3 needed to be adjusted to the new features desired for e-nose v2.

3.3.1.1 Delivery system of e-nose v2

The delivery system is composed of two air pumps (the exposure and the recovery pumps). These pumps are the same model: *Marina 200*, with a constant flow rate set to 5 L/min.

The sample chamber is the same type used in e-nose v1. The tubes and connectors are also made of silicone and polypropylene, respectively. Similarly to e-nose v1, two non-return valves were applied at the entrance of the detection chamber to avoid backflow.

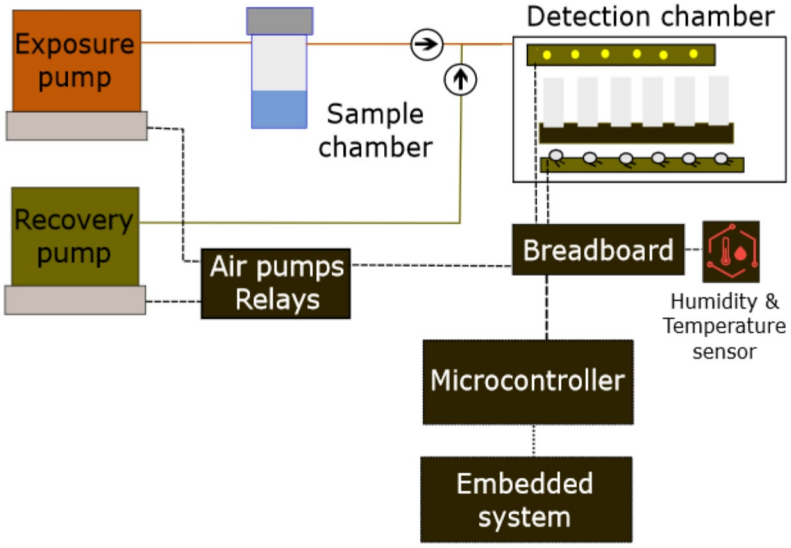

Figure 3.1: Schematic of e-nose v2 with the optical detection chamber.

3.3.1.2 Data acquisition and control system of e-nose v2

The architecture of the e-nose v2 data acquisition and control system is very similar to the one applied for e-nose v1, based on *Arduino Due* and *Raspberry Pi 2 Model B*. *Arduino Due* was used instead of *Ardunino Uno* (used in e-nose v1), because the electrical detection chamber was initially design to accommodate 12 electrical sensors. *Arduino Due* has 12 analogue inputs, whereas *Arduino Uno* has only six. Additionally, real-time signals visualisation was implemented based on *bokeh server* – see the interface in Figure 3.2.

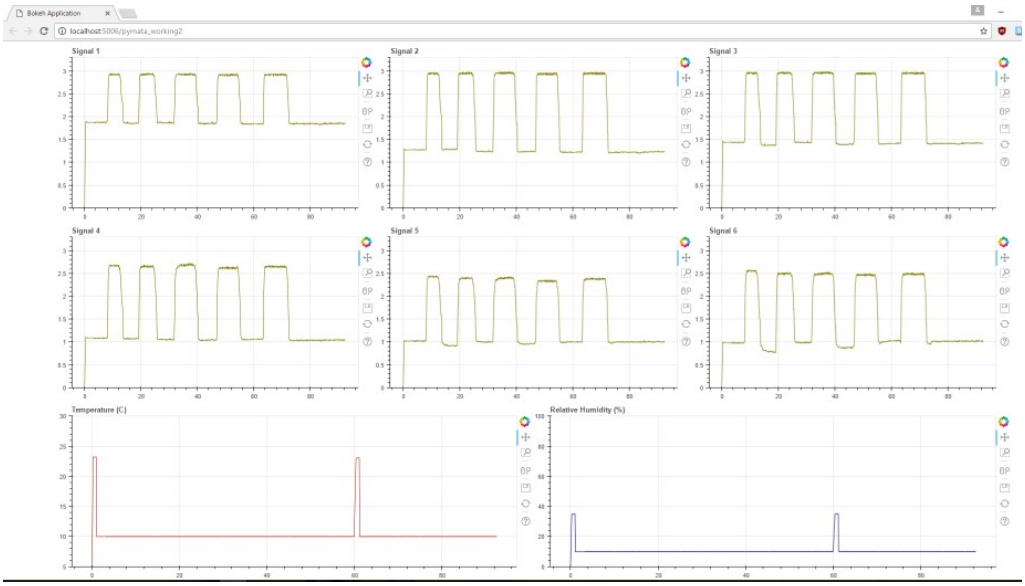

Figure 3.2: Interface for signals' visualisation in real-time based on *bokeh server*.

A humidity and temperature sensor *HTU21D* from *Adafruit* was included in the e-nose instrumentation to measure the room conditions. This I^2C digital humidity sensor

has a typical accuracy of ±2 % with an operating range that is optimised from 5 % to 95 % relative humidity. The temperature output has an accuracy of ±1 °C from -30 °C to + 90 °C. The system has a PTFE filter to keep the sensor clean, protecting it from dust and splashes.

The relays unit was wired according to the schematic shown in Figure 3.3.

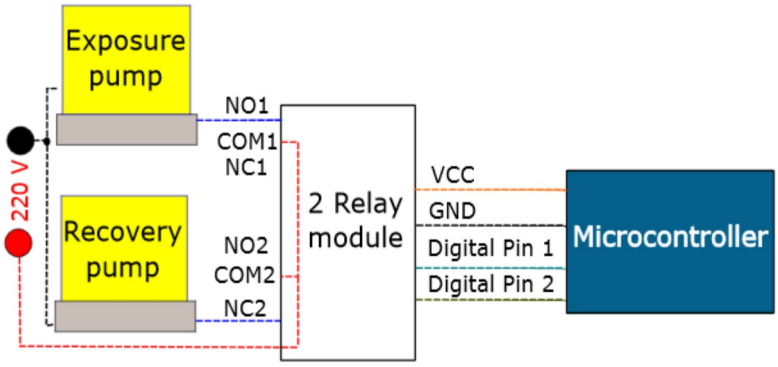

Figure 3.3: Schematic of relays unit. NO: normally open; NC: normally closed; VCC: power supply ; GND: ground.

3.3.1.3 Detection chamber of e-nose v2

The detection chamber is the e-nose component where the analytes interact with the sensing materials.

Optical detection chamber of e-nose v2

The optical detection chamber is composed of:

- An external box (chamber with lid) Figure 3.4 - (1);
- An internal support for sensing films with a glass chamber on it - Figure 3.4 - (2);
- PCBs for the emission circuit (using LEDs) - Figure 3.4 - (3A) and for the detection circuit (using LDRs) - Figure 3.4 - (3B).

The external structure of the detection chamber was designed using a solid modeling computer-aided design and computer-aided engineering program, *SolidWorks 2016*. This chamber contains the PCBs with the emission and detection circuits, the internal support with sensing films (see technical drawing in Figure C.4 of Appendix C) and an internal glass chamber on it.

It is black and opaque, avoiding the interference of background light sources with the tests performed. This chamber is made of Polylactic Acid (PLA), and was built in an *Ultimaker* 3D-printer. Pictures are shown in Figure 3.5, including the views with the box opened and closed.

The internal chamber is composed of a support for sensing films and of a glass chamber on it to concentrate the VOCs near the sensing films. To assemble it, firstly the sensing

Figure 3.4: Detection chamber of e-nose v2. 1 - External structure; 2 - Internal support for sensing films and glass chamber; 3A - PCB for the emission circuit; 3B - PCB for the detection circuit.

(a) Chamber with lid (closed).

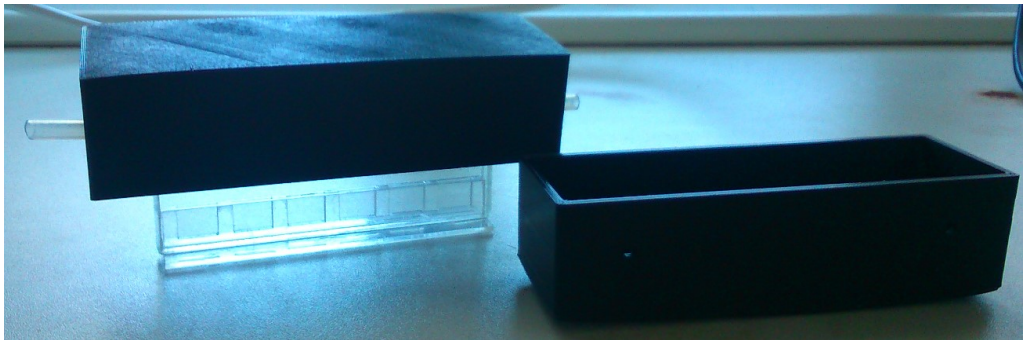

(b) Opened chamber.

Figure 3.5: Structure of the detection chamber.

films are inserted in the slots of the support, as shown in Figure 3.6a. Then, the glass cover is inserted in a slot and on a rubber roofing membrane strip made of Ethylene Propylene Diene Terpolymer (EPDM) - Figure 3.6b. This rubber allows to close the chamber hermetically (for the pressures applied in the system) when the external structure of the detection chamber is closed, because the lid of the external structure forces it against the rubber.

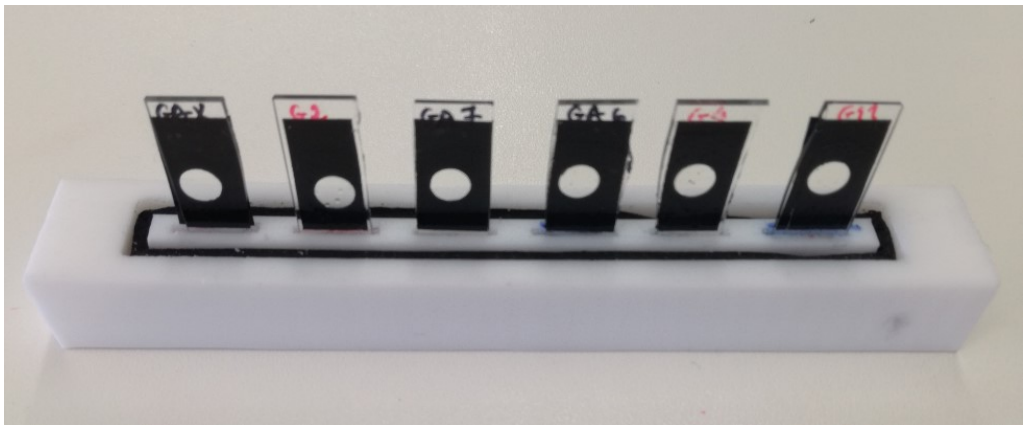

(a) Sensing films placed in the support.

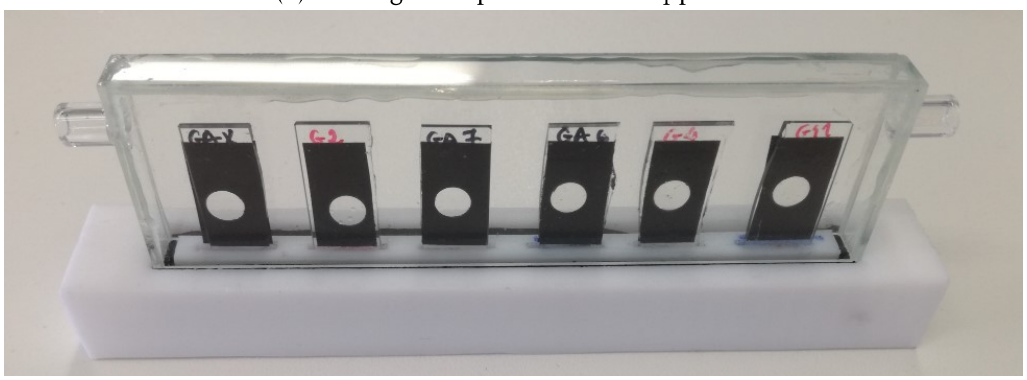

(b) Glass chamber placed on the support.

Figure 3.6: Assembly of internal chamber.

The support for sensing films was also designed using *SolidWorks 2016* - Figure 3.7. Then, it was built at the physics' department workshop, at FCT-NOVA. Its constituent material is PTFE.

The glass cover was made at VICARTE (at FCT-NOVA), using glass plates, which were cut in the desired dimensions, and then pasted with a glue for glass (*Araldite Rapid*).

The PCBs for the emission and detection circuits of e-nose v2 are similar to the ones used in e-nose v1, but having an array of six LEDs/LDRs in parallel instead of four. The components used are through-hole technology mounting type. The schematic of the emission circuit is represented in Figure 3.8a, and the schematic of the detection circuit is shown in Figure 3.8b. The 6 LDR were selected among a group of 30, by selecting the group of 6 which presented more similar responses in the two conditions tested: inside a black box, with a LED ON pointing directly at the LDR (when the LDR presents minimum

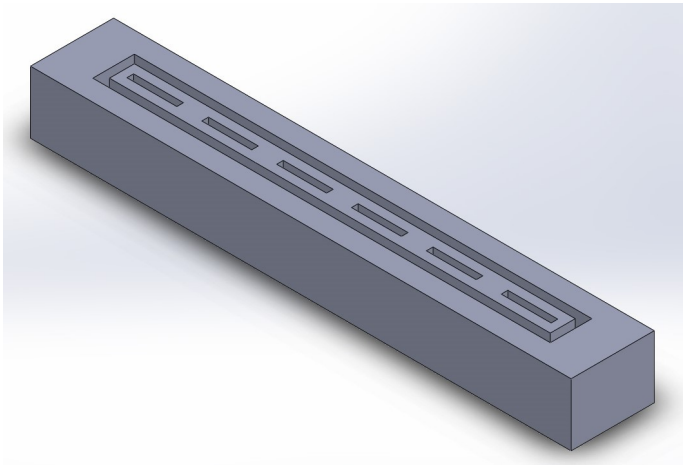

Figure 3.7: 3D-project of the support for sensing films.

resistance) and with the LED OFF (when the LDR has maximum resistance).

There is another difference in the detection circuit of e-nose v2 compared to e-nose v1. Its power supply is 3.3 V, whereas for e-nose v1 it was 5 V. This modification was necessary because an analogue input value higher than 3.3 V may damage the *Arduino Due* inputs (used in e-nose v2).

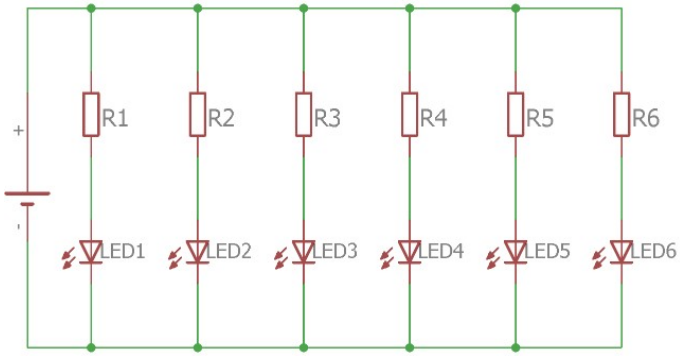

(a) Schematic of emission circuit.

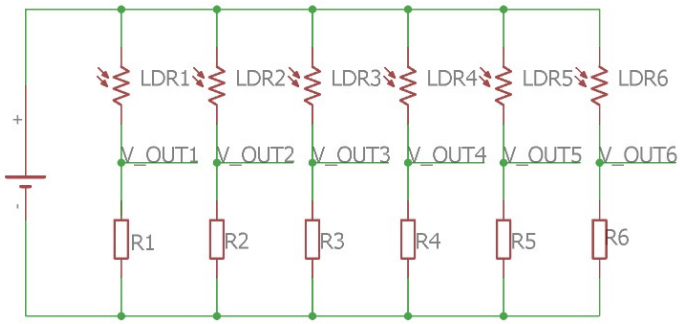

(b) Schematic of detection circuit.

Figure 3.8: PCBs' circuits of e-nose v2.

The characteristics of the LEDs used are described in Table 3.1, and the specification of the LDRs are summarised in Table 3.2.

Table 3.1: Specifications of the selected LEDs for e-nose v2.

Model	L-5T47UW5C-D1
Lamp diameter (mm)	5
Chip - Raw material	GaInN
Chip - Emitted color	Ultra white
Lens colour	Clear water
View angle (°)	18
Typical forward voltage @ 20 mA (V)	3.5
Typical luminous intensity (mcd) @ 20 mA (V)	6500

Table 3.2: Specifications of the selected LDRs.

Supplier	Robert Mauser (ref. 005-0033)
Power (mW)	90
Resistance at 100 lx ($k\Omega$)	15
Resistance at 10 lx ($k\Omega$)	340
Resistance at 0 lx ($k\Omega$)	15000
Wavelength at the point of max. sensitivity (nm)	600

Electrical detection chamber of e-nose v2

The electrical detection chamber can be used in e-nose v2, substituting the optical detection chamber to acquire electrical signals - Figure 3.9. The electrical e-nose v2 uses the same delivery, and data acquisition and control system implemented for the optical e-nose v2.

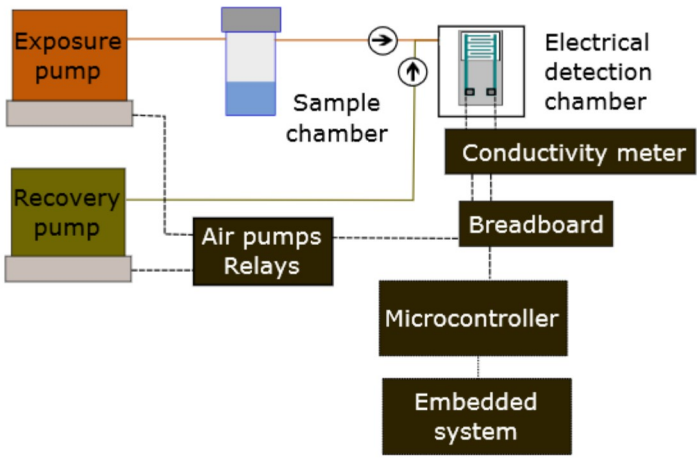

Figure 3.9: Schematic of e-nose v2 with the electrical detection chamber.

As a first approach, the interdigitated electrodes with sensing gels on the top were wired to a circuit represented in the schematic of Figure 3.10.

In this case, DC was applied to the electrodes. However, the sensing films tested

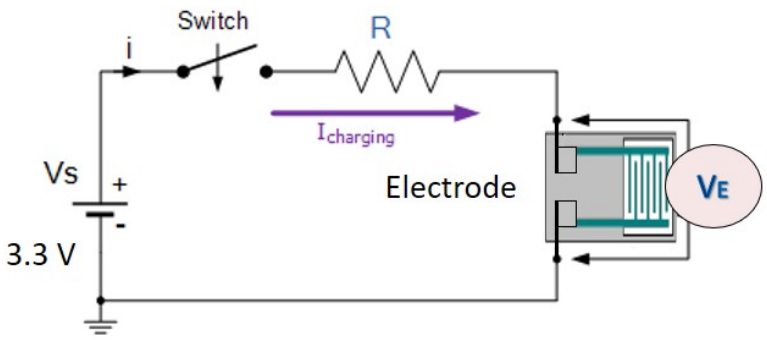

Figure 3.10: Circuit with DC applied to an electrode.

exhibited none or negligible amplitude of response in the signals obtained, due to the capacitive effects that occur in the interdigitated electrodes.

The electrodes wired to a DC voltage source behave like capacitors saturating due to capacitive charging. When an electrode is connected to this kind of circuit (see Figure 3.10), the current begins to flow into the electrodes via the resistor. The electrode continues charging up and the voltage difference between V_S and V_E reduces, until the electrode is fully charged. At this point, the current passing through the electrode decreases; and the voltage drop occurs almost entirely across it. Since this effect interferes with the voltage drop across the electrodes, this also inhibits the occurrence of voltage changes related to the interaction of the VOCs with the electrodes.

A solution for this problem is to use Alternating Current (AC), because the capacitive electrodes block DC, but not AC. In the case of AC, the voltage applied by the source, V_S, changes its polarity. Therefore, the electrodes are being continuously polarised and depolarised, enabling the study of the conductivity changes that occur on the electrical sensors due to interactions with VOCs – Figure 3.11.

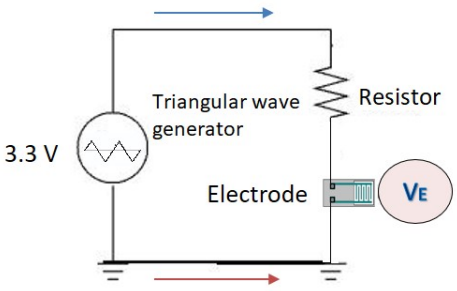

Figure 3.11: Circuit with AC applied to an electrode.

An electrical field is generated between the interdigitated electrodes and passes through the sensing film, which in turn changes the impedance of the electrical sensor when exposed to VOCs. By measuring the changes in voltage across the electrodes, a signal is obtained and it is representative of the interaction with the VOCs.

To detect the conductance changes that occur in the electrode while interacting with

the VOCs, the conductivity meter described in [103] was implemented. The schematic of the conductivity meter is shown in Figure 3.12.

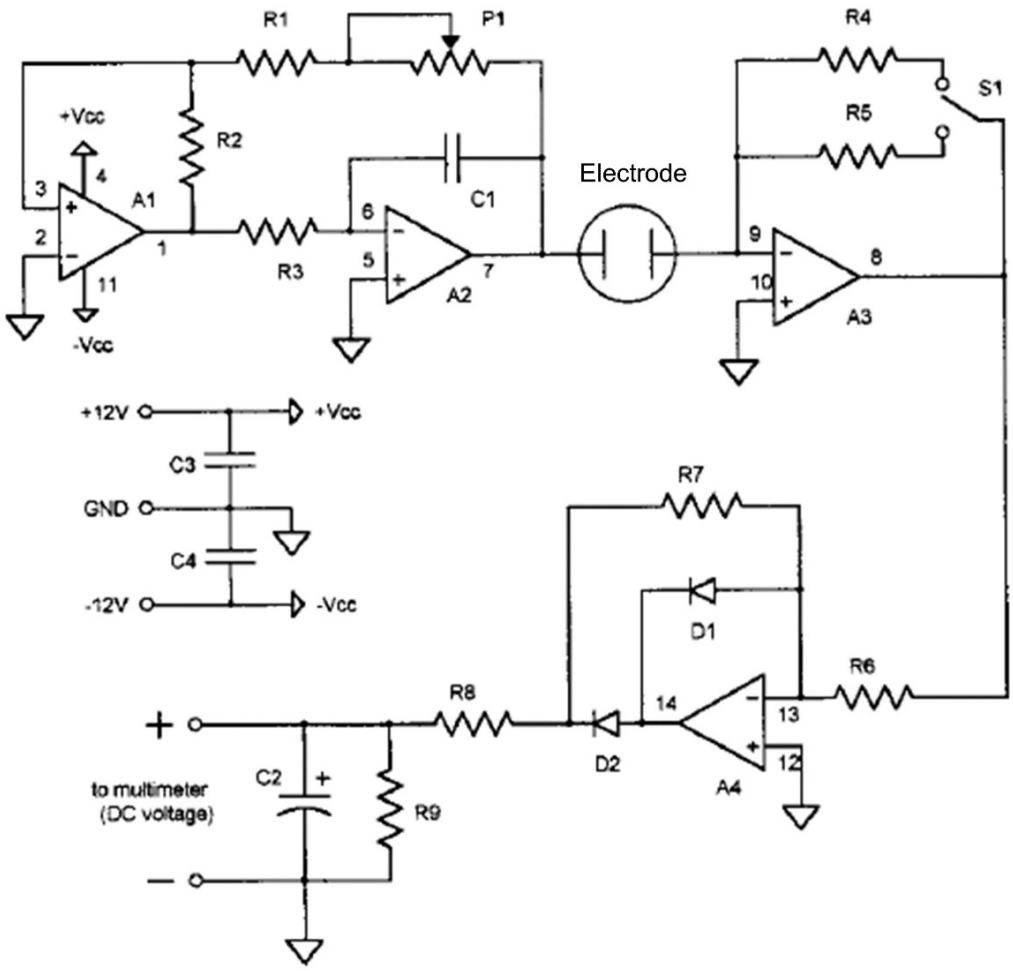

Figure 3.12: Schematic of the conductivity meter. Details about the values of the components can be found in the origin article of this image: [103]

.

Figure 3.9 shows its connection to the electrodes and to the microcontroller (in this case the *Arduino Due*). The diagram in Figure 3.13 explains how the conductivity meter works.

The first block consists of an oscillator which generates a triangular wave (Figure 3.13 - A). This wave is applied to one of the electrode terminals. The other electrode terminal is coupled to the input of a current-to-voltage converter (Figure 3.13 - B) . After rectification (Figure 3.13 - C) and filtering (Figure 3.13 - D), the output voltage becomes proportional to the conductance of the electrode.

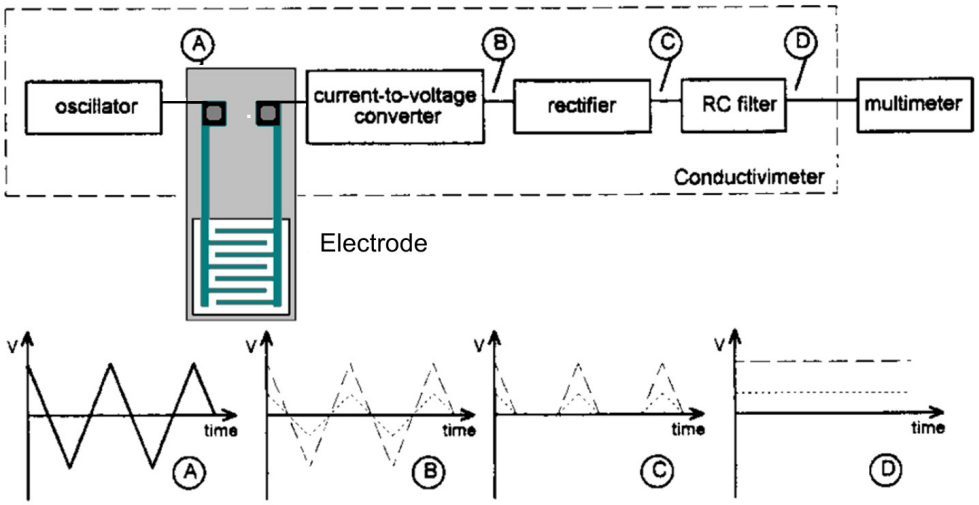

Figure 3.13: Diagram of conductivity meter. Adapted from [103]

.

3.3.2 Methodologies applied for experiments

In this subsection, the methodologies applied to prepare the sensing films used in the experiments performed with e-nose v2 are described. This includes the sensing films' composition, the spreading techniques and the sensors' array preparation.

3.3.2.1 Optical sensors for e-nose v2

For experiments with the optical e-nose v2, the optical detection chamber (which has an array of six optical sensors inside) was used. The optical sensors are called A, B, C, D, E and F (see Figure 3.14). A is the optical sensor closer to the detection chamber entrance and F is the optical sensor closer to the detection chamber exit. The sensing gels produced were based on [BMIM DCA] as IL, 5 CB as LC, water, and Bovine Skin Gelatin (BSG) as polymer.

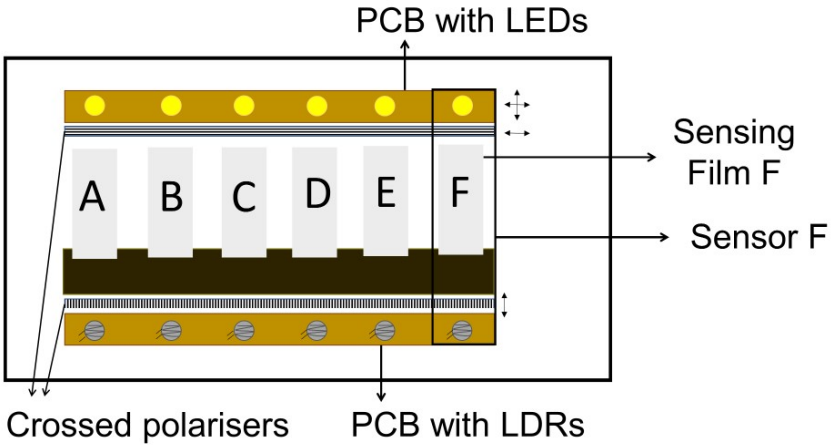

Figure 3.14: Schematic of e-nose v2's sensor array

3.3.2.2 Reproducibility studies

The gel's recipe applied to produce the sensing films for the reproducibility studies corresponds to the composition of the standard recipe described in the previous subsection 3.3.2.1 , using not only BSG but also sorbitol as polymers. This is the same recipe that was used for the optical sensor B in the proof of concept performed with e-nose v1, because this was the sensing film which allowed to distinguish the 13 different VOCs tested.

After the batch production, a drop of gel was deposited on each microscope glass slide (with dimensions 26 mm x 10 mm), and manually spread over it using a roll-on technique.

To perform reproducibility studies, six sensing films having the same composition and produced using the same parameters were applied in the sensor's array, because the goal was to test sensing films' reproducibility when exposed to the same experiment conditions, and study the sensing gels' response stability in different days.

For the first reproducibility test carried out, the sensing films were inserted in the support and kept at the same position for a week. In five different days of the week (days 1, 2, 5, 6 and 7), the sensing films were cyclically exposed to acetone for five minutes. The experiment's conditions of the first reproducibility test were the following:

- **Sample and quantity:** 5 mL of acetone
- **Sample temperature:** 36 °C
- **Room temperature:** 20 °C
- **Exposure time:** 10 s
- **Recovery time**: 50 s
- **Experiment duration**: 5 min
- **Sampling rate**: 5 Hz

To study the signals behaviour in a longer temporal window, for the second test performed, the total duration of the experiment was extended to 50 minutes. Therefore, each daily signal was acquired for 50 minutes. However, the first five minutes of each signal were not considered for data analysis, because during this period the dynamics of the system are still stabilising. Hence, each daily study includes 135 signal cycles acquired for 45 minutes. Both the exposure and recovery times were reduced comparing with the previous study. Again, an array of six sensing films was placed inside the detection chamber, and kept at the same position for 10 days. All the sensing films' were produced from the same batch, and their recipe was the same used in the previous study.

The experiment's conditions are described below.

- **Sample and quantity:** 5 mL of acetone

- **Sample temperature:** 36 °C
- **Room temperature:** 21-23 °C
- **Exposure time:** 5 s
- **Recovery time**: 15 s
- **Duration**: 50 min
- **Sampling rate**: 5 Hz

To evaluate the reproducibility of the responses given by the six optical sensors, a method for reproducibility analysis was created (see schematic in Figure 3.15).

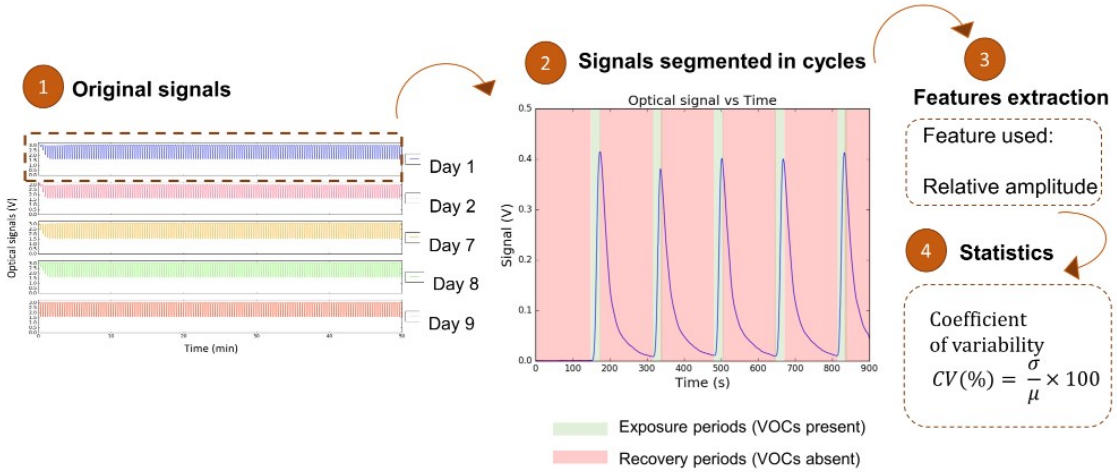

Figure 3.15: Method used for reproducibility analysis of optical signals obtained with e-nose v2.

Firstly, the original signals were segmented in cycles. Next, the relative amplitude (Ra) - equation 3.1 - of each cycle was calculated.

$$Ra = \frac{max(s) - min(s)}{min(s)} \tag{3.1}$$

And, finally, the Coefficient of Variability (CV) was determined by equation 3.2. It is given by the standard deviation of the signal cycles' relative amplitude divided by the mean of the cycles' relative amplitude, and the value is then converted in percentage.

$$CV = \frac{\sigma}{\mu} \times 100 \tag{3.2}$$

Hence, the parameter CV was accessed for each day of experiment and compared among the several days of the experiment.

3.3.2.3 Study on sensing films' spreading method

For studies about the impact of sensing film's production method on classification accuracy by the e-nose, six optical sensors were used in the sensor array (see Figure 3.16 a). A set of sensing films was produced with a black mask on the back (see figure 3.16 b). The masks have hole with five millimetres of diameter, which delimiters the area of detection. The sensing gel's base composition was the standard, having a biopolymer matrix with droplets of LC self-assembled in the presence of IL.

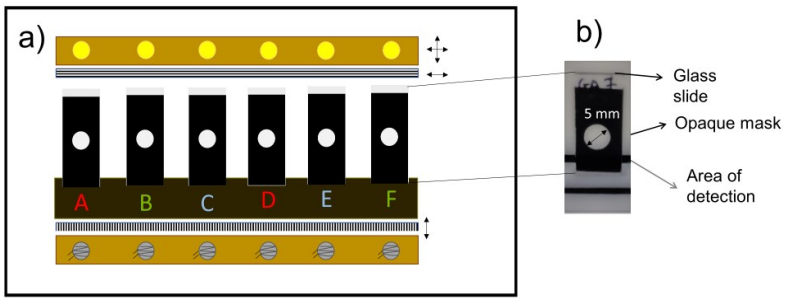

Figure 3.16: a) Schematic of sensor array. ; b) Sensing film.

In the present study, sensors D and E have sensing films produced by a standard recipe described in subsection 3.3.2.1, and sensors A and C have sensing films produced by the standard recipe, plus adding a cross-linking agent to the standard recipe, named GA. Sensing films A, B and D were spread by FC, whereas sensing films C, E and F were spread by SC. Sensors B and F are controls: sensing film B does not have LC and sensing film F does not contain IL. A brief description of each sensor is provided in Table 3.3.

Table 3.3: Sensor array of the e-nose.

Sensor	Sensing film description	Spreading technique
A	STD gel + GA	FC
B	Control (without LC)	FC
C	STD gel + GA	SC
D	STD gel	FC
E	STD gel	SC
F	Control (without IL)	SC

STD = Standard ; GA = Glutaraldehyde ; FC = Film coating ; SC = Spin coating ; LC = Liquid Crystal ; IL = Ionic Liquid.

The thickness of the sensing films produced by FC is 30 μm, and the drop quantity of gel used was 15 μL. Finally, the optical sensing films with light polarisation properties were obtained.

The experiment performed consisted in exposing the same array of sensors (Table 3.3), placed inside the detection chamber, to a set of 13 VOCs, sequentially, in the following order: acetone, isopropanol, ethanol, methanol, hexane, heptane, toluene, xylene, benzene, chloroform, dichloromethane, diethyl ether, and ethyl acetate. The experiment conditions are described in the list below:

- **VOC quantity:** 20 mL
- **Sample temperature:** 37 °C
- **Exposure time:** 5 s
- **Recovery time**: 15 s
- **Duration**: 20 min
- **Sampling rate**: 5 Hz

The data was collected by the e-nose data transduction and acquisition system.

This study intended to evaluate the influence of the selected sensing film spreading method on the classification capabilities of the e-nose. The methodology followed consisted of performing an experiment where the e-nose was exposed to 13 different pure VOCs. The sensors' array had two sensing films produced by FC, and other two produced by SC. After data collection, a set of features was extracted from the original signal curves, and the best were selected by Recursive Feature Elimination (RFE). Then, the classification performance of different machine learning algorithms was evaluated for VOCs discrimination.

Data collection and data analysis

An example of a set of 6 signals (one per sensor) acquired for exposure to acetone is shown in Figure 3.17.

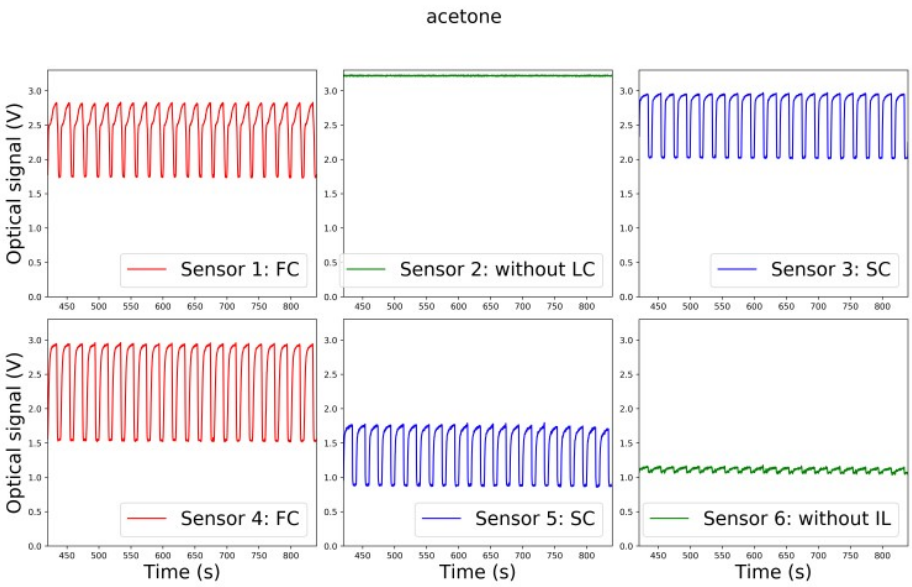

Figure 3.17: Examples of cycles from signals collected when the sensor array is cyclically exposed to acetone for 5 min, during the 20 min experiment.
FC: sensor with sensing film spread by film coating; SC: sensor with sensing film spread by spin coating; IL: Ionic Liquid; LC: Liquid Crystal.

After data collection, the features related to each individual sensor were extracted. The mathematical formula and illustration of these features are presented in Section 2.3.5, in particular in Figure 2.7. Table 3.4 describes the eight features extracted per sensor, and also explains the physico-chemical meaning of each feature. Since the sensor array is composed of six sensors, the number of original features that can be used is given by $6x8 = 48$.

Table 3.4: Features extracted from the signals.

Feature name	Description / Meaning
arelv (+ ns)	signal's relative amplitude
amax (+ ns)	x coordinate of signal's maximum
max (+ ns)	y coordinate of signal's maximum
amaxdv (+ ns)	x coordinate of maximum of signal's first derivative
maxdv (+ ns)	y coordinate of maximum of signal's first derivative
amindv (+ ns)	x coordinate of minimum of signal's first derivative
mindv (+ ns)	y coordinate of minimum of signal's first derivative
onset (+ ns)	time when signal raises above noise since exposure time started
arelv (+ ns)	Influenced by VOC's concentration and affinity for sensing gel
amax (+ ns)	Time needed for maximum detection of VOC
max (+ ns)	Level of maximum VOC detection
amaxdv (+ ns)	Time when the rate of interaction VOC-sensing film is higher
maxdv (+ ns)	Maximum rate of interaction VOC-sensing film
amindv (+ ns)	Time when the rate of unlink VOC-sensing film is higher
mindv (+ ns)	Maximum rate of unlink VOC-sensing film
onset (+ ns)	Time needed for the sensor to start the response

ns =number of sensor;

Then, auto-scaling was exploited for data pre-processing, using a standardisation technique, according to Eq. 3.3:

$$Z_j = \frac{\left(x_j - \bar{x_l}\right)}{\bar{s_l}} \tag{3.3}$$

where Z_j is the value of x_j after auto-scaling. x_j is defined as the variable before scaling. $\bar{x_l}$ is the variable mean and $\bar{s_l}$ is the standard deviation of the variable. The final value Z_j varies around the mean zero with standard deviation one.

Features selection

We were interested in comparing the optical responses given by sensors in which sensing films spread by FC were applied, versus from sensors with sensing films spread by SC.

Therefore, the original set of 48 features was divided into three sub-groups (see Figure 3.18). One group is composed by 16 features of sensing films produced by FC (sensors 1 and 4 - red signals in Figure 3.17), the other is composed by 16 features of sensing films produced by SC (sensors 3 and 5 - blue signals in Figure 3.17), and another one is related

to the control signals (this group was excluded for feature analysis because these sensors do not respond to the presence of VOCs).

For each group of features, we were interested in knowing the best number of features to select, and what features were more interesting for VOCs classification.

Initially, each sub-group has 16 features. To know the more relevant features for differentiating the VOCs, RFE was performed. The estimator 'svc' was used to assign weights to features. This estimator was trained on the initial set of features and the importance of each one was obtained. Then, the RFE method removes the weakest features and selects them by recursively considering smaller and smaller sets of features. The procedure is recursively repeated on the pruned set until a specific number of features to select is reached. For each sub-group of features, RFE was used to select the best number of features, and the top best were selected by cross-validation (2 folds).

Note that the *GaussianNB()*, *DecisionTreeClassifier*($maxdepth = 15$) and *LogisticRegression*($C = 32768$, $tol = 0.0001$, solver='liblinear', multiclass='ovr') classifiers were also tested as estimators in RFE, before applying NB, DT, and MLR respectively as classification models (see next steps of the methodology applied in this Subchapter), but an identical accuracy rate given by the classifiers was obtained comparing to when the 'svc' classifier was used in RFE.

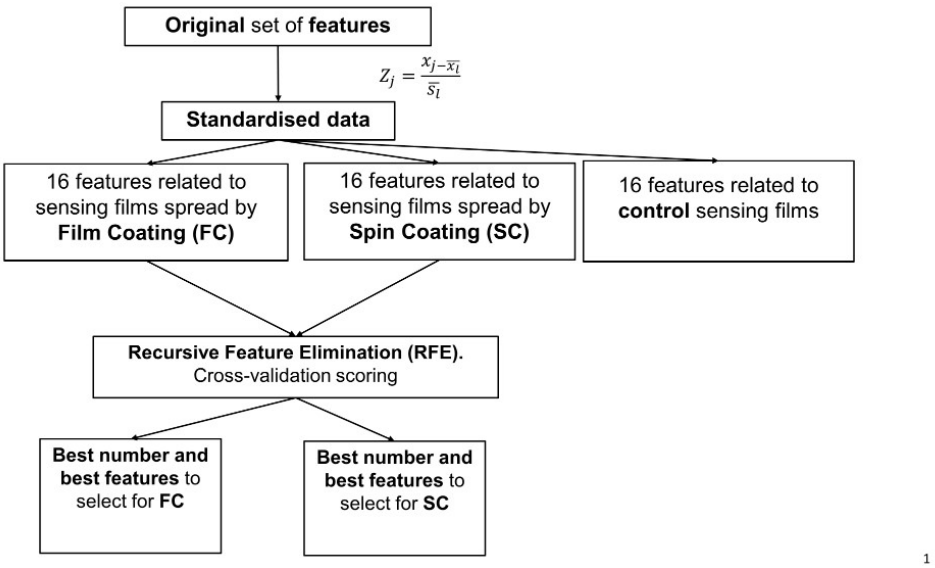

Figure 3.18: Schematic of features selection algorithm.

Classification models

We decided to test three machine learning algorithms, since other authors had reported the capability of other e-noses to perform classification of samples in a fast and reliable way using those methods [50, 51, 101]. In case we were not able to achieve good performance, we intended to apply more advanced computational techniques to enhance classification accuracy. Taking into account the results obtained in the previous studies,

our study was focused on the performance of MLR, DT and NB as data classification methods. Finally, the class discrimination capabilities of these classifiers were compared.

We studied which classification model works best for sensors with sensing films produced by SC and FC.

Figure 3.19 shows the procedure used for each classifier. Each group of best features related to FC or SC was randomly divided in training data (70 %) and test data (30 %).

Cross-validation (10-fold) was applied on the train data. This means that the train set was randomly divided in ten subsets, using nine for training the model and the remaining to validate it. Firstly, the model was built on the train set, then the training error was calculated; the validation set was tested separately and the validation error was also obtained. This procedure was repeated nine more times, each time using a different subset for validation. The average over classes of cross-validation for the different classification techniques was reported. The parameters of the models associated to a lower validation error were selected for classifiers optimisation.

The parameters of optimisation were then applied on the classifier for prediction on the Test data. Finally, for each classifier, the estimated error was calculated, and the McNemar's test was used to compare the classifiers.

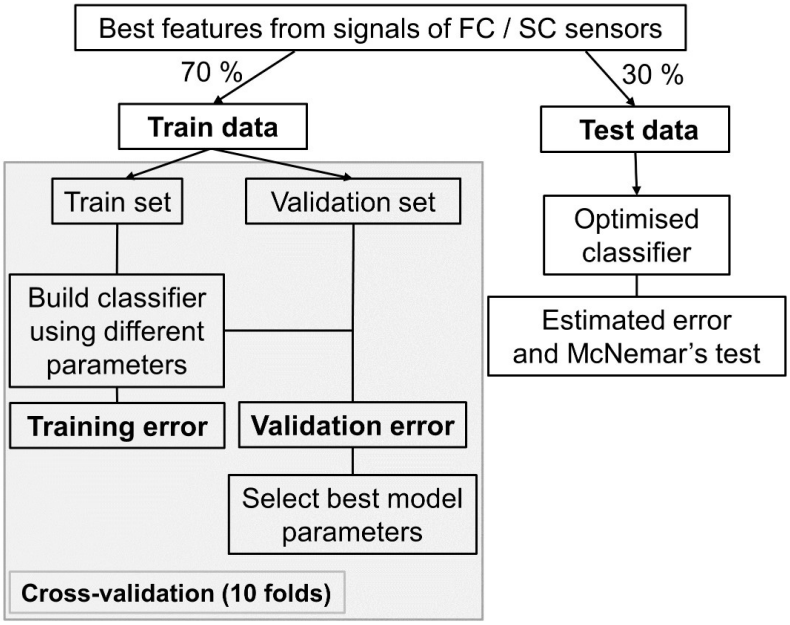

Figure 3.19: Schematic of classifiers' algorithm.

Naïve Bayes

NB methods are a set of probabilistic classification algorithms based on applying Bayes' theorem with independence assumption between every pair of features.

For this work, we assumed the likelihood of the features to be Gaussian. We applied the *GaussianNB* function from the *scikit-learn* library to implement the Gaussian NB algorithm for classification.

Decision Tree

DT is a flowchart, where each branch represents the outcome of a decision, and each terminal node holds a class label. It is a method simple to understand, interpret and visualise data.

The DT applied was the *DecisionTreeClassifier* from *scikit-learn* library, and its best maximum depth was studied.

Multinomial logistic regression

MLR generalises logistic regression to multiclass problems, i.e. with more than two possible discrete outcomes.

We used the Logistic regression classifier from the *scikit-learn* library. The one-vs-all methodology was applied. Our dataset is composed by several classes, therefore we need to decompose our training set into 13 different binary classification problems, where one of the classes/labels corresponds to 1, and the remaining labels correspond to 0. Each logistic regression classifier is defined by:

$$h_{\Theta}^{(i)}(x) = P(y = i \mid x; \Theta), i = (1, 2, ...13) \tag{3.4}$$

We train the logistic classifier for each class i to predict the probability of an input y that $y = i$. When we want to predict a new input x, we pick the class that maximises the probability of x belonging to a certain class:

$$max_i \, h_{\Theta}^{(i)}(x) \tag{3.5}$$

3.3.2.4 Study on the inclusion of a cross-linking agent in the gel's composition

The sensing films applied in the sensor array for the experiment on the impact of the spreading method technique in classification accuracy were also used for a study on the inclusion of GA as a crosslinking agent in the gel's composition. The conditions of the experiment perfomed are described in the previous subsection 3.3.2.3. In particular, details about the sensing films' composition and spreading method used can be found in Table 3.3.

Before being placed in the array of sensors, the sensing films were observed in the microscope, and an image of each one of them was taken. Figure 3.20 shows an example of an image of a sensing film before exposure to VOCs, taken from a *Zeiss* high resolution microscope where it was placed between two crossed polarisers.

On *FIJI - Image J* we imported the images of the sensing films before exposure to the VOC, and converted them to binary, following these steps:

1. Convert image to 8-bit grayscale.

2. Adjust the image threshold and convert it to binary.

Again, on *FIJI - Image J*, the particles in the images were detected and quantified using the following steps:

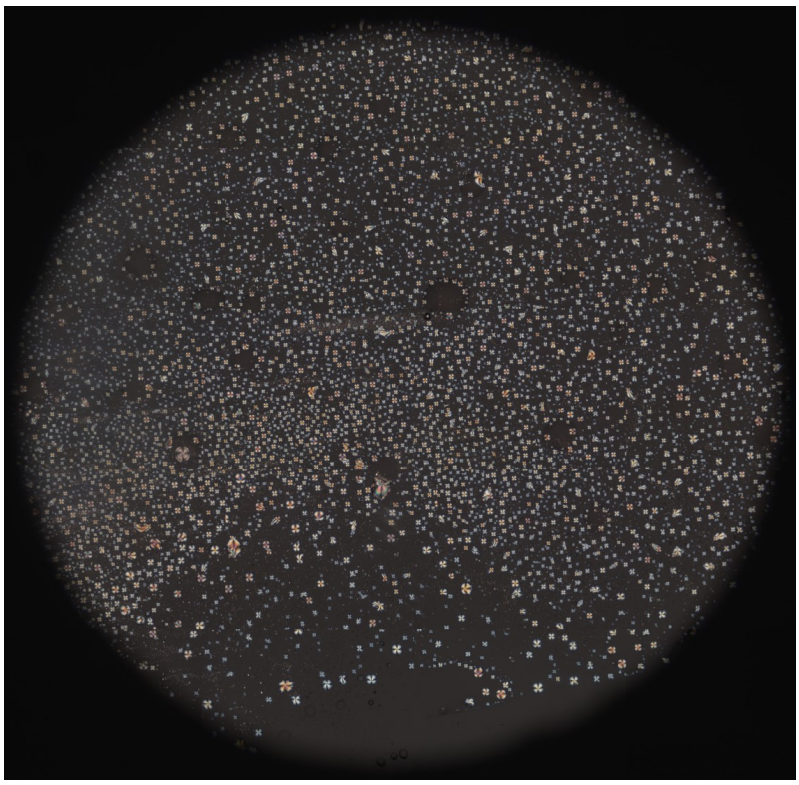

Figure 3.20: Microscopic image of sensing film before exposure to a VOC.

1. Dilate the objects (droplets) if necessary.
2. Click on "Analyse particles".
3. Save measurements of particles' parameters in a file.

The parameters that describe the sensing films were manually added to the name of the file that contains information about the particles in the image. The sensing films' parameters added to the file name were the following:

- VOC: volatile to which the sensing film was exposed.
- Film type: control-gel or GA-gel.
- Film name: film identifier (e.g. GA1, CONT2).
- Time: before or after exposure to the VOC.
- Threshold and dilate: values applied to convert the original image to binary on *Image J*.

The file content includes the number of particles identified in the analysed image, the area of each particle (number of pixels that constitute each particle), and the ferret's diameter of each particle, among other features that characterise each particle.

Then, a python script was created. The code implemented in this script extracts the useful information and performs statistics using the files with raw data about the particles' parameters, and generates a spreadsheet with the data of interest organised. The script works according to the flowchart presented in Figure 3.21.

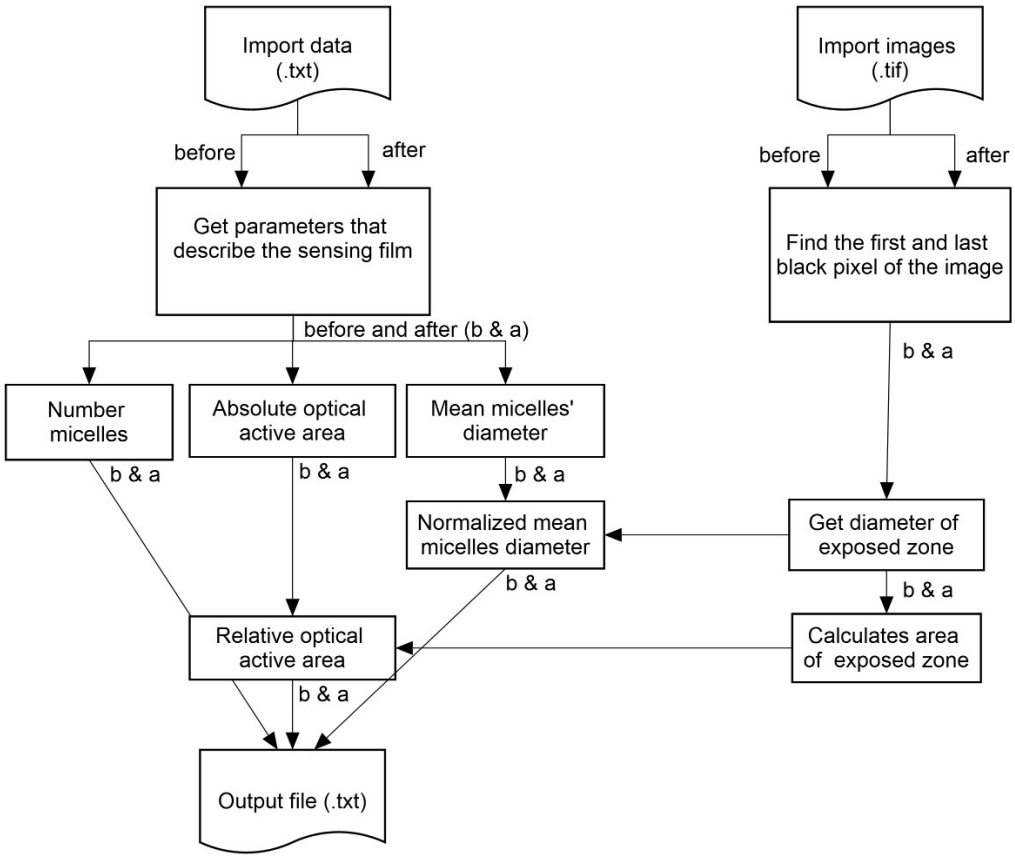

Figure 3.21: Flowchart of script for extracting and performing statistics regarding droplet's parameters using information from the files obtained on *Image J*.

Table 3.5 represents the output files' structure showing an example of an output obtained for a sensing film with GA exposed to acetone. The file content can be then plotted in graphics.

Table 3.5: Output file obtained for a sensing film with GA exposed to acetone

Time	Film name	Droplets' number	Droplets' optically active area (0-1)	Droplets' mean diameter (μm)
after	g11	12345	0.070	13.976
before	g11	9964	0.096	19.845
after	g2	14247	0.219	23.262
before	g2	15923	0.085	15.685
after	g6	15144	0.183	18.107
before	g6	10559	0.142	20.842

ga = glutaraldehyde;

The results of this experiment and their respective discussion and conclusions are

provided in Section 3.4.3.

3.3.2.5 Electrical sensors for e-nose v2

For the first study using the electrical detection chamber, an array of four interdigitated electrodes with 100 μm spacing and four interdigitated electrodes with 200 μm spacing was prepared. Four electrodes with gels having different compositions (A, B, C and D) were used and the recipe of each type is described in Table 3.6. The compositions of the gels applied in the electrodes were similar to the ones used in the proof of concept of the optical e-nose v1. After the batch production, a drop of gel was deposited on each electrode, and manually spread over it using a roll-on technique.

Table 3.6: Composition of gels applied in electrodes

Gel type	IL	LC	Polymer	Water
A	[BMIM][DCA]	5 CB	BSG + Dextran	MilliQ water
B	[BMIM][DCA]	5 CB	BSG + Sorbitol	MilliQ water
C	[EMIM][DCA]	5 CB	BSG + Dextran	MilliQ water
D	[BMIM][Cl]	5 CB	BSG + Dextran	MilliQ water

IL: Ionic Liquid; LC: Liquid Crystal; BSG: Bovine Skin Gelatin; 5CB: 4-Cyano-4'-pentylbiphenyl; [BMIM][DCA]: 1-Butyl-3-methylimidazolium dicyanamide; [EMIM][DCA]: 1-Ethyl-3-methylimidazolium dicyanamide; [BMIM][Cl]: 1-Butyl-3-methylimidazolium chloride.

In this context, the electrodes with sensing gels are called electrical sensors. The produced electrical sensors were then tested one by one in the detection chamber. The experiment conditions were the following:

- **VOC quantity:** 5 mL
- **Sample temperature:** 37 °C
- **Exposure time:** 10 s
- **Recovery time**: 50 s
- **Duration**: 4 min
- **Sampling rate**: 10 Hz
- **Room temperature**: 20 °C
- **Frequency of triangular wave**: 1.68 kHz
- R_5: 200 $k\Omega$

3.3.2.6 Preparation of sensing films for studies on electrodes' corrosion

The interdigitated electrodes used are composed of a substrate (fiberglass), a copper layer and a finishing surface. The finishing surface is applied on the top to protect the copper layers from corrosion. Our electrodes have one layer of nickel (with 3 μm) and one layer of gold (with 0.05 μm) on top as finishing surfaces.

The electrical sensors are interdigitated electrodes with a layer of sensing gel spread on the top. Corrosion was observed on the electrodes at different levels depending on the composition of the applied sensing gel. It is important to guarantee that the finishing surface of the electrodes is resistant to the sensing gels applied on the top of them. To test other types of finishing surfaces, a test against corrosion was performed by applying four different sensing gels compositions on PCBs having different finishing surfaces. The finishing surfaces tested were: immersion tin, Hot Air Solder Leveling (HASL), HASL lead free, and Electroless Nickel Immersion Gold (ENIG) (0.05 – 0.2 μm of gold over 3 – 6 μm of nickel). The compositions of the different gel categories are described in Table 3.7. The different categories of gels having distinct ionic liquids and polymers in their composition were spread on the PCBs used for the tests. They were observed each week, during four weeks, to determine the point in time when the process of corrosion caused by the sensing gel starts.

Table 3.7: Composition of gels used for corrosion tests

Gel category	IL	LC	Polymer	Water
A	[BMIM][DCA]	5 CB	BSG + Sorbitol	MilliQ water
B	[BMIM][DCA]	5 CB	BSG + Dextran	MilliQ water
C	[bmim][Fe(III)Cl_4]	5 CB	BSG + Dextran	MilliQ water
D	[BMIM][Cl]	5 CB	BSG + Dextran	MilliQ water

IL: Ionic Liquid; LC: Liquid Crystal; [BMIM][DCA]: 1-Butyl-3-methylimidazolium dicyanamide; [bmim][Fe(III)Cl_4]: 1-butyl-3-methylimidazolium tetrachloroferrate; [BMIM][Cl]: 1-Butyl-3-methylimidazolium chloride; 5CB: 4-Cyano-4'-pentylbiphenyl; BSG: Bovine Skin Gelatin.

3.4 Results and Discussion

3.4.1 Reproducibility tests with e-nose v2

The first experiment using the e-nose v2 intended to study the reproducibility of the results obtained. The sensing films were inserted in the support and kept at the same position for five days.

Figure 3.22 shows an example of the signal obtained for the optical sensor C.

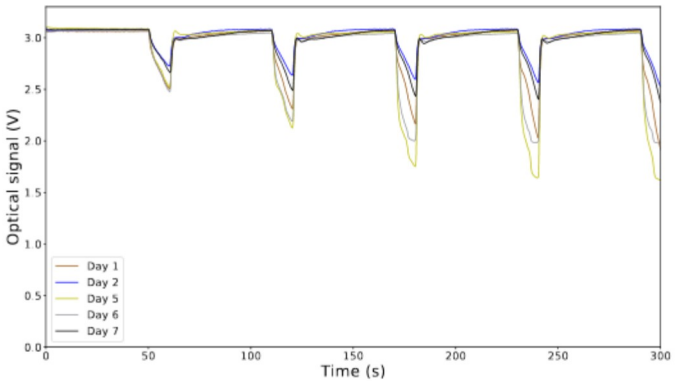

Figure 3.22: Optical signals given by sensor C placed at the same position in e-nose v2 when cyclically exposed to acetone along a week for experiment of 5 min.

The signals obtained varied in amplitude during the cycles of the five minutes experiment. For studying the signals behaviour in a longer temporal window, the duration of the experiments was extended to 50 minutes. The exposure and the recovery times became shorter. The array of six sensing films was placed inside the detection chamber, and kept at the same position for a 10 days experiment.

As example, Figures 3.23 and 3.24 are provided to show the signals given by sensing films used in the optical sensors C and E, in five of the 10 days of experiment.

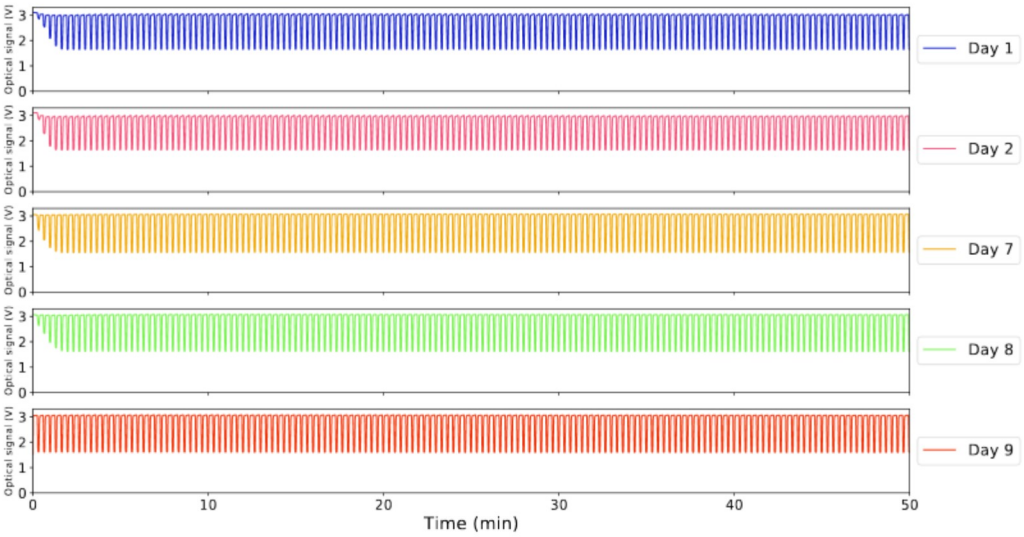

Figure 3.23: Optical signals given by sensor C placed in e-nose v2 when cyclically exposed to acetone along some of the days of experiment.

Observing the results for the optical sensor C - Figure 3.25 - we noticed that only after 2 minutes the signal starts stabilising. The x-axis ranges from 0 to 50 min. After

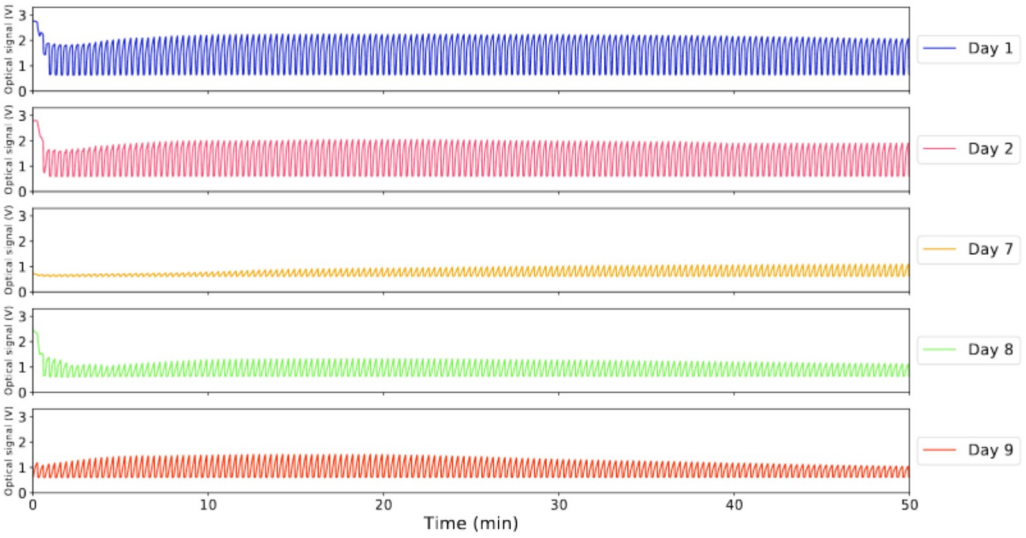

Figure 3.24: Optical signals given by sensor E placed in e-nose v2 when cyclically exposed to acetone along some of the days of experiment.

the first 2 min of each signal, the cycles are apparently similar regarding wave shape and amplitude of response along the days of experiment.

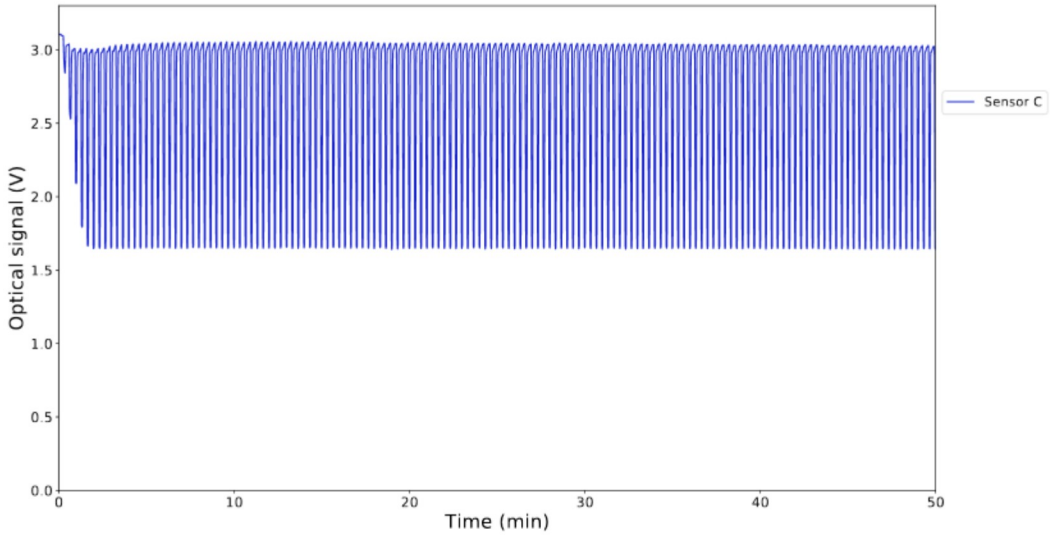

Figure 3.25: Optical signals given by sensor C placed in e-nose v2 when cyclically exposed to acetone at day 1 of experiment.

However, for the optical sensor E, the signals' amplitude changed along the days of experiment - Figure 3.24. The optical sensor E exhibits a response with similar amplitude from day 1 until day 2. However, in the next day, the amplitude of response significantly

decreased. In days 7-9, the sensing film became less responsive.

To evaluate the reproducibility of the responses given by the six optical sensors, a method for reproducibility analysis was created (see Section 3.3.2.2). The graph of Figure 3.26 represents the relative variation of the cycles' relative amplitude along a 45 min experiment, in each one of the 10 days experiment.

The original experiment ran for 50 min. Then, for signal analysis, the first five minutes of each signal were not considered for the study, because the sensors are still stabilising during this period of time. Therefore, this study on the daily variation of the cycles' relative amplitude includes 135 cycles acquired for 45 minutes each day.

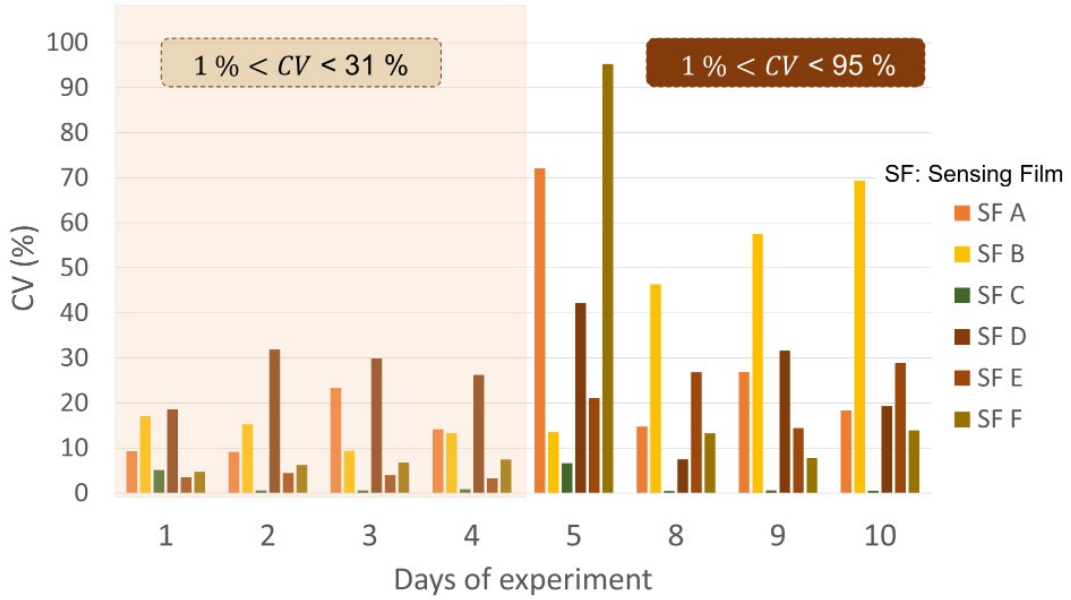

Figure 3.26: Daily variation of the cycles' relative amplitude for 45 min experiments.

In the first four days of experiment, the CV was lower than 32 % for all the sensing films, whereas in the following days the relative variation along the experiment significantly increased.

These results suggest that the sensing films give more stable responses in the first four days of experiment, because the signal's relative amplitude varies less during the experiments performed.

Therefore, these results arise questions, about the factors that affect the stability of the responses given by the optical films. Some possible reasons were identified: the variation of the ambient room conditions (humidity and temperature) along the days; the sensing gels' spreading method was not adequate to spread the gel in a way that the droplets are stable along the days; and the stability of the sensing films might be compromised after a certain number of cycles of exposure to the VOC.

We decided to test automatic spreading techniques (see study performed on the next Subsection 3.4.2). Moreover, we explored the effect of cross-linking on the sensing films

for droplets' stability and we studied the effect of a set of VOCs on the sensing film's morphology, when these are cyclically exposed to them for four hours (see Subsection 3.4.3).

Therefore, the next steps could be described as an attempt to overcome the signal variations inherent to some sensing films, and consequently achieve reproducibility.

3.4.2 Testing automatic sensing films' spreading techniques

Since our goal was to compare the performance of sensing films' spread by FC with those spread by SC, two groups were created. For each group, 16 features were extracted and RFE was applied in order to get the best number of features for classifications. The two groups were studied separately, but applying the same methodology to both, and their classification accuracy was compared.

For classification purposes, the best number of features for VOCs classification using sensing films produced by FC is six, according to RFE - see Figure 3.27a. As can be seen in the plot, the lower error rate of the classifier with 2-fold cross-validation occurs for six features. Figure 3.27b shows that the best number of features for VOCs classification using sensing films produced by SC is 13. However, the error decreases less than 5 % using 13 features, compared to the use of six features. Since a lower number of features improves the computation performance, we decided to use also 6 features for this group of sensors. Therefore, in the next steps, only the best six features per group were selected.

The ranking obtained by RFE indicated that the six features with a higher score were: arelv1, mv1, maxdv1, arelv4, mv4 and maxdv4 for FC; and arelv3, mv3, maxdv3, mindv3, arelv5, and mv5 for SC. Therefore, these features were the only used for training and testing in the classification models performed.

The next step was to optimise the selected classifiers. We studied the best parameter C for logistic regression, and the best maximum depth of DT, using features extracted from the signals given by sensors where sensing films produced by FC were used, and by sensors where sensing films produced by SC were used. Then, we assessed the accuracy of the three classification models: MLR, DT and NB.

3.4.2.1 Classification using sensors with sensing films produced by film coating

The value of parameter C for Logistic Regression was optimised - Figure 3.28a , as well as the best value for depth in DT - Figure 3.28b.

Using sensing films produced by FC in the sensors, the best value of parameter C for Logistic Regression is 65536 - Figure 3.28a. And the best depth for DT is 15 - Figure 3.28b. Hence, these values were selected to be used in the classifiers' models.

The estimated errors calculated on the Test set were 2.75 % for MLR, 3.15 % for DT, and 3.15 % for NB.

We also compared the difference in accuracy between the classifiers using the McNemar's test. This test is used to comapred two classifiers. The formule uses e_{01} and e_{10} to

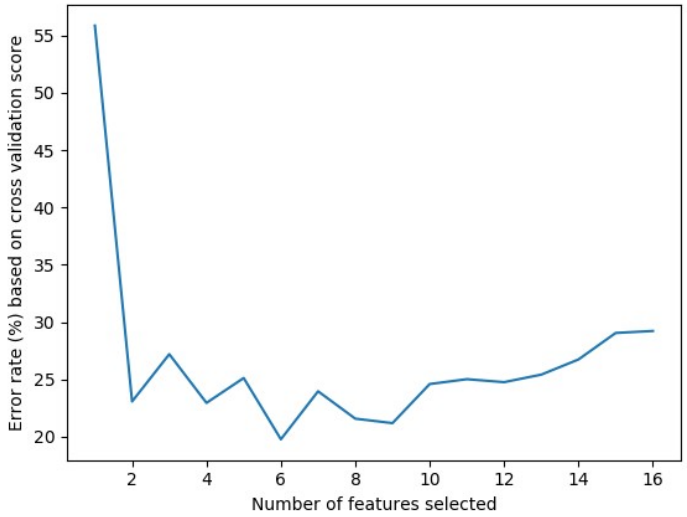

(a) Features extracted from signals obtained from sensors with sensing films produced by FC.

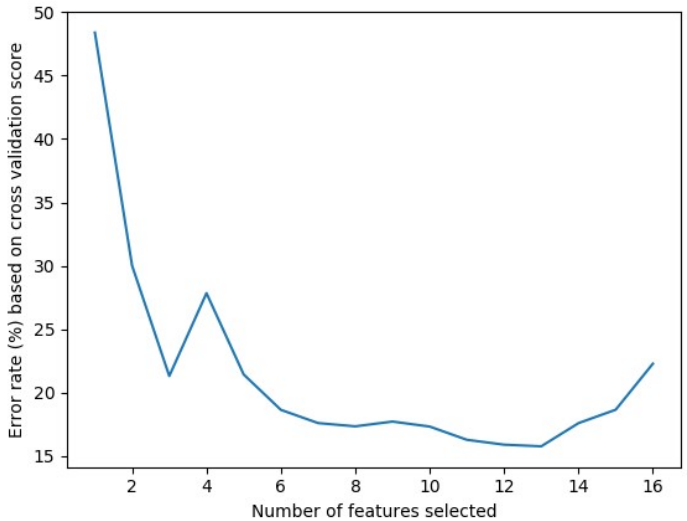

(b) Features extracted from signals obtained from sensors with sensing films produced by SC.

Figure 3.27: Correlation between cross-validation scores of RFE *vs* number of features extracted from signals.

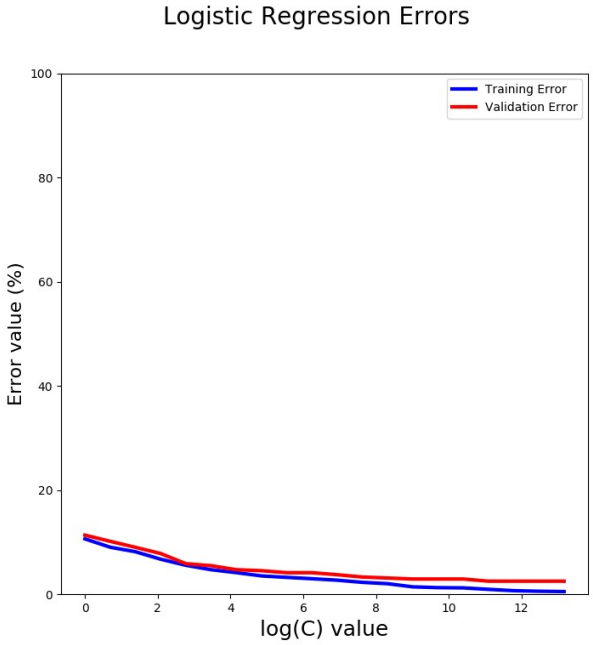

(a) C parameter for Logistic Regression *vs* Accuracy errors.

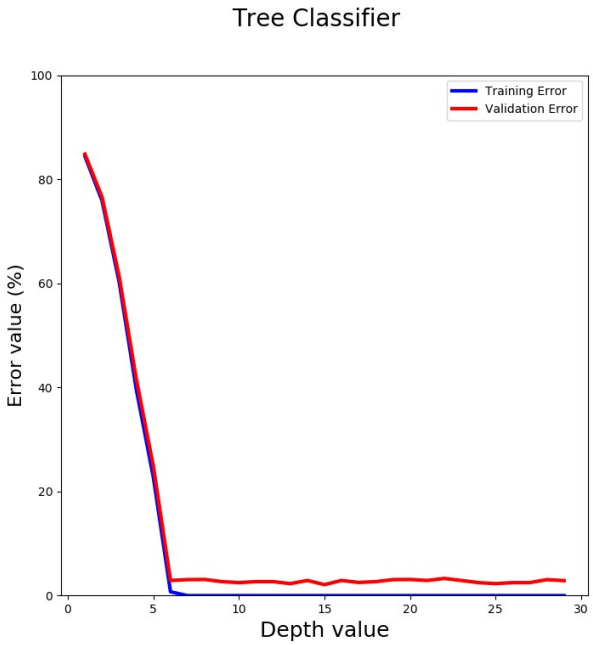

(b) Depth parameter for Decision Tree *vs* Accuracy errors.

Figure 3.28: Optimisation of algorithms' parameters using sensing films produced by FC.

count samples wrong in one and correct in the other. According to this test, the classifiers are significantly different (with 95 % confidence) if the value of equation 3.6 is ≥ 3.84.

$$\frac{(|e_{01} + e_{10}| - 1)^2}{e_{01} + e_{10}} \approx {X_1}^2 \tag{3.6}$$

The results of the McNemar's test comparing two classifiers applied to data from experiments where sensing films spread by FC were used are given in Table 3.8

Table 3.8: Results of McNemar's test comparing two classifiers applied to data from experiments where sensing films spread by FC were used.

Classifiers compared	Value of McNemar's test
MLR vs DT	0.0
MLR vs NB	0.0
DT vs NB	0.1

MLR = Multinomial Logistic Regression; DT = Decision Tree; NB = Naïve Bayes

The results presented in Table 3.8 indicate that there is no significant difference between the accuracy of the three classifiers used.

3.4.2.2 Classification using sensors with sensing films produced by spin coating

Using sensing films produced by SC in the sensors, the best value of parameter C for Logistic Regression is 32768 - Figure 3.29a. And the best depth for DT is eight - Figure 3.29b. Hence, these values were selected to be used in the classifiers' models.

The estimated errors calculated on the Test set were 2.76 % for MLR, 3.15 % for DT, and 3.94 % for NB.

The McNemar's test was performed to compare the classifiers between each other, according to equation 3.6 . The results for the classifications where sensing films spread by SC were used in the sensor array are given in Table 3.9.

Table 3.9: Results of McNemar's test comparing two classifiers applied to data from experiments where sensing films spread by SC were used.

Classifiers compared	Value of McNemar's test
MLR vs DT	0.00
MLR vs NB	0.36
DT vs NB	0.08

MLR = Multinomial Logistic Regression; DT = Decision Tree; NB = Naïve Bayes

The results above indicate that there is no significant difference among the accuracy results of Multinomial Logistic Regression, DT and NB for classification using data from experiments where sensing films spread by SC were used .

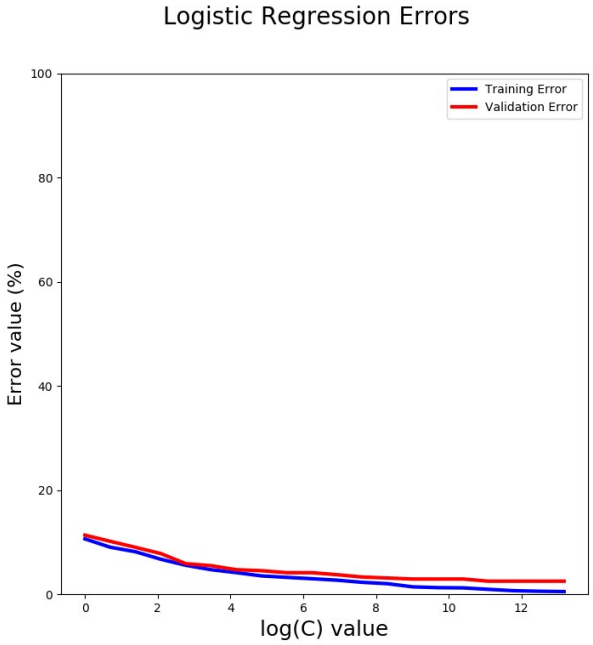

(a) C parameter for Logistic Regression *vs* Accuracy errors.

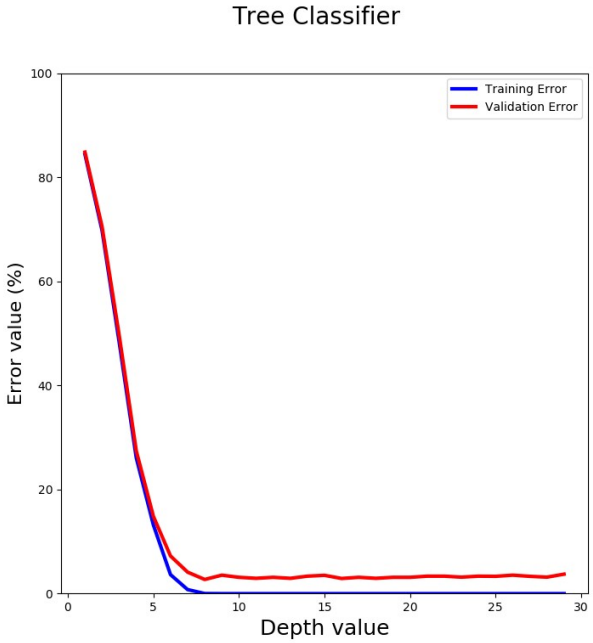

(b) Depth parameter for Decision Tree *vs* Accuracy errors.

Figure 3.29: Optimisation of algorithms' parameters using sensing films produced by SC.

3.4.3 Study on the incorporation of a cross-linking agent on the sensing film's optical stability

The following figures represent the changes that occur in the droplets of the sensing films due to cyclical exposure to a certain VOC during four hours. The variation in the exposure zone of the sensing film's was quantified regarding the number of droplets (Figure 3.30), the optically active area (Figure 3.31), and the droplet's diameter (Figure 3.32). In x-axis of the plots, the VOCs are disposed from more apolar to more polar.

Figure 3.30 shows that overall the number of droplets changed significantly among the different VOCs and sensing films' types. This variation ranged from - 75 % to + 60 %. For sensing films exposed to hexane, the number of droplets tended to decrease. For diethylether and ethyl acetate the tendency was different for standard sensing films and sensing films with GA. Having GA the number of droplets tends to decrease, whereas it tends to increase for standard sensing films. For acetone and isopropanol the number of droplets increased for both sensing films' types. And for ethanol, the number of droplets increased for sensing films with GA and decreased for the standard sensing films.

The sensing films' optically active area presented a variation inferior to 10 % for exposure to each one of the VOCs, except for standard sensing films exposed to diethylether (see Figure 3.31). Taking into account the variability bars, there are no significant differences in the optically active area variation comparing standard sensing films' and sensing films' with GA.

Regarding the droplets' diameter, as can be infered from Figure 3.32 the mean variation was in the range -9 μm to + 7.5 μm. In general, taking into acount the variability bars, the presence of GA did not interfere with the rate of increase/decrease in droplets' size.

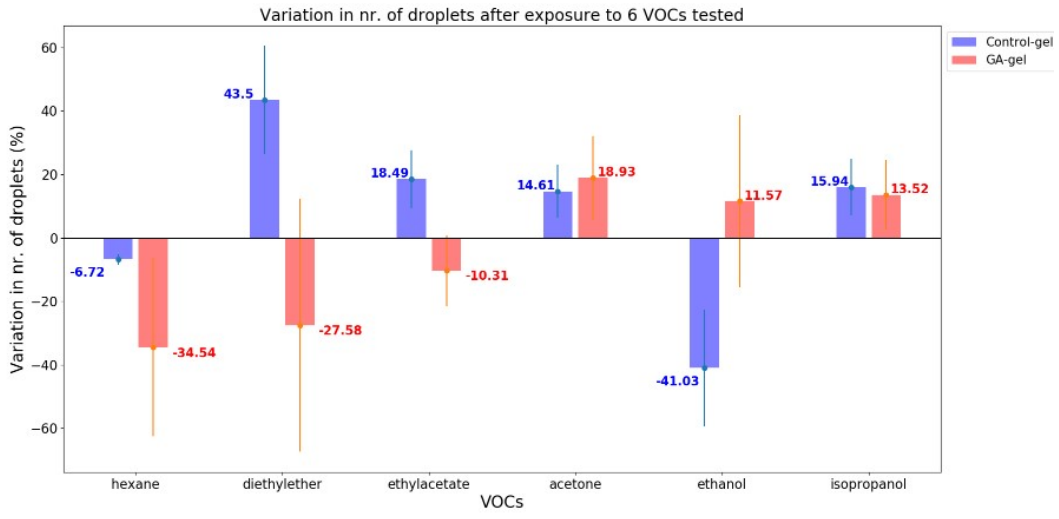

Figure 3.30: Variation in the number of droplets of sensing films comparing before and after cyclical exposure to a certain VOC for four hours.

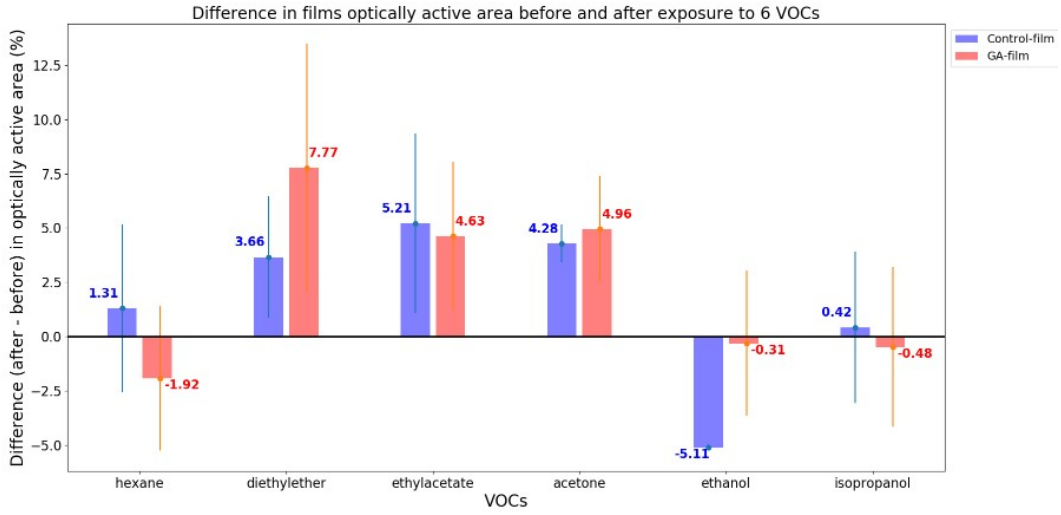

Figure 3.31: Variation in optically active are of sensing films comparing before and after cyclical exposure to a certain VOC for four hours.

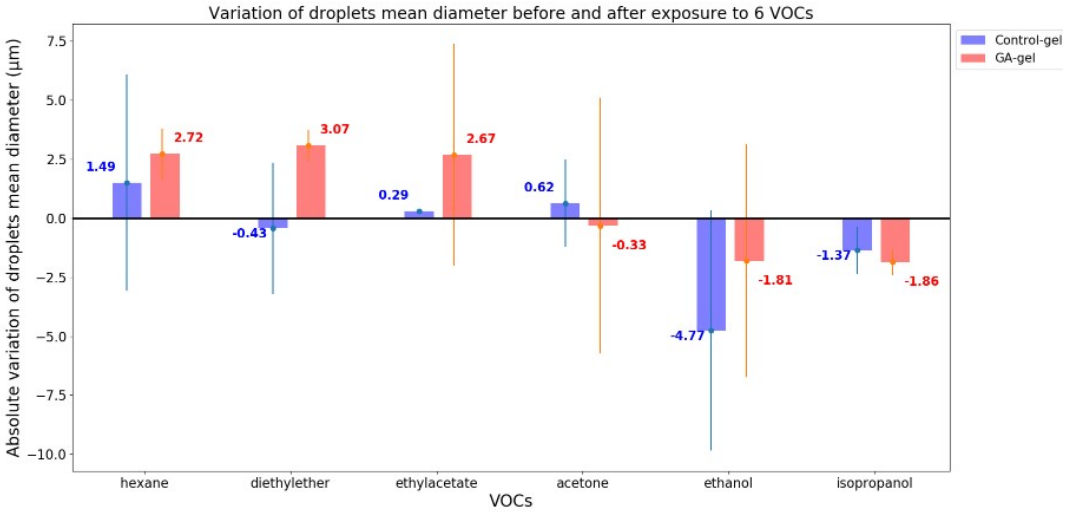

Figure 3.32: Variation in droplet's mean diameter of sensing films comparing before and after cyclical exposure to a certain VOC for four hours.

3.4.4 First electrical responses

Two different types of interdigitated electrodes (with 100 μm and 200 μm spacing) were tested using four different gel recipes (see Table 3.6 in Section 3.3.2.5). From the eight combinations tested, the only one that gave an electrical response when exposed to VOCs was the gel composition B on interdigitated electrodes with 200 μm spacing.

Examples of signals obtained for acetone, ethanol, ethyl acetate and diethyl ether using the electrode with sensing gels of recipe B are shown in Figure 3.33. In this plot, the baseline of the signals was set to zero to enable an easier comparison among the different VOC's signals.

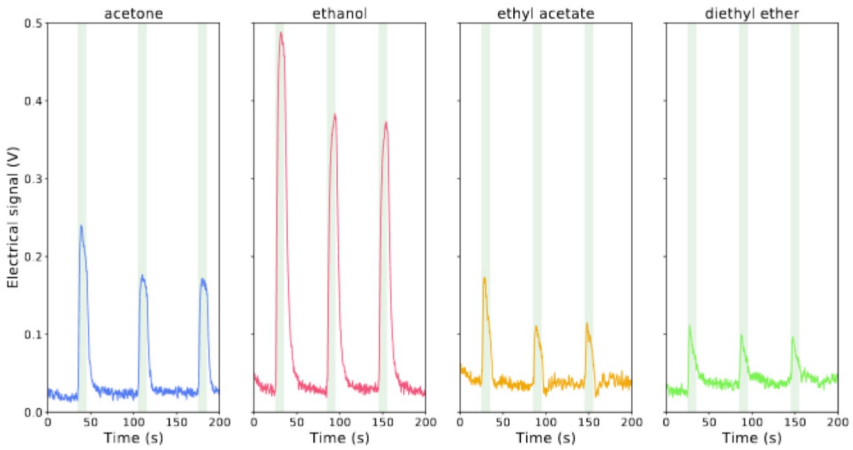

Figure 3.33: Electrical signals obtained using e-nose v2.

.

When the electrical sensors are exposed to a VOC (exposure periods), their conductance alters.

Then, to optimise the conductivity meter parameters, namely the triangular wave frequency, a study was conducted to test the influence of the triangular wave frequency on the relative amplitude of the output signal. The results are shown in Table 3.10.

Table 3.10: Study the effect of the triangular wave frequency on the relative amplitude of the output DC signal.

Frequency of triangular wave (Hz)	**Capacitor C_1 (nF)**	**Relative amplitude of DC output signal (average of 5 cycles)**
215	880	0.11
780	220	0.10
1680	100	0.05
2330	68	0.07
3340	47	0.05
4910	20	0.04
10290	10	0.02

The conclusion from this study was that generating a triangular wave (f = 215 Hz), using C_1 = 880 nF, we get a DC output signal with higher relative amplitude (from the range tested: 215 Hz – 10.29 kHz).

3.4.5 Study on the corrosion of the electrodes' finishing surface

The PCBs with different finishing surfaces (immersion tin, HASL, HASL lead free and ENIG (0.05 - 0.2 μm of gold over 3-6 μm of nickel) with gels of different compositions spread on them (see Table 3.7 in Section 3.3.2.6) were observed every week until the first signs of corrosion started being seen by naked eye. Corrosion can be identified due to a change in the electrodes' finishing surface colour (to green, brown or yellow) depending on the electrodes' finishing surface composition. The results are shown in Figure 3.34.

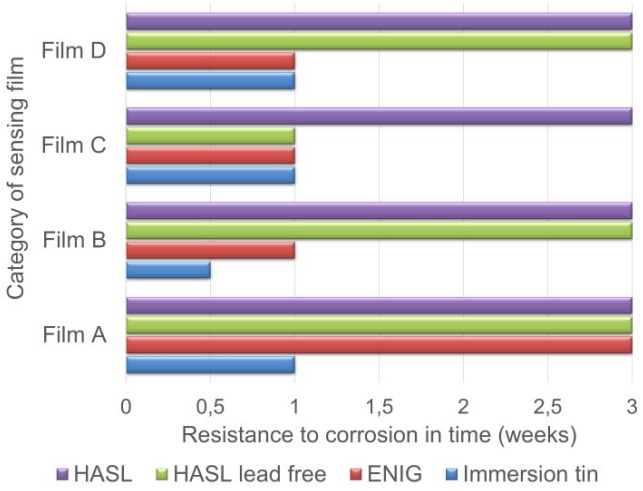

Figure 3.34: Study on the resistance of different finishing surfaces to corrosion caused by sensing films.

From this study, it was concluded that the finishing surface more resistant to corrosion caused by the four categories of sensing films was the HASL (and also HASL lead free except for the gel C). The HASL presented the first signs of corrosion, observed by naked eye, three weeks after the sensing gels had been spread on the PCBs. HASL lead free also resisted three weeks to corrosion when in contact with sensing gels A, B and D; but it only resisted one week to gel composition C. ENIG resisted three weeks to the corrosion caused by film A, but only one week for the other films' categories. Immersion tin can only resist one week to corrosion, but this period is even shorter for the recipe of film B for which the corrosion started half a week later. Overall, none of the finishing surfaces tested resisted more than 3 weeks to the effects of corrosion caused by the sensing gel's components.

3.5 Conclusions

E-nose v2 became more stable and faster, since the acquisition rate doubled compared to e-nose v1, mainly due to the new detection chamber implemented. This chamber was miniaturised, which allowed to reduce the overall device volume and also decrease the times (exposure and recovery times) required to acquire the exposure signals. In this

version, two optical sensors were added to the optical sensor array as well. These factors allow the acquisition of more data in less time.

The electrical detection chamber was designed and assembled in order to explore another sensing films' property that changes while interacting with VOCs: conductance. The electrical detection chamber enables to detect those variations, which are converted into signals by the data acquisition system. A humidity and temperature sensor was also added to the system to collect information about the environment/room conditions, which might influence sensing films' stability.

The reproducibility tests performed with e-nose v2 indicate that in the first minutes of experiments the optical sensors are still stabilising, and therefore the first cycles should not be considered for analysis. When analysing the signals' stability along 10 days the results showed that, for the first four days of experiment, the responses given by the sensing films are more stable, based on the evaluation of the signals' relative amplitude variation. After four days, the CV of the signals' relative amplitude increased significantly.

Some factors that might possibly interfere with sensing films' stability could be: the sensing films' spreading method (in this case, the manual roll-on technique) did not allow to make homogeneous and stable gels along the days; the gel's composition may not be stable along the days, due to its own internal properties; the droplets' structure in the sensing films might be affected by sequential exposure to the VOCs; and also, the variation of the environmental conditions (humidity, temperature) could affect the sensing films' response.

To overcome the issue of manually spreading the gels over the sensing films, we decided to test two automatic spreading techniques (SC and FC) to spread the gels on the microscope glass slides. Both sensing film production types demonstrated capability to distinguish the different VOCs in a quick, simple and accurate way, using NB, MLR and DT as machine learning algorithms. In this study, the RFE results indicate that the most effective features for classification are: relative amplitude, maximum of the signal, and maximum and minimum of signal's first derivative. For distinction of 13 different VOCs, the three simple classification methods studied were effective, with estimated error inferior to 4 % for all of them. Comparing the results obtained for sensors with sensing films produced by FC *vs* sensing films produced by SC, the values did not vary significantly for any of the classifiers. Therefore, we conclude that both spreading techniques are very good for sensing films production.

We also explored the effect of cross-linking on the sensing films for droplets' stability, when these are cyclically exposed to VOCs for four hours. The results showed that there was no significant differences between sensing films produced using the standard recipe and those that were produced with GA. The variations regarding sensing films' optically active area and droplets' number and diameter do not seem to be reduced due to the the inclusion of GA in the gels' composition.

As a general conclusion, for the current sensing gels production method used, the spreading techniques applied - FC and SC - can be used to create sensing films capable of

distinguishing pure VOCs. Also, the machine learning methods applied (NB, MLR and DT) were effective for VOCs prediction. As a future perspective, new methodologies for droplets' stability should be explored (e.g. other cross-linking agents or other production methods based on microfluidics).

For the electrical sensing films, the gel composition based on [BMIM][DCA], 5 CB and with bovin skin gelatin and sorbitol as polymers applied on interdigitated electrodes with 200 μm spacing enabled the acquisition of electrical responses, when exposed to four different VOCs (acetone, ethanol, ethyl acetate and diethyl ether).

Also, the conductivity meter components were optimised by studying the influence of the triangular wave frequency on the relative amplitude of the output signal. The best relative amplitude found was 0.11 V when a triangular wave with 215 Hz was applied in the conductivity meter (using a capacitor with $C = 880nF$).

Since we noticed corrosion appearing in the electrodes, we carried on a study to test different finishing surfaces (HASL, HASL lead free, ENIG and Immersion tin), exposing them to gels with different compositions. None of them resisted more than three weeks to corrosion. The more resistant was HASL, because it was the one that resisted more time to corrosion cause by the four compositions tested. HASL lead free could also resist three weeks to three of the four compositions tested. ENIG also resisted three weeks to one type of gel. Immersion tin could only resist one week at maximum to corrosion caused by the gels. In the future, other finishing surfaces, such as silver and platinum should be further tested as options. The thickness of the layer may also affect the results, therefore a more complete study using other materials and diverse thickness for the layers should be performed in the future.

Chapter 4

Making the device scalable and user-friendly: E-nose v3

In this chapter, firstly a brief introduction to summarise the main features of the previous e-noses assembled is provided. Then, the materials and methods applied to design and assemble a more stable and user-friendly device, e-nose v3, are described.

The new data acquisition system was developed in collaboration with the LIBPhys group of the Physics department in FCT-NOVA. An interface and real-time signals visualisation tool was implemented, and we established a network layer among the several elements (e-noses, users' computers, and database). To get there, we had to create new control algorithms for the data acquisition and control, and a database.

Finally, an overview of the work developed in this project is given, including conclusions from the results obtained and future perspectives.

4.1 Introduction

The first e-nose prototype, e-nose v0, was not easy-to-use, due to a non-practical mechanism used to open and close the detection chamber. Moreover, flow losses were identified at the detection chamber and at pipelines of the delivery system. Regarding the transduction system, the signal-to-noise ratio was too low. Moreover, it was expensive, due to the use of a data acquisition and control system composed by a computer and a *National Instruments board myDAQ*.

Parts of the work presented in this chapter were published in Pádua *et al.* (2019) in *Proceedings of the 11th International Joint Conference on Biomedical Engineering Systems and Technologies - Vol. 1.* [104] , and presented in *BIODEVICES 2019* conference, in the oral presentation entitled *An Optimized E-nose for Efficient Volatile Sensing and Discrimination*, and in Pádua *et al.* (2018) in *Proceedings of the 11th International Joint Conference on Biomedical Engineering Systems and Technologies - Vol. 1.* [105] , and presented at *BIODEVICES 2018* conference in a poster entitled *Scalable and Easy-to-use System Architecture for Electronic Noses*.

Therefore, this version was improved to be more robust, easy-to-handle and economic, resulting in e-nose v1.

In the next e-nose version, e-nose v2, the detection chamber became more stable and less bulky. Having less volume, the exposure and recovery times could be reduced and the analysis time became faster. This version became significantly cheaper, due to the use of a data acquisition system composed by an *Arduino Uno* microcontroller and a *Raspberry Pi 2 Model B*. The mechanisms for data acquisition became approximately 2.5 times faster compared to the previous version.

Still, this version presented some negative aspects: it kept having flow losses, the detection chamber was too big and it was difficult to change sensing films between experiments. As so, e-nose v2 was designed to be easier-to-handle, stable and miniaturised.

The assembled e-nose v2 was mainly improved concerning the detection chamber. Firstly, it is important to highlight that the device is hybrid since two different alternative detection chambers (optical and electrical) can be used. An electrical detection chamber and its respective sensors were implemented.

The optical detection chamber of e-nose v2 is easier-to-handle because it has a vertical configuration (instead of the horizontal structure used in e-nose v1), thus the sensing films can be easily placed and removed. In addition, the chamber is more stable because the sensing films are placed in fixed positions. The number of sensors in the array was increased, which allows the acquisition of more data simultaneously. Another important improvement, is the fact that the detection system is hermetic for the pressures being applied in the system. Moreover, the chamber volume was reduced from 1.2 L to 20 mL from version 1 to version 2. As a result, the exposure and recovery times were reduced to half. In respect of the data acquisition system, a humidity and temperature sensor was implemented.

Nevertheless, more improvements were needed. The detection chamber should be more stable regarding easy of use and sensors' positions. A more user-friendly interface should be implemented, because e-nose v2 interface requires to use the command line, which is not intuitive to use for a non-trained person.

4.2 Objectives

E-nose v3 should be improved to be more stable and user-friendly than e-nose v2. One of the main goals was to make the detection chamber more stable. Its structure should enable the placement of the LEDs and the photo-detectors perfectly aligned with each other, and also with the sensing films between them. Moreover, the mechanism to open and close the detection chamber should be improved, without compromising the hermetic effect achieved with e-nose v2.

The interface used to insert the input experiment parameters should be improved to be more user-friendly for every researcher, independently of his/her background knowledge. Real-time data acquisition visualisation should also be implemented to allow the

detection of some malfunctions that can happen while the experiments are running. Additionally, the data collected should be stored in a common database. This would positively impact data analysis, due to having a more organised and significant database available.

4.3 Materials and methods

The schematic of e-nose v3 is represented in Figure 4.1.

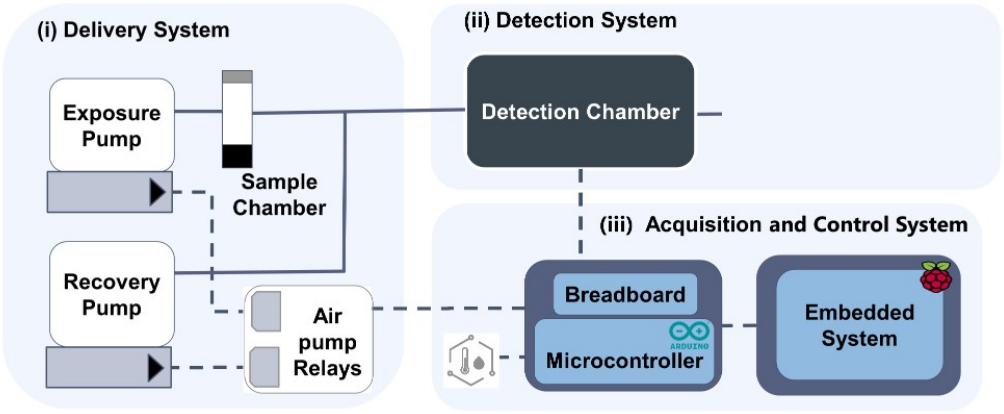

Figure 4.1: Schematic of e-nose v3

4.3.1 Device systems

The delivery system is a replica of the system assembled for the e-nose v2. The pumps flow rate is 3 L/min. The flow rate at the detection chamber entrance is 1.8 L/min in the exposure circuit, and 2.5 L/min in the recovery circuit.

The detection chamber is one of the innovative aspects of this version. It should be much more stable and easy-to-handle than the previous versions. It is composed of an external box with a lid, and an internal structure inside. Both were designed using the software *SolidWorks 2016*, and printed in PLA using an *Ultimaker* 3D-printer. Figure 4.2 describes how to assemble these pieces, preparing the detection chamber for an experiment.

The external box was designed using *SolidWorks 2016*. The 3D drawings of the external box and respective lid are shown in Figure 4.3.

The external box - Figure 4.4a - is composed of a black box with a lid (see the technical drawings in Figure C.1 and Figure C.2, respectively, of Appendix C). It has two important functions. One of them is to close the chamber hermetically. Through a very simple and intuitive procedure (activating the locker) the lid closes the chamber, pressurizing the glass chamber (part of the internal chamber) - see Figure 4.4b. The EPDM strip placed on the lid is compressed between the lid and the internal chamber. Another EPDM strip is placed in the slot of the internal structure support, and it is also compressed by the glass

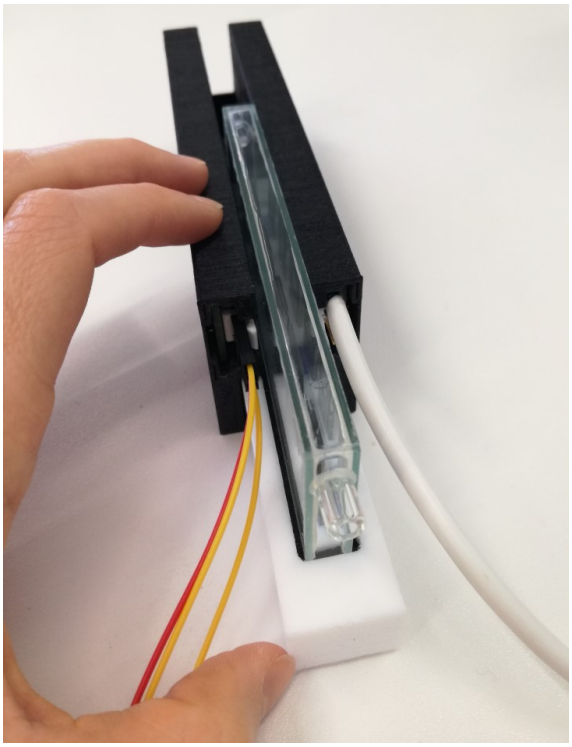

(a) Support for sensing films being inserted in the internal structure.

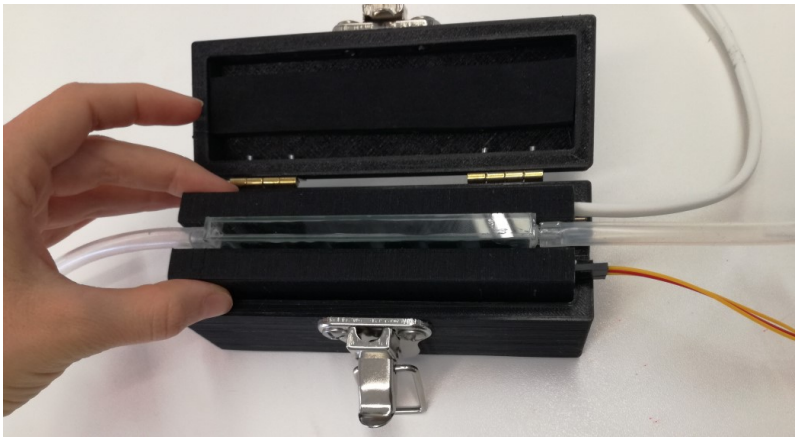

(b) Assembled internal structure being placed inside the external box.

Figure 4.2: Photo-description of how to prepare the detection chamber of e-nose v3 for an experiment.

chamber. This compression is enough to close the chamber hermetically, for the pressures being applied in the system.

The other function of the external box is to isolate the sensors from ambient light. Moreover, it also increases the chamber robustness.

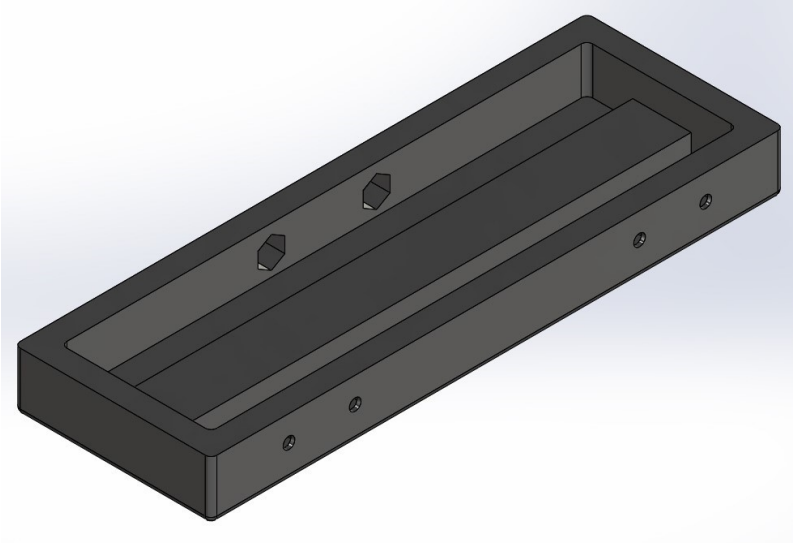

(a) Lid.

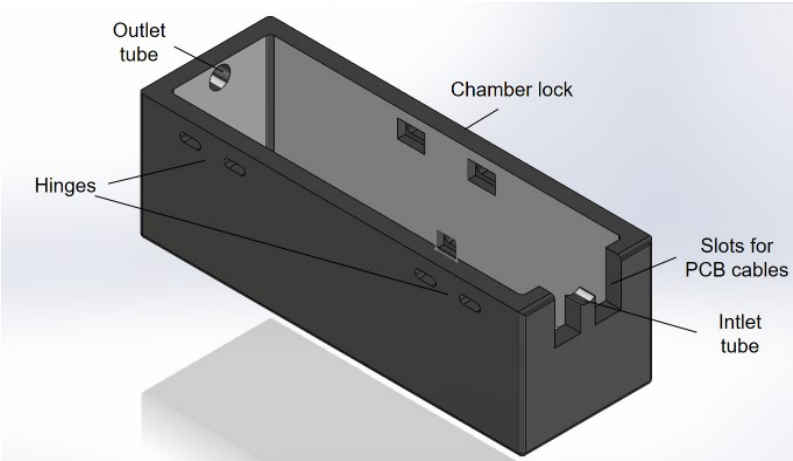

(b) External box.

Figure 4.3: Design of external box using *SolidWorks 2016*.

The internal structure (see Figure 4.5 and the technical drawing in Figure C.3 in Appendix C) serves as support for the PCBs and polarising films, and accommodates the sensing films' internal support. It has two slots to insert the PCBs: one that has an emission circuit with LEDs, and other that has a detection circuit based on photodiodes. These are aligned in front of each other. This way, each LED is placed exactly in front of its corresponding photodiode. There are also slots to insert the polarising films - see Figure 4.5.

Moreover, the light tunnels prevent interference of the light from other neighbour LEDs on the results of each individual LED/photodiode pair.

(a) Closed external box.

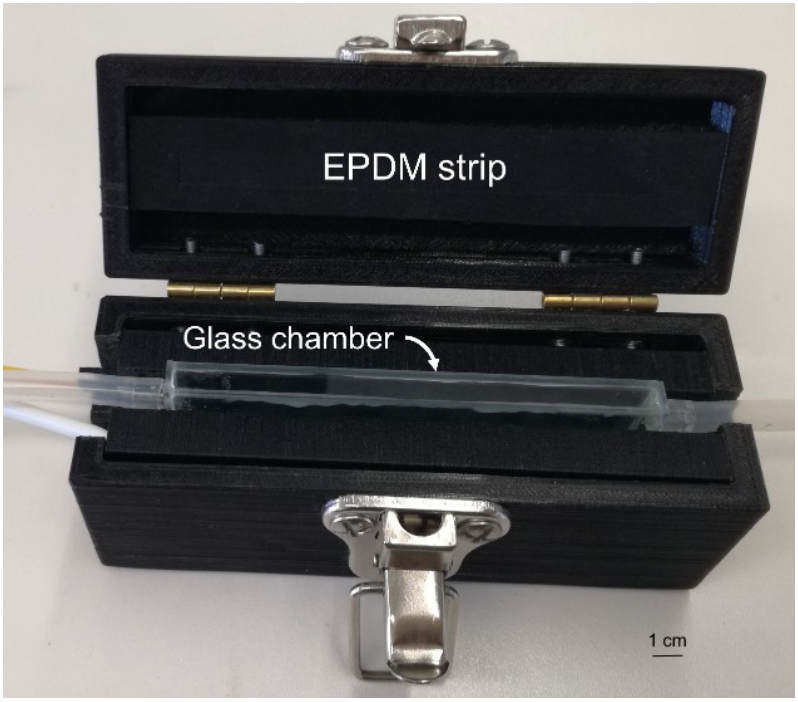

(b) Opened external box, enclosing the internal structure and respective connections.

Figure 4.4: Picture of the assembled external box.

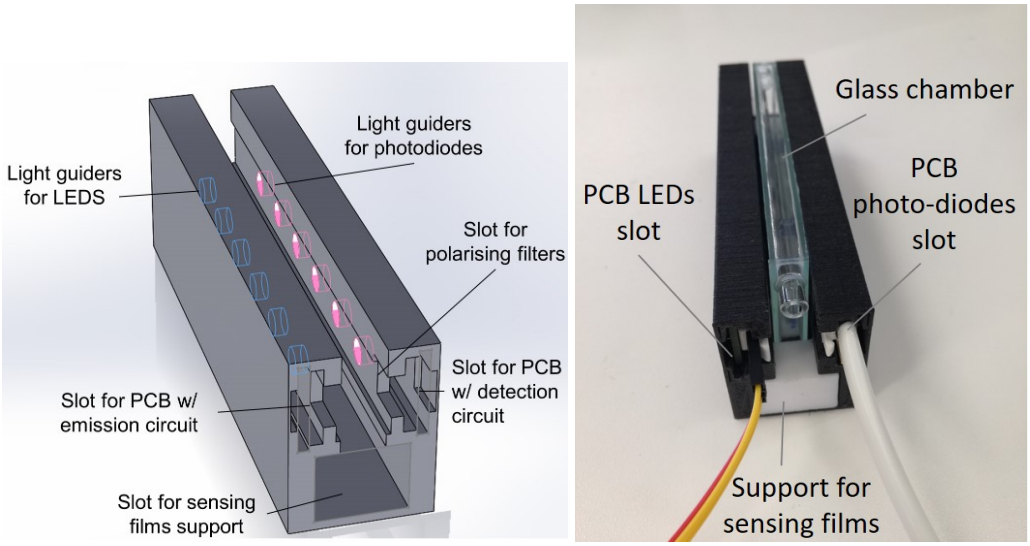

(a) Design of internal structure.

(b) Picture of assembled internal structure.

Figure 4.5: Internal structure of e-nose v3.

Previous e-nose versions used handmade solder boards which usually resulted in alignment problems between the light emitters and the light detectors. Those versions used through-hole components: LEDs, resistors and LDRs. For the e-nose v3 PCBs, Surface-Mount Technology (SMT) was used to guarantee proper alignment. This combined with tailor-made 3D printed structures solved the alignment problems. These changes allowed to assemble an improved version with increased viability.

The schematics of the emission and detection circuits were designed, and then projected using *Eagle software*, to produce the PCBs.

The emission circuit is composed of six LEDs. The six LEDs are wired in series with a resistance and in parallel with the voltage source (5 V). Theoretically, the current is evenly distributed through all the LEDs. Consequently, the LEDs emit light with equal intensity. Also, a transistor in the common ground line acts as a switch to control the LEDs state (ON or OFF). Some important specifications of the LEDs chosen are described in Table 4.1.

A photo of the emission PCB assembled is presented in Figure 4.6. And a schematic of a single unit of the LEDs' array is represented in Figure 4.7. The value of the resistors, $(R_x, x = 2,3,4,5,6,7)$, is calculated by equation 4.1. According to that, the resistor selected was $R_x = 100\ \Omega$.

$$\begin{aligned} & V_{R2} = V_{DD} - V_{LED} \Leftrightarrow V_{R2} = V_{DD} - V_{LED} \Leftrightarrow \\ & \Leftrightarrow V_{R2} = 5 - 3.25 \Leftrightarrow V_{R2} = 1.75V \Leftrightarrow \\ & \Leftrightarrow R2 \times I_{LED} = 1.75 \Leftrightarrow R2 = \frac{1.75}{20 \times 10^{-3}} \Leftrightarrow \\ & \Leftrightarrow R2 = 87.5\Omega \approx 100\Omega \end{aligned} \tag{4.1}$$

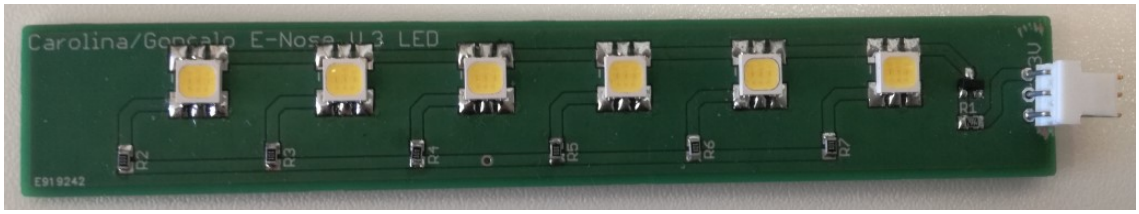

Figure 4.6: Picture of the PCB with the emission circuit of e-nose v3.

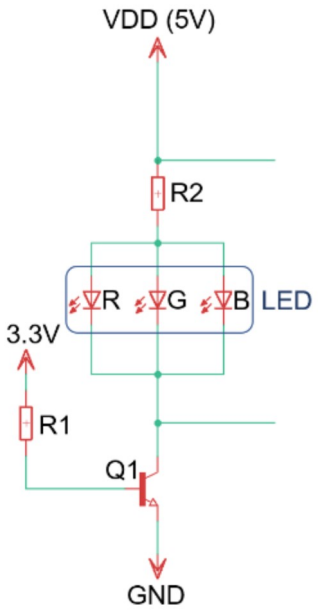

Figure 4.7: Schematic of the LED´s circuit. Only one LED is represented for illustration purposes.

In e-nose v3, for light-intensity measurements, the photoresistors were replaced by photodiodes which have been reported to be more sensitive. Photodiodes are one of the most popular sensor types for many light-based measurements. In the e-nose case, the analyte detection relies on photodiodes for precision light measurement.

Table 4.1: Specifications of the selected LEDs for e-nose v3.

Chip - material	InGaN
Emitted colour	White
Reverse voltage	5 V
Forward current (I_F)	20 mA
Forward voltage (V_F)	2.9 to 3.6 V
Viewing angle	120 °
Operating temperature	- 40 °C to + 85 °C
Storage temperature	- 40 °C to + 90 °C
e-noses current @ $I_F = 30mA$	50μA
Luminous intensity	6000 (mcd)

Photodiodes generate a current proportional to the light that strikes their active area. The current needs to be converted into voltage, since the *Arduino* analogue input pins measure voltage variations, and not current variations. Therefore, a circuit using a current to voltage converter (also called transimpedance amplifier) was implemented.

The circuit operates the photodiode in photoconductive mode. Usually, for the photo-conductive mode, shown in the Figure 4.8 (below), an external reverse bias is applied ($V_{bias} < 0$).

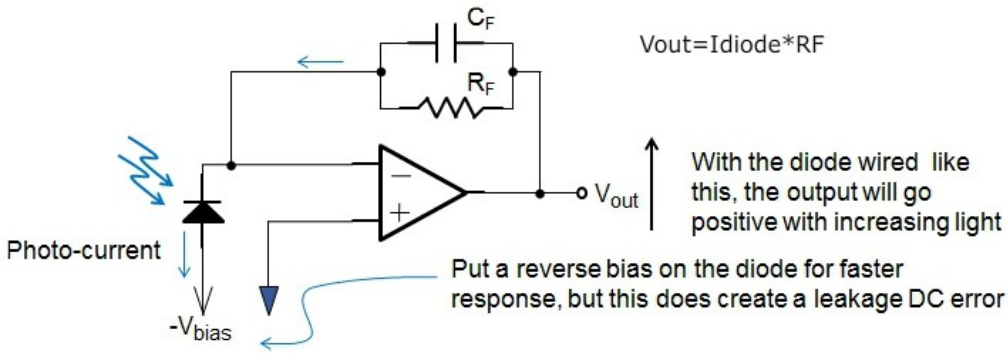

Figure 4.8: Photodiode with reverse bias applied operating in photo-conductive mode.

As an overview, when light hits the photodiode, it generates a current. Since the operational amplifier (op-amp) input current is ideally zero, the photodiode current is forced through the feedback resistor, R_F. This gives a voltage difference at the output of the amplifier V_{out} equal to photodiode current times the resistor value, $V_{out} = -I_{diode} \times R_F$.

However, the Arduino does not supply negative voltage. Therefore, the photodiode was flipped around, having the cathode connected to the source, and the anode connected to the op-amp. In the new configuration shown in Figure 4.9, the current flows in the opposite direction comparing to Figure 4.8. The schematic of the photodiode´s reverse polarising circuit is also represented in Figure 4.10 (b).

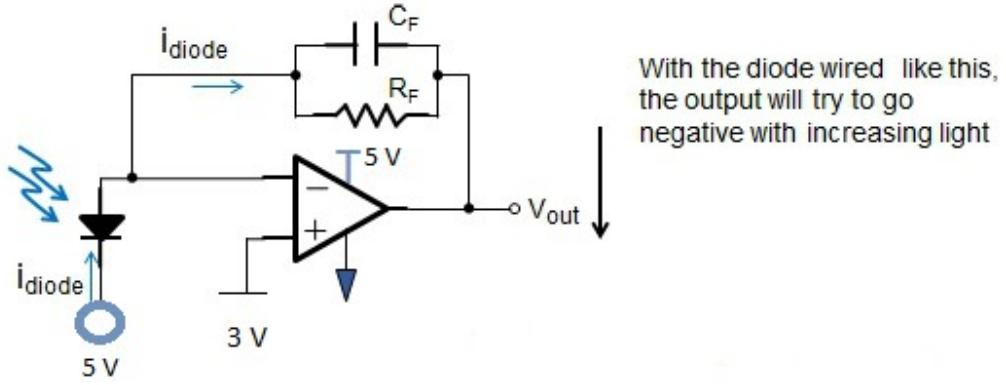

Figure 4.9: Photodiode connected in reverse on a photoconductive mode circuit.

To get an output voltage exclusively in the range of Arduino input pins (0 – 3.3 V), the positive input of the op-amp, V_{DIV} - was connected to 3.0 V. The maximum output

voltage is directly defined by V_{DIV} through the op-amp positive input (In+), therefore it forces the DC output to have a maximum of 3.0 V. This value was obtained using the voltage divider described in Figure 4.10 (a). The value of V_{DIV} was established as a compromise between the output voltage window and the reverse polarisation of the photodiodes.

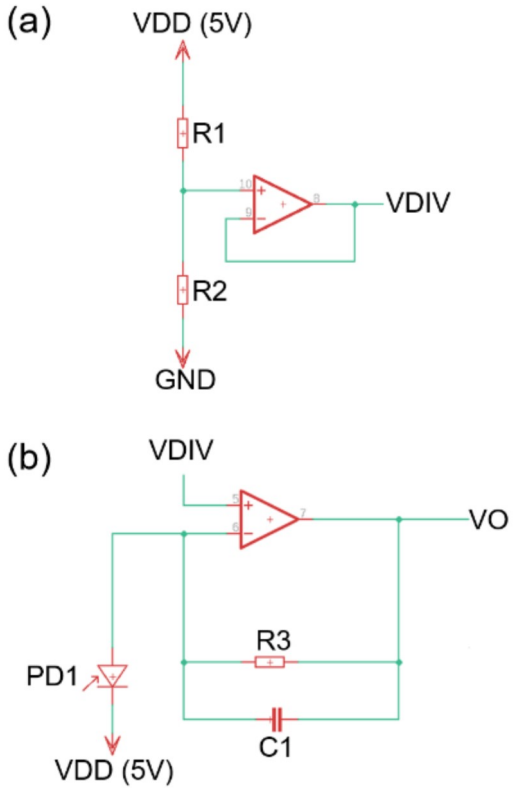

Figure 4.10: Single unit of the photodiodes array. (a) Generic voltage divider to generate V_{DIV}. (b) Schematic of photodiode's reverse polarising circuit. Only one light-sensor is represented for illustration purpose.

Photodiode's reverse polarisation voltage, V_{DRP}, is given by equation 4.2.

$$V_{DRP} = V_{DD} - V_{DIV} \tag{4.2}$$

If V_{DIV} is higher, the output range V_{out} will increase but V_{DRP} will decrease. Photodiodes become more sensitive to light when the polarisation voltages are higher. Consequently, a decrease in V_{DRP} has a negative impact on the performance of the photodiodes. To contribute to increase the photodiode depletion area, the cathode was wired to $V_{DD} = 5V$, which improves its sensitivity to light, resulting in a higher current value.

When the photons from the light reach the photodiode active area, the current will flow in the anode direction, and the output will go negative with increasing light intensity. Since the In+ of the op-amp forces the DC output to be 3.0 V at maximum, this voltage will decrease when the light intensity increases according to equation 4.3.

$$V_{out} = V_{DIV} - I_{Diode} \times R_F \tag{4.3}$$

The photodiodes selected are model *SFH2430-Z* and their specifications are described in Table 4.2 below.

Table 4.2: Specifications of the selected photodiodes for e-nose v3.

Photo-current (I_{DIODE} for $V_R = 5V$)	6.3 μA
Spectral sensitivity ($V_R = 5V$)	6.3 nA/lux
Spectral range of sensitivity (typ)	400 nm - 900 nm
Reverse voltage (V_R)	6 (V)
Max. power dissipation	150 mW
Forward voltage (I_F = 100 mA, E = 0)	1.2 V
Half angle	±60°
Operating and storage temperature	- 40 °C to + 100 °C

To determine the best value of the resistance R_F, different values were tested, under two different conditions (A and B), similar to the calibration conditions of the e-nose. The photodiode was placed in front of the LED and aligned with it. The distance between them was 15 mm. The components were placed inside a little box without interference of environmental light.

Condition A: Two parallel polarisers were placed between the LED and the photodiode.

Condition B: Two crossed polarisers were placed between the LED and the photodiode.

Note: The LEDs and photodiodes used in both conditions were the same selected to be used in the e-nose v3. The results obtained are shown in Table 4.3.

Table 4.3: R_F values tested under conditions A) and B). V_{out} of circuit shown in Figure 4.9, tested using different R_F values.

R_F ($k\Omega$)	$V_{out}(V)$ for condition A Parallel polarisers	$V_{out}(V)$ for condition B Crossed polarisers
220	1.5	2.9
300	0.75	2.9
386	0.06	2.9
440	0.055	2.9
510	0.045	2.9
520	0.045	2.9
530	0.045	2.9
540	0.045	2.9
550	0.045	2.9
560	0.045	2.9
570	0.045	2.9
620	0.045	2.9
730	0.045	2.9

A potentiometer was used to find the more suitable R_F. According to Table 4.3, using $R_F > 440\ k\Omega$, the circuit starts saturating for condition A. The value $R_F = 386\ k\Omega$ was the selected, because it results in the higher voltage drop from condition B to condition A, without fall in the saturation zone for condition A.

The capacitor C_F value was calculated using the Nyquist theorem, which states that the cut-off frequency (f_c) should be half of the sampling rate (s_r). Assuming that the maximum sampling rate we intend to use in the e-nose is sf = 1 kHz, then we can calculate C_F using equation 4.4.

$$f_c = \frac{f_r}{2} \Leftrightarrow \frac{1}{2 \times \pi \times R \times C_F} = 500 \Leftrightarrow \frac{1}{2 \times \pi \times 386 \times 10^3 \times C_F} = 500 \Leftrightarrow C_F \approx 820 \times 10^{-12} \quad (4.4)$$

Finally, the circuit was designed using $R_F = 383\ k\Omega$, $C_F = 820$ pF and integrated circuits *LM324* (with 4 op-amps each). A picture of the final PCB with the detection circuit already mounted is represented in Figure 4.11.

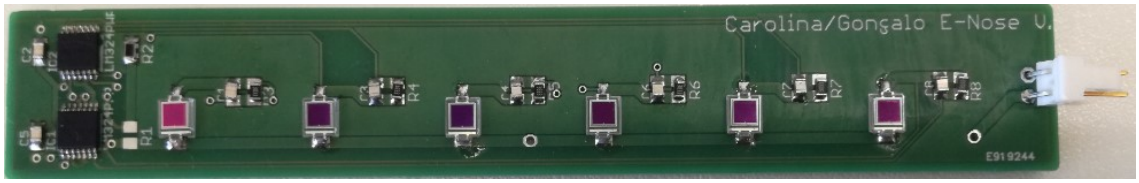

Figure 4.11: PCB with the detection circuit of e-nose v3.

4.3.2 Scalable and easy-to-use data acquisition system for e-noses

The data acquisition system was re-designed and implemented to be easily scalable for several e-noses with data storage in a common database.

Since we were interested in acquiring large datasets simultaneously from different e-nose devices, the idea of creating a common data acquisition system to all the e-noses in the laboratory emerged. The data should be stored in the *Raspberry Pi* of each e-nose, and in a common database to all e-noses for backup. Moreover, an easily scalable system architecture should be implemented, with automatic temperature and humidity measurements, and that would enable real-time visualisation of the signals acquired.

The process of scale-up the e-noses acquisition and control system is important to acquire and store more data from several e-noses at the same time, as well as enabling real-time signals visualisation. Currently, we have three e-nose prototypes working in the laboratory. It is useful for research purposes to increase the number of devices, having different e-noses attributed to different researchers, which allows the acquisition of large amounts of data simultaneously from different e-noses. The acquired data can be then compared, analysed and processed.

In this section, it is explained how the data acquisition system elements interact in the process of control, acquisition and visualisation, how the interface is used for setting

the session configurations and for signals visualisation. Flowcharts of the scripts are also presented, and it is described how the Arduino actions are controlled by a python script.

To give an overview about the system architecture and how the user can interact with the system: Firstly, the user establishes remote connection to the Network Attached Storage (NAS), and runs the script that creates the interface - Step 1 in Figure 4.12.

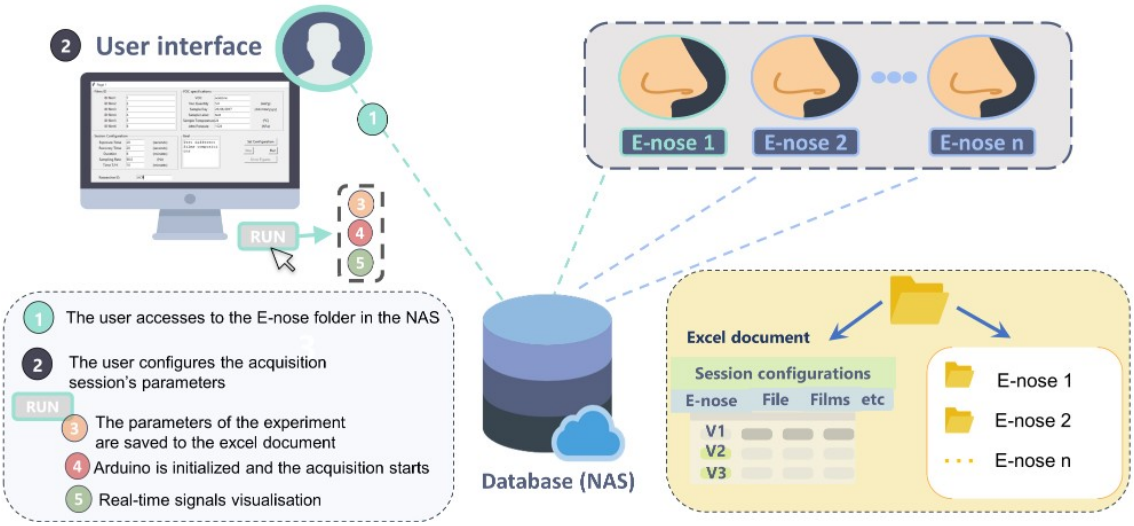

Figure 4.12: Integrated data acquisition system architecture.

Then, the user fills in the parameters of the interface, allowing the definition of the experiment conditions - Step 2 in Figure 4.12. By clicking in the "Run" button on the interface - Step 3 in Figure 4.12, the user starts the main script, which saves the session parameters to the database, controls the exposure and recovery periods, and acquires the data from the photo-detectors and from the humidity and temperature sensor. This data is saved in the *Raspberry Pi*, as well as in the NAS.

After that, the real-time visualisation of the signals acquired is launched in the personal computer of the user using *PyQtGraph*, a graphics and user interface library for python.

4.3.2.1 Interface, control and visualisation

The user interface was implemented using a python GUI library, named *TKinter*. This interface was built due to the need of having an interface easy-to-use, independently of the user's background knowledge, and avoiding the use of the command line.

The interface runs in the user's personal computer, and coordinates all the processes that run during the session. As explained in Figure 4.13, it connects to the *Raspberry Pi*, where the main process runs, via SSH. And, it controls the visualisation process, which also runs in the user's personal computer.

As described in the flowchart in Figure 4.13, firstly, the code starts by initialising the App interface.

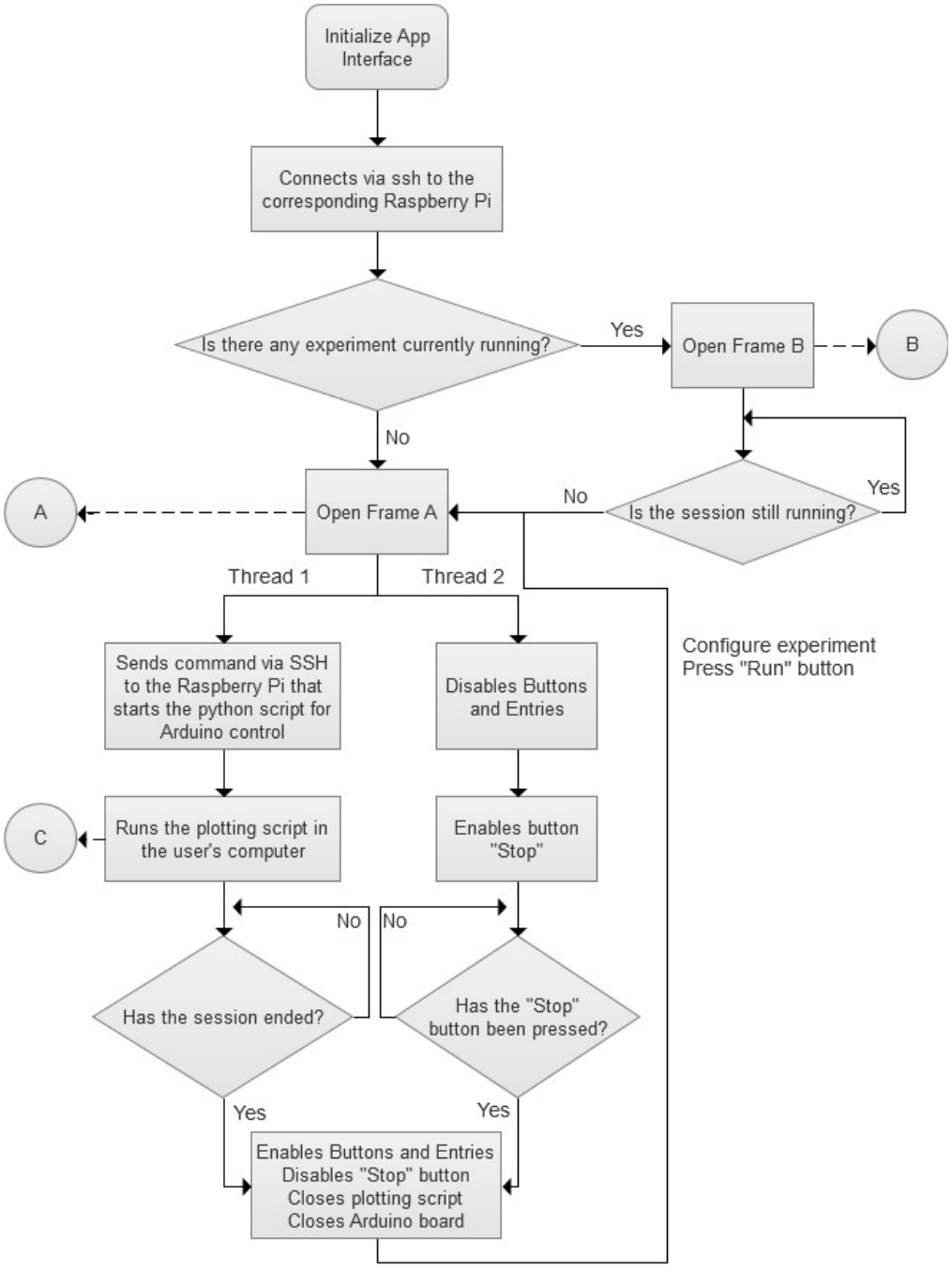

Figure 4.13: Flowchart representative of the python file that implements the interface.

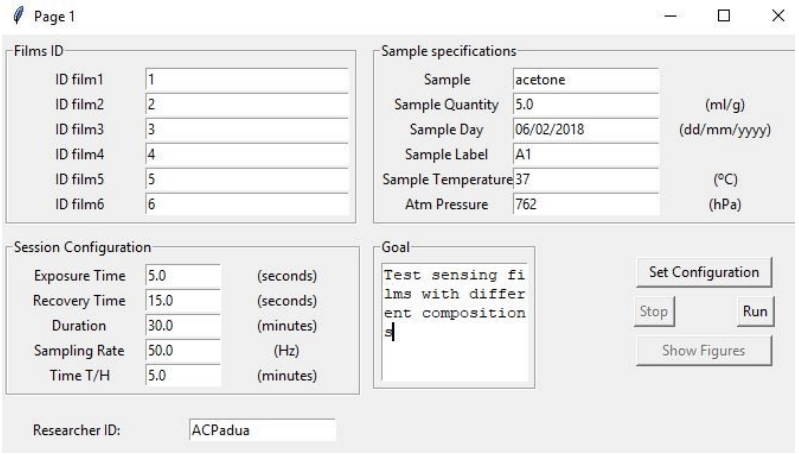

(a) Frame A.

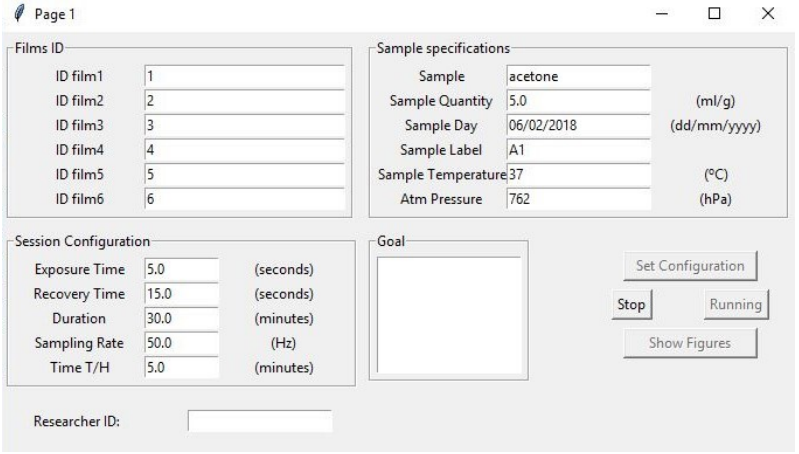

(b) Frame B.

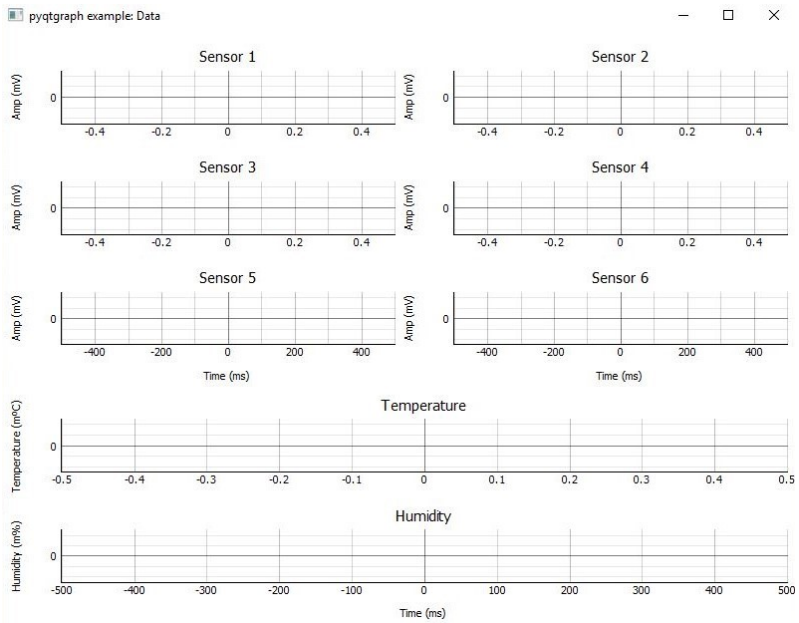

(c) C: Window for signals visualisation in real-time.

Figure 4.14: Interface frames.

Then, the interface connects via SSH to the corresponding *Raspberry Pi* (each e-nose is associated to a *Raspberry Pi* with a static IP). Once connected, it checks if there is any session already running. If so, it opens Frame B (see Figure 4.14b), where the only button enabled is button "Stop". This button can be pressed by the user to finish the experiment if needed.

In case there is not an experiment currently running, Frame A (see Figure 4.14a) is opened. In this page, the user can configure the conditions in which the experiment will be conducted, by specifying the details that characterise the experiment: sensing films' identifiers (IDs), the session parameters, the researcher identification number, the sample specifications, and the goal of the experiment. Initially, the fields are filled according to the default configuration file (named $default\_config.json$, located in the folder $eNose/rasps/eNose\_Vx\_raspxxx/config\_files$). The default configuration intends to be useful when many experiment parameters are the same for several experiments running consecutively. This way, the user does not need to insert repeatedly all the parameters at the beginning of each session. When necessary, the fields content can be changed by the user, according to the parameters of the new experiment. For each entry, the input text type is validated (e.g. the 'Sample name' should be string, and the 'Sample quantity' should be float).

When the configuration is done, the user can press the button "Run" to start the experiment. This action triggers two threads.

Thread 1 runs the python script which controls the *Arduino*, by sending a command to the *Raspberry Pi* via SSH. Additionally, this thread calls a subprocess that launches the real-time signals visualisation (see Figure 4.14c), running the plotting script in the user's computer. This process ends when the duration of the experiment has elapsed.

Thread 2 disables all the buttons and entities, and enables "Stop" button. In case this button is pressed, the session ends.

When one of the two threads ends, the *Arduino* board and the visualisation script are closed. Next, the buttons and entities become enabled, and the "Stop" button becomes disabled.

The interface and the processes that are launched are completely independent. If the interface is closed, the main process that controls the *Arduino* will still be active, as well as the visualisation subprocess. This procedure guarantees that the experiment does not fail by means of any unexpected occurrence.

4.3.2.2 Acquisition and control

In each e-nose version, the *Arduino* board controls the pump relays module, acquires the data from the photo-receptors and reads the temperature and humidity values.

The *Arduino* board also supplies power to the PCBs (placed inside the detection chamber). The output signals from the photo-receptors board are connected to the analogue

input pins, while the humidity and temperature sensor is connected to the SDA (data line) and SCL (clock line) pins, using the I^2C protocol.

For each e-nose, the *Arduino* has been flashed with *StandardFirmataPlus* firmware. Therefore it can be controlled by a python script (explained in the flowchart of Figure 4.15) that runs in the *Raspberry Pi*, using a python library that supports the complete *StandardFirmata* protocol.

Figure 4.15 depicts the flowchart of the process that controls the *Arduino* board. After setting the main parameters, the main cycle starts and a first recovery cycle is performed to clean the detection chamber conditions to a reference state. Further, the acquisition cycle (main cycle) starts and will last for the duration specified initially.

As shown in Figure 4.15, in each iteration of the main cycle the period of the current activated pump, and the time for acquiring the room temperature and humidity are checked. When the period of the pump cycle has elapsed, the pump mode (exposition or recovery) is switched and the pump timer is reset. The temperature and humidity values are acquired at defined periods. This process is repeated in each iteration, ending when the duration of the experiment session has elapsed.

The data acquired from the photodetectors and humidity and temperature (H&T) sensor are constantly being written in temporary and in the final text file. The temporary files contemplate only 100 samples each. They are accessed and read by the plotting process and erased afterwards. This is important for simplifying the access to data from the NAS. A single file containing a large dataset makes the process slower.

Due to the need of I^2C protocol, the library *pymata_aio* was chosen. Comparing the two most used libraries used to control *Arduino* flashed with *StandardFirmataPlus* firmware, this one provides a simplest implementation.

All the code and architecture was prepared to run on the performance lagging *Raspberry Pi*, the version 2. In the purposed architecture, the *Raspberry Pi* is only responsible for saving the data and controlling the *Arduino*.

4.3.2.3 Network layer

In order to make the system as scalable as possible, each acquisition module must be able to easily connect to the NAS and to the user.

Firstly, the NAS, *Raspberry Pi* of the e-nose, and the user's computer must be connected to the same network, in this case the internal local area network of the laboratory. With all the components connected this way, the IP of both the NAS and the *Raspberry Pi* must be set to a static IP in order to make the connection easier. In the case of the *Raspberry Pi*'s, the static Internet Protocol address (IP) also gives a unique identification number to each of them.

Each *Raspberry Pi* connects to a particular folder in the NAS to save the data acquired and to a common folder containing the Excel file. Each *Raspberry Pi* folder is named using its own IP, e.g., eNose108 is the NAS folder where the *Raspberry Pi* with the 108 ending

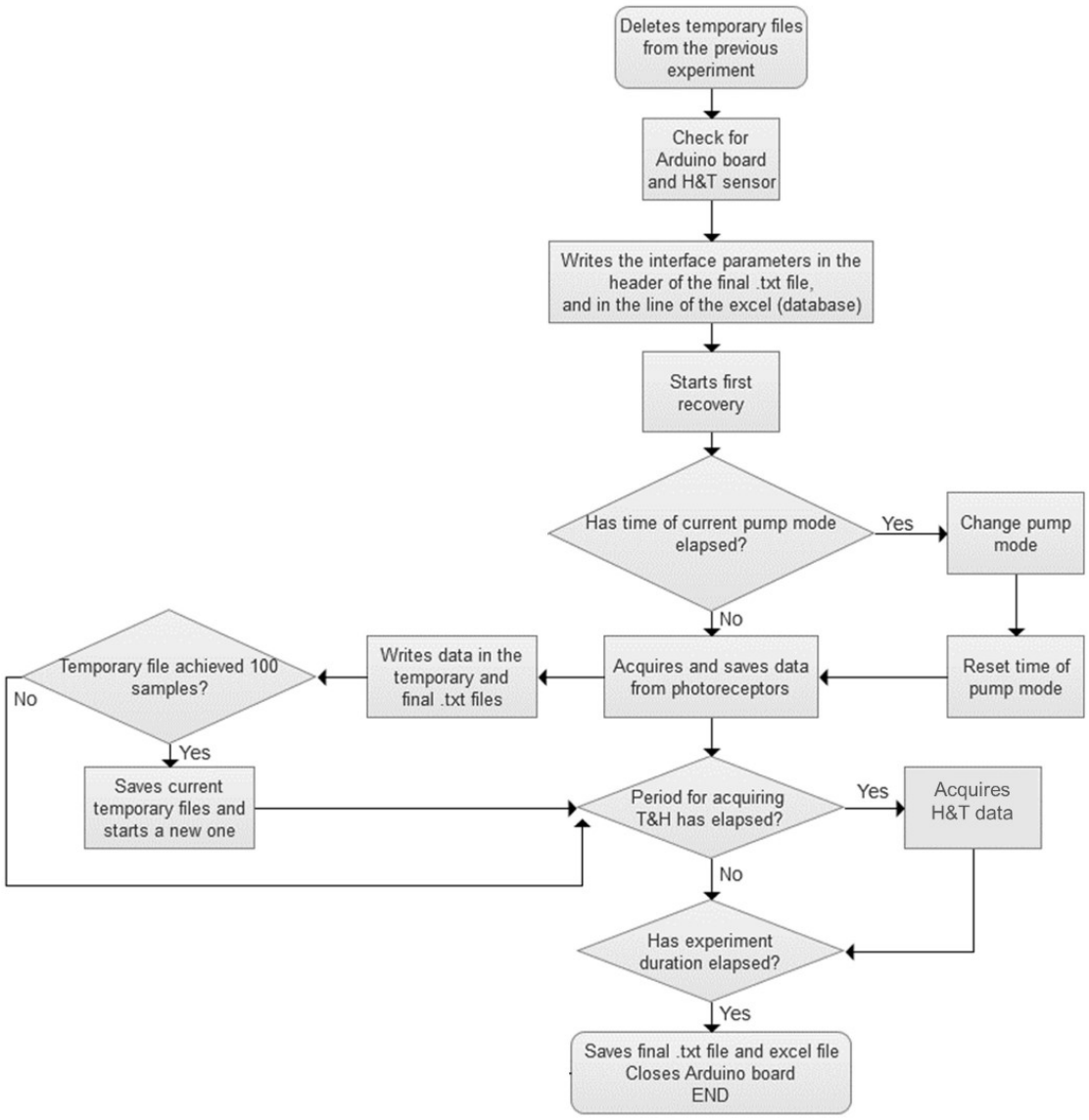

Figure 4.15: Flowchart representative of the python file that implements the acquisition and control.

IP connects to. The user also mounts the NAS folders in the personal computer in order to access the files for setting up, controlling and visualising the experiments.

To communicate with the *Raspberry Pi* via a PC, the SSH protocol was used. To use this protocol in python, the *paramiko* library was used. This library implements the SSHv2 protocol. This library is used to run the data acquisition script, query the *Raspberry Pi* if there is any script running and to stop the script if the user deems necessary.

4.3.2.4 Database

The data is stored in the NAS for a convenient and organised storage of the information that is acquired in each e-nose. The NAS used in this project is a QNAP TS-453A. Each e-nose has a individual directory in the NAS, and the devices also share a common excel file (where the configurations of each experiment session are stored).

The database is composed by four tables: the sensors table, the pictures table, and the two experiments tables. The sensors table should be written by the user prior to the experiment. The pictures table should contain the sensing film images, visualised under 90-degree crossed polarising films at the microscope (magnification: 5x), before and after the experiment. For more details about how to fill this database consult Table A.3 in Appendix A. Lastly, the experiments tables fields are automatically written by the script, while the experiment is running.

Instructions about how the fields of the sensing films' table should be filled are described in Table A.1 of Appendix A. All the fields are identified as obligatory or optional.

There are two experiments tables: one that contemplates all the experiments performed (including even the aborted experiments), and another that just contains the completed experiments. Both the experiments tables have the columns described in Table A.2 of Appendix A.

4.4 Discussion and Conclusions

E-nose v3 can be described as a robust, stable and user-friendly device. Regarding the detection chamber, the number of sensors was increased and the chamber became more solid, compact and reproducible. Due to the way it was designed, the sensing films are centrally aligned with the emission and detection components of the PCBs. To achieve so, an internal structure with specific slots to insert the PCBs and the sensing films' support was placed inside the detection chamber. The internal structure also has light tunnels incorporated to prevent the interaction between neighbour optical pairs. This, together with the use of PCBs with surface-mount technology was enough to guarantee proper alignment of the sensors.

Moreover, this device is hermetic for the pressures being applied in the system and the use of a small volume detection chamber allows a 10 times faster analysis, comparing to the initial prototype (e-nose v0).

The new data acquisition system implemented has an easy-to-use interface, that allows the user to configure all the parameters of an acquisition. A real-time visualisation signals solution is also provided, allowing for an interactive experiment. The architecture developed is able to be easily scaled up, taking only 6 steps to setup a new node. These experiments can run in all the current iteration of the e-nose and up to a sampling rate of 100 Hz. This means that the same experiment can run in any one of the in-house developed e-noses, even if some have the *Raspberry Pi 2* and others the *Raspberry Pi 3*.

Comparing to other e-noses described in the literature - see Table 4.4 - our device presents an innovative detection system. The sensing materials are biodegradable and possibly reusable. In addition, our materials and sensing device operate at ambient conditions as opposed to MOS. The number of sensors is not disparate comparing to the other e-noses, although it's still possible to increase the number of units if necessary. For research purposes, the detection system could benefit from the use of a longer array of LED/photodiode pairs. This would allow a wider combination of different sensor types or a larger number of replicas, which have a positive impact in the VOCs prediction algorithms or reproducibility tests, respectively. The PCBs can also be more compact than they are currently. For that, a new design would be required to create mini-PCBs.

Some e-noses described in the literature include the use of miniaturised air pumps and mass flow controllers for the delivery system. In terms of our device evolution, the next version should include those micropumps in the delivery system. The delivery system is flexible, because mass flow controllers (MFCs) can be installed instead of air pumps to control the concentration of VOCs inside the detection chamber. This is useful for making controlled dilutions of VOCs in nitrogen. Therefore, it enables to study the detection limits of the system. In respect of the data acquisition system, ours differentiate from the remaining. It is more well-described and benefits from the use of open-source hardware and software.

E-nose v3 has been used to address many scientific questions which are under study at the moment, mostly in four different categories: influence of external factors on the signals' response; determination of detection limits [1]; stability and properties of sensing films with different compositions [106] [2] [3]; and efficient data analysis.

As future perspectives, an improvement could be the introduction of a scheduler (a table where the users can schedule the experiments). Using this, the interface would be used to fill the schedule table. This would allow for the experiment to be programmed outside the lab if, for example, an on-line spreadsheet service was used. A physical button connected either to the *Raspberry Pi* or the *Arduino* could be incorporated into the system architecture in order to abruptly stop the experiment. This would mitigate against software problems or emergency situations.

[1] Article under submission process

[2] Work presented as poster entitled "The effect of 8CB on the self-assembly and performance of gas responsive gels" at ECLC2019 by Ramou E.

[3] Work entitled "Molecular recognition with tunable gas sensing liquid crystal gels" orally presented at ECLC2019 by Ramou E.

Future studies can be performed in order to explore the application of the e-nose in many different sectors, such as food and beverage evaluation, environmental safety or medical research.

Table 4.4: Comparative table of different e-noses reported in the literature

Reference	Detection system	Delivery system	Data acquisition system	Applications
[107]	6 piezoelectric QC-based sensors	Oven at 230 ° C used to extract VOCs; VOCs carried by nitrogen stream.	NI board / LabVIEW	Cheese maturation
[108]	6-MOS + 1 PID sensors	Uses mass flow controllers	R software	Determination of odours interactions in gas mixtures
[36]	7 MOS sensors	Home-made olfactometer	Measurement computing board + PC	Chocolate classification
[8]	40 colorimetric sensors	Internal micropump	Contact image sensor / MATLAB	Discrimination of individual analytes associated to explosives
[109]	8 nano-sensors based on QCM	Syringe pump	Ellipsometer	Identification of explosives
[96]	8 MOS	Micropumps	NI board / LabVIEW	Pulp and paper indutry's gasous emissions
[110]	Chemiresponsive nanomaterials integrated into the circuitry of commercial NFC tags	n.a.	smartphone	Discrimination of amonia
[111]	Carbon nanotube-based	Nitrogen gas stream of constant flow rate	n.d.	Detection of ethylene to identify fruit ripeness
E-nose v3	6 optical sensor	VOCs carried by atmospheric air	Arduino + Raspberry Pi / Python	Detection of harmful toxicants

NI: National Instruments
NFC: Near-Field Communication

Chapter 5

Conclusions and future prospects

5.1 Device evolution

This subsection provides a brief overview of the device upgrade along this project. Table B.1 in Appendix B summarises the main differences of the three e-nose versions, facilitating their comparison.

The signals obtained with e-nose v0 were very unstable due to variations among the optical pairs. Therefore, before data acquisition with e-nose v1, optical signals' calibration was done. Moreover, the sensing gels were not homogeneously spread over the glass slides. To solve this, in e-nose v1, opaque black masks were applied on the back of the glass slides to control the exposed area.

A proof of concept was conducted with e-nose v1. For each solvent tested, the signals obtained presented different baselines in the different tests (1, 2 and 3). Nevertheless, their wave shape was identical. This indicates that the characteristic signals resultant from the interaction of a specific solvent with a sensing film, may be described by a mathematical model, independently on the factor(s) that cause baseline drift.

Then, several classification methods were explored. Analysing the PCA using data from a single test (test 1), and selecting the two best features, it is possible to identify a clear separation of all the 13 solvents. 100 % of the total variance was covered by the two principal components. The accuracy of NB, DT, k-NN, and SVM for VOCs prediction was evaluated. The best results were found using SVM which had 100 % accuracy for the classifications performed.

The sensing films were removed and placed again in the detection chamber for reproducibility tests. However, this time, when we analysed the PCA using data from the three tests, it was not possible to observe a separation of the solvents in clusters. For the other classification methods tested, the best result was 85 % of accuracy using the DT.

These results indicated lack of reproducibility for the three tests. This could be due to the fact that the sensing films were not placed in fixes positions in the sensors' array, and the user needed to remove the upper part of the transduction system (where the detection PCB was placed) to insert the sensing films. Therefore, for the next e-nose version (e-nose v2), a new support for sensing films was designed and a horizontal structure was applied instead of a vertical one. This allowed to place the sensing films in fixed positions, without need of touching in the PCBs to change the films.

Then, the next device version - e-nose v2 - was assembled. To test the new device, reproducibility tests were performed. The time required for the signals to stabilise with e-nose v2 was inferior to five minutes.The 10-days reproducibility test revealed that the CV of the signals' relative amplitude was lower than 32 % in the first four days of experiment for all the sensing films, whereas in the following days this parameter significantly increased. The unstability of the optical responses given by the optical sensing films might be caused by: the variation of the humidity and temperature along the days of experiment; the droplets that compose the sensing gels might change in number and/or size along the days; and the stability of the sensing films can be affected due to exposure to the VOCs.

In order to produce more uniform and controlled sensing films, two new gels' spreading techniques were explored: spin coating and film coating. Both were reported as effective to produce sensing films able to distinguish each one of the 13 VOCs tested. The classification accuracy using both sensing film production methods was higher than 96 % for all the three classification methods used (DT, NB, MLR).

Another attempt to achieve reproducible sensing films was the inclusion of GA in the sensing films recipe to promote cross-linking. A microscopic analysis of the sensing films before and after exposure to the VOCs was used to study the variation in the number and size of the droplets. The goal was to verify if adding this compound to the gels' recipe, the droplets' stability would be improved. After sensing films exposure to VOCs, we reported a change in the number and size of droplets. The sensing films having glutaraldehyde did not exhibit significantly different variations compared to the standard recipe. Therefore, different methods to stabilise the droplets should be explored.

Preliminary responses given by electrical sensing films were obtained for one of the gel compositions tested, using 200 μm spacing interdigitated electrodes connected to a conductivity meter. The best frequency for the triangular wave generated by the conductivity meter was f = 220 Hz, which results in a DC output signal with higher relative amplitude (from the range tested: 220 Hz – 10.38 kHz).

E-nose v3 was built to be a robust and user-friendly device. The detection chamber is hand-size and hermetic for the pressures being applied. The mechanical structure (ready to replicate using a 3-D printer) and PCBs implemented (easily reproducible) for e-nose v3 contributed to make the device easily scalable. A suggestion for improvement in the future is a reduction in the size of the detection chamber. Reducing its volume would enable shorter cycle periods, and consequently a faster analysis. As estimation, it can be

reduced in 50 % without changing the current configuration, if the size of the sensing films would be reduced too.

In the PCBs, the advantages of using photodiodes is that they are more sensitive and have a quicker response time than photoresistors. Since the composition of the sensing films make them vary their number, size and morphology of droplets, their optical properties vary in a wide range. That's why a possible correction for the future is to use adjustable resistances for a detection system that could be automatically adapted to diverse sensing films.

The non-return valves currently used in the system are susceptible to degradation caused by VOCs interaction. To avoid that, these can be replaced by PTFE non-return valves.

The data acquisition and control system based on *Arduino* and *Raspberry Pi* constitute a low-cost and independent unit. The sampling rate of 90 Hz was enough to guarantee informative signal acquisition. The assembled system was able to distinguish 11 tested VOCs [104]. Although the identification of the VOCs was not made in real time, a step towards making this e-nose able to make automatic classification was taken. Signal pre-processing (including features extraction) can be improved, as well as more machine learning algorithms can be explored.

The results showed that the methodology applied is fast, low-cost and reliable to detect pure VOCs. Nevertheless, future studies are necessary to evaluate if the e-nose can predict the VOCs of interest when they are present in real conditions, in which many different VOCs are mixed together.

The signals acquired by the e-nose should be correlated with the ambient conditions, and more tests to study the effect of the temperature and humidity on the signals obtained are needed.

To produce the sensing films, it will be important to explore the use of different LCs, ILs and polymers. For example, chiral LCs can be explored due to their quick response time, but also others specially if they have a stable phase at room temperature. Other cross-linking methods should also be investigated as an attempt to achieve sensing films' stability. Microfuidics is another possible different approach to produce sensing films that should be considered.

For the electrical part, the conductivity meter should be implemented in a PCB using SMT to improve stability and to reduce the size. Moreover, the possibility of generating an input digital wave should be explored. Furthermore, the electrodes finishing surface should be more corrosion-resistant (the use of nickel and gold, or platinum might be a solution).

Currently, the main drawback of the e-nose is the sensitivity limits, because at least 0.5 % (v/v) is needed to detect VOCs in the system. An ideia to increase the information extracted from the sensing films and possibly improve the detection limits is the inclusion of a mini-camera with microscopic functionality that would record what happens to the sensing films while interacting with VOCs. Videos recorded from polarised

optical microscopy showed the dynamics of the droplets in the sensing films' changing in different ways while interacting with distinct VOCs. Therefore, deep learning could be interesting to predict the VOCs based on features changing in the droplets while the interaction occurs.

Accuracy, stability, and scalability are imperative to get to a device, that can be explored towards several applications in environmental protection, security, product quality, or medical research. And hopefully in the future a portable and user-friendly e-nose can be in our hands to improve our quality of life, or even to prevent and diagnose diseases.

5.2 Contributions

This Ph.D. project contributed to create better devices to test sensing films, and to have tools for data acquisition and data analysis. The tests carried out generated important datasets containing varied and well-organized information that can be easily accessed in the future.

Hardware

- Creation of three devices (e-nose v1, v2 and v3) available and ready-to-use for experiments in the laboratory.
  - E-nose v1: The prototype became smaller, easier-to-handle and more stable compared to the previous version.
    - Better stability was achieved due to the new configurations adopted for the detection system and sample chamber.
    - The transduction system was improved regarding both mechanical and electronic parts.
    - A new data acquisition and control system based on *Arduino* and *Raspberry Pi* was developed. This allowed to acquire optical signal less noisy, which significantly improves the quality of the data that will be further analysed and processed.
  - E-nose v2: hybrid prototype including both optical and electrical responses.
    - Design and assembly of a new miniaturized, hermetic and easier-to-use optical detection chamber.
    - Design and assembly of the first electrical detection chamber.
    - Replication and adaptation of the delivery system and data acquisition system of e-nose v1 for e-nose v2.
    - Implementation of a conductivity meter for reading the electrical signals from the electrodes.

        * Optimization of the conductivity meter by selecting the more efficient electrical components.
    - E-nose v3: reproducible and scalable prototype.
        * Design and assembly of a new detection chamber configuration with internal support for sensing films, slots for PCBs, and light guiders incorporated.
        * Design of new PCBs using SMT.
        * Design of a new delivery system to allow the control of VOCs concentration transferred to the detection chamber, and made with different materials to be more resistant to interaction with VOCs.

- Exploration on the production of optical sensing films varying their composition (IL, LC and polymers), and applying different spreading methods (manual roll-on technique, film coating and spin coating).

- Production of electrical sensing films with several compositions (based on IL, water, polymers, and LC); and using different types of interdigitated electrodes.

Software

- Optical sensors calibration.

- Explored several classification methods.

- Integration of a humidity and temperature sensor in the e-nose to measure the room conditions automatically during the experiments.

- Development of a methodology for droplets' analysis in images of optical sensing films' obtained from the microscope.

- Implementation of a scalable and easy-to-use architecture for electronic noses:
    - User-friendly interface that allows the user to easily configure the parameters of the experiments.
    - Implementation of real-time data visualization.
    - Creation of a database composed by four tables: the sensors table, the images table, and two experiments tables containing information about the experiments' parameters.

Dataset

- Review on commercial e-noses and gas sensors in the market and their applications.

- First optical signals generated by e-nose v1.

- Optical signals obtained using e-nose v1 for a proof of concept.
- Optical signals obtained with e-nose v2 for studying the reproducibility of the responses along a day, a week and a month.
- First electrical signals obtained using e-nose v2 and their optimization.
- Optical signals from sensing films spread by film coating vs sensing films spread by spin coating.
- Optical signals for studying the effect of cross-linking by glutaraldehyde on the sensing films stability.
- Microscopic images of sensing films (standard and cross-linked with glutaraldehyde) before and after exposure to VOCs.

5.3 Publications and presentations

Peer-reviewed articles

- **Pádua, A.**; Gruber, J.; Gamboa, H. and Roque, A. (2019). Impact of Sensing Film's Production Method on Classification Accuracy by Electronic Nose.In Proceedings of the 12^{th} International Joint Conference on Biomedical Engineering Systems and Technologies - Vol. 1: BIODEVICES, ISBN 978-989-758-353-7, pages 56-64. DOI: 10.5220/0007401900560064
- Santos, G.; Alves, C.; **Pádua, A.**; Palma, S.; Gamboa, H. and Roque, A. (2019). An Optimized E-nose for Efficient Volatile Sensing and Discrimination.In Proceedings of the 12^{th} International Joint Conference on Biomedical Engineering Systems and Technologies - Vol. 1: BIODEVICES, ISBN 978-989-758-353-7, pages 36-46. DOI: 10.5220/0007390700360046
- **Pádua A.**, Palma S., Gruber J., Gamboa H. and Roque A. (2018). Design and Evolution of an Optoelectronic Device for VOCs Detection. In Proceedings of the 11^{th} International Joint Conference on Biomedical Engineering Systems and Technologies - Vol. 1: BIODEVICES, ISBN 978-989-758-277-6, p. 48-55.
- **Pádua A.**, Osório D., Rodrigues J., Santos G., Porteira A., Palma S., Roque A. and Gamboa H. (2018). Scalable and Easy-to-use System Architecture for Electronic Noses. In Proceedings of the 11^{th} International Joint Conference on Biomedical Engineering Systems and Technologies - Vol. 1: BIODEVICES, ISBN 978-989-758-277-6, p. 179-186. DOI: 10.5220/0006597101790186.
- Hussain A., Semeano, A., Palma S., Pina A., Almeida J., Medrado B., **Pádua A.**, Carvalho A., Dionísio M., Li R., Gamboa H., Ulijn R., Gruber J., Roque A. (2017).

Tunable Gas Sensing Gels by Cooperative Assembly. Advanced Functional Materials, 27(27), p. 1–14. DOI: 10.1002/adfm.201700803.

Conferences

2019/06: ICMAT 2019 conference in Singapore.

- Poster presented by Wellington Gonçalves entitled "Ionogel Doped with Functionalized Fe3O4 Particles as Sensitive Layer in Gas Sensors for Electronic Nose Application". Authors: Gonçalves W., **Pádua A.**, Santos G., Li R., Roque A., Gruber J.

2019/05: ISOEN 2019 conference in Osaka (Japan).

- Oral presentation by Susana Palma entitled "Enhanced gas sensing with soft functional materials". Authors: Palma S., Esteves C., **Pádua A.**, Alves C., Santos G., Costa H., Dionísio M., Gamboa H., Gruber J., Roque A.

2019/01: BIODEVICES 2019 conference in Prague (Chez Republic).

- Oral presentation entitled "Impact of Sensing Film's Production Method on Classification Accuracy by Electronic Nose". Authors: **Pádua, A.**; Gruber, J.; Gamboa, H. and Roque, A.
- Oral presentation by Gonçalo Santos entitled "An Optimized E-nose for Efficient Volatile Sensing and Discrimination An Optimized E-nose for Efficient Volatile Sensing and Discrimination". Authors: Santos, G.; Alves, C.; **Pádua, A.**; Palma, S.; Gamboa, H. and Roque, A.

2018/02: BIODEVICES 2018 conference. (Madeira - Portugal)

- Oral presentation entitled "Design and Evolution of an Opto-electronic Device for gas sensing".
- Poster presentation entitled "Scalable and Easy-to-use System Architecture for Electronic Noses".

Events

- **Oral presentations**
  - 2018/11: Oral presentation entitled "Design of an electronic nose for odours detection", in the 9^{th} Ph.D. students meeting at ITQB-NOVA (Oeiras).
  - 2017/10: Final oral presentation of Bioentrepreneurship course (included in the Ph.D. program curricular units) entitled "What is the best first application for our electronic nose?" at ITQB-NOVA.2017/10: Final oral presentation of Bioentrepreneurship course (included in the Ph.D. program curricular units) entitled "What is the best first application for our electronic nose?" at ITQB-NOVA.

  - 2015/06: Oral presentation entitled “Principal Component Analysis for bacteria identification” in Society for Industrial at Applied Mathematics (SIAM) student chapter’s annual meeting at FCT-NOVA University.

- **Posters**

  - 2016/11: 8th Ph.D. students meeting at ITQB - Oeiras. Title: Design and assembly of a prototype opto-electronic nose.

- **Demonstrations**

  - 2018/07 and 2017/07: Electronic nose demo in the event "Science and Technology summit in Portugal", at Lisbon Congress Centre.
  - 2017/09: Activity entitled "The smell of Science: gels sensible to smells and electronic noses’ in the ’European Researchers Night", at the National Museum of Natural History and Science of Lisbon.

- **Award**

  - 2015/12: 2^{nd} prize of StartUp Pirates - Hardware edition. In this intensive bootcamp the team explored future applications for the electronic nose as a medical device. Designed and built a prototype of a final product: an e-nose for smelling biological samples. The prototype developed was portable, handheld and had a LCD exhibiting the set of pathogenic bacteria present in the sample. The team worked on a business model for this product, did market analysis and presented the final work to the public. The awards was attributed by Productized.

Bibliography

[1] A. Loutfi, S. Coradeschi, G. K. Mani, P. Shankar, and J. B. B. Rayappan. "Review: Electronic noses for food quality: A review." In: *Journal of Food Engineering* 144 (2015), pp. 103 –111. ISSN: 0260-8774.

[2] S. Singh. "Sensors—An effective approach for the detection of explosives." In: *Journal of Hazardous Materials* 144.1 (2007), pp. 15 –28. ISSN: 0304-3894. DOI: https://doi.org/10.1016/j.jhazmat.2007.02.018. URL: http://www.sciencedirect.com/science/article/pii/S0304389407002397.

[3] S. E. Stitzel, M. J. Aernecke, and D. R. Walt. "Artificial Noses." In: *Annual Review of Biomedical Engineering* 13 (2011), p. 1. ISSN: 15239829.

[4] F. Buljubasic and G. Buchbauer. "The scent of human diseases: a review on specific volatile organic compounds as diagnostic biomarkers." In: *Flavour Fragrance Journal* 30.1 (2015), p. 5. ISSN: 08825734.

[5] R. P. Arasaradnam, J. A. Covington, C Harmston, and C. U. Nwokolo. "Review article: next generation diagnostic modalities in gastroenterology–gas phase volatile compound biomarker detection." In: *Alimentary Pharmacology Therapeutics* 39.8 (2014), pp. 780 –789. ISSN: 1365-2036.

[6] A. Sanaeifar, H. ZakiDizaji, A. Jafari, and M. d. l. Guardia. "Early detection of contamination and defect in foodstuffs by electronic nose: A review." In: *Trends in Analytical Chemistry* 97 (2017), pp. 257 –271. ISSN: 0165-9936.

[7] A. Manuel, C. Juan M., A. Teresa, and H. M. C. "Quantification of Wine Mixtures with an Electronic Nose and a Human Panel." In: *Frontiers in Bioengineering and Biotechnology, Vol 6 (2018)* (2018). ISSN: 2296-4185.

[8] J. R. Askim, Z. Li, M. K. LaGasse, J. M. Rankin, and K. S. Suslick. "An optoelectronic nose for identification of explosives." In: *Chemical Science* 7.1 (2016), p. 199. ISSN: 20416520.

[9] R. Stuetz. "Chapter 12 Application of electronic nose technology for monitoring water and wastewater." In: *Comprehensive Analytical Chemistry* 39.Integrated Analytical Systems (2003), pp. 513 –539. ISSN: 0166-526X.

[10] C. Laura, S. Selena, and R. Renato Del. "Electronic Noses for Environmental Monitoring Applications." In: *Sensors, Vol 14* 11 (2014), pp. 19979–20007. ISSN: 1424-8220.

[11] T. Saidi, O. Zaim, M. Moufid, N. El Bari, R. Ionescu, and B. Bouchikhi. "Exhaled breath analysis using electronic nose and gas chromatography–mass spectrometry for non-invasive diagnosis of chronic kidney disease, diabetes mellitus and healthy subjects." In: *Sensors & Actuators B: Chemical* 257 (2018), pp. 178 –188. ISSN: 09254005.

[12] Z. Tang, Y. Liu, and Y. Duan. "Review: Breath analysis: technical developments and challenges in the monitoring of human exposure to volatile organic compounds." In: *Journal of Chromatography B* 1002 (2015), pp. 285 –299. ISSN: 1570-0232.

[13] S. Dragonieri, G. Pennazza, P. Carratu, and O. Resta. "Electronic Nose Technology in Respiratory Diseases." In: *Lung* 195.2 (2017), pp. 157 –165. ISSN: 03412040.

[14] A. W. Boots, A Smolinska, J. J. B. N. v. Berkel, R. R. R. Fijten, E. E. Stobberingh, M. L. L. Boumans, E. J. Moonen, E. F. M. Wouters, J. W. Dallinga, and F. J. V. Schooten. "Identification of microorganisms based on headspace analysis of volatile organic compounds by gas chromatography–mass spectrometry." In: *Journal of Breath Research* 8.2 (2014), p. 1. ISSN: 17527155.

[15] M. Cauchi, D. Fowler, C. Walton, C. Turner, W. Jia, R. Whitehead, L. Griffiths, C. Dawson, H. Bai, R. Waring, D. Ramsden, J. Hunter, J. Cole, and C. Bessant. "Application of gas chromatography mass spectrometry (GC-MS) in conjunction with multivariate classification for the diagnosis of gastrointestinal diseases." In: *Metabolomics* 10.6 (2014), pp. 1113 –1120. ISSN: 15733882.

[16] A. W. Boots, L. D. Bos, M. P. van der Schee, F.-J. van Schooten, and P. J. Sterk. "Exhaled Molecular Fingerprinting in Diagnosis and Monitoring: Validating Volatile Promises." In: *Trends in Molecular Medicine* 21.10 (2015), pp. 633 –644. ISSN: 14714914.

[17] R. A. Allardyce, V. S. Langford, A. L. Hill, and D. R. Murdoch. "Detection of volatile metabolites produced by bacterial growth in blood culture media by selected ion flow tube mass spectrometry (SIFT-MS)." In: *Journal of Microbiological Methods* 65.2 (2006), pp. 361 –365. ISSN: 01677012.

[18] D. Smith and P. Španěl. "Direct, rapid quantitative analyses of BVOCs using SIFT-MS and PTR-MS obviating sample collection." In: *Trends in Analytical Chemistry* 30.Biogenic Volatile Organic Compounds S.I. (2011), pp. 945 –959. ISSN: 0165-9936.

[19] B. Lieuwe D J, S. Peter J, and S. Marcus J. "Volatile metabolites of pathogens: a systematic review." In: *PLoS Pathogens, Vol 9, Iss 5, p e1003311 (2013)* 5 (2013), e1003311. ISSN: 1553-7366.

[20] H. Handa, A. Usuba, S. Maddula, J. I. Baumbach, M. Mineshita, and T. Miyazawa. "Exhaled Breath Analysis for Lung Cancer Detection Using Ion Mobility Spectrometry." In: *PLoS ONE* 9.12 (2014), pp. 1 –13. ISSN: 19326203.

[21] W. F. Wilkens and J. D. Hartman. "An Electronic Analog for the Olfactory Processes." In: *Journal of Food Science* 29.3 (1964), p. 372. ISSN: 00221147.

[22] A. Dravnieks and P. J. Trotter. "Polar vapour detector based on thermal modulation of contact potential." In: *Journal of Scientific Instruments* 42.8 (1965), p. 1. ISSN: 09507671.

[23] K. Persaud and G. Dodd. "Analysis of discrimination mechanisms in the mammalian olfactory system using a model nose." In: *Nature* 299.5881 (1982), p. 352. ISSN: 00280836.

[24] M. Kaneyasu, A. Ikegami, H. Arima, and S. Iwanaga. "Smell Identification Using a Thick-Film Hybrid Gas Sensor." In: *IEEE Transactions on Components, Hybrids, and Manufacturing Technology* 10.2 (1987), pp. 267–273. ISSN: 0148-6411. DOI: 10.1109/TCHMT.1987.1134730.

[25] A. P. Turner and N. Magan. "Electronic noses and disease diagnostics." In: *Nature Reviews Microbiology* 2.2 (2004), p. 161. ISSN: 17401526.

[26] T. Kea-Tiong and C. Shih-Wen. "Towards a Chemiresistive Sensor-Integrated Electronic Nose: A Review." In: *Sensors, Vol 13* 10 (2013), pp. 14214–14247. ISSN: 1424-8220.

[27] S. Sankaran, L. R. Khot, and S. Panigrahi. "Review: Biology and applications of olfactory sensing system: A review." In: *Sensors & Actuators: B. Chemical* 171-172 (2012), pp. 1 –17. ISSN: 0925-4005.

[28] *Exploring Nature Science Education Resource: Life Science, Earth Science, and Physical Science Resources for K-12.* Access date: October 2018. URL: www.exploringnature.org.

[29] *Home Page: BioNinja.* Access date: October 2018. URL: http://ib.bioninja.com.au.

[30] Y. Jia, G. Xiuzhen, D. Shukai, J. Pengfei, W. Lidan, P. Chao, and Z. Songlin. "Electronic Nose Feature Extraction Methods: A Review." In: *Sensors, Vol 15, Iss 11, Pp 27804-27831 (2015)* 11 (2015), p. 27804. ISSN: 1424-8220.

[31] J. Burlachenko, I. Kruglenko, B. Snopok, and K. Persaud. "Sample handling for electronic nose technology: State of the art and future trends." In: *Trends in Analytical Chemistry: TRAC* 82 (2016), pp. 222 –236. ISSN: 01659936.

[32] N. Bhattacharya, B. Tudu, A. Jana, D. Ghosh, R. Bandhopadhyaya, and A. B. Saha. "Illumination heating and physical raking for increasing sensitivity of electronic nose measurements with black tea." In: *Sensors & Actuators: B. Chemical* 131.Special Issue: Selected Papers from the 12th International Symposium on Olfaction and Electronic Noses ISOEN 2007 (2008), pp. 37 –42. ISSN: 0925-4005.

[33] S. Deshmukh, A. Jana, N. Bhattacharyya, R. Bandyopadhyay, and R. Pandey. "Quantitative determination of pulp and paper industry emissions and associated odor intensity in methyl mercaptan equivalent using electronic nose." In: *Atmospheric Environment* 82 (2014), pp. 401 –409. ISSN: 1352-2310.

[34] T. Wen, L. Zheng, S. Dong, Z. Gong, M. Sang, X. Long, M. Luo, and H. Peng. "Rapid detection and classification of citrus fruits infestation by Bactrocera dorsalis (Hendel) based on electronic nose." In: *Postharvest Biology and Technology* 147 (2019), pp. 156 –165. ISSN: 0925-5214.

[35] A. Taurino, D. D. Monaco, S. Capone, M. Epifani, R. Rella, P. Siciliano, L. Ferrara, G. Maglione, A. Basso, and D. Balzarano. "Analysis of dry salami by means of an electronic nose and correlation with microbiological methods." In: *Sensors & Actuators: B. Chemical* 95.Selected Papers from Eurosensors XVI (2003), pp. 123 –131. ISSN: 0925-4005.

[36] L. F. Valdez and J. M. Gutiérrez. "Chocolate Classification by an Electronic Nose with Pressure Controlled Generated Stimulation." In: *Sensors (14248220)* 16.10 (2016), pp. 1 –12. ISSN: 14248220.

[37] J. H. Sohn, N. Hudson, E. Gallagher, M. Dunlop, L. Zeller, and M. Atzeni. "Implementation of an electronic nose for continuous odour monitoring in a poultry shed." In: *Sensors and Actuators B: Chemical* 133.1 (2008), pp. 60 –69. ISSN: 0925-4005.

[38] S. Deshmukh, R. Bandyopadhyay, N. Bhattacharyya, R. Pandey, and A. Jana. "Application of electronic nose for industrial odors and gaseous emissions measurement and monitoring – An overview." In: *Talanta* 144 (2015), pp. 329 –340. ISSN: 0039-9140.

[39] J. Gutiérrez and M. Horrillo. "Advances in artificial olfaction: Sensors and applications." In: *Talanta* 124 (2014), pp. 95 –105. ISSN: 00399140.

[40] S. E. Zohora, A. M. Khan, and N. Hundewale. "Chemical Sensors Employed in Electronic Noses: A Review." In: *Advances in Computing Information Technology* (2013), p. 177. ISSN: 9783642315992.

[41] S. Gaoquan and B. Hua. "Gas Sensors Based on Conducting Polymers." In: *Sensors, Vol 7, Iss 3, Pp 267-307 (2007)* 3 (2007), p. 267. ISSN: 1424-8220.

[42] G. Rui, X. Dong, Z. Luyuan, Y. Longwei, and W. Chengxiang. "Metal Oxide Gas Sensors: Sensitivity and Influencing Factors." In: *Sensors, Vol 10, Iss 3, Pp 2088-2106 (2010)* 3 (2010), p. 2088. ISSN: 1424-8220.

[43] L. O. Péres, R. W. Li, E. Y. Yamauchi, R. Lippi, and J. Gruber. "Conductive polymer gas sensor for quantitative detection of methanol in Brazilian sugar-cane spirit." In: *Food Chemistry* 130.4 (2012), pp. 1105 –1107. ISSN: 03088146.

[44] J. R. Cordeiro, R. W. C. Li, r. S. Takahashi, G. P. Rehder, G. Ceccantini, and J. Gruber. "Wood identification by a portable low-cost polymer-based electronic nose." In: *RSC Advances* 6.111 (2016), p. 109945. ISSN: 20462069.

[45] "New composite porphyrin-conductive polymer gas sensors for application in electronic noses." In: *Sensors & Actuators: B. Chemical* 193 (2014), pp. 136 –141. ISSN: 0925-4005.

[46] "A colorimetric sensor array for identification of toxic gases below permissible exposure limits." In: *Chemical Communications* 46.12 (2010), p. 2037. ISSN: 13597345.

[47] Q. Chen, A. Liu, J. Zhao, Q. Ouyang, Z. Sun, and L. Huang. "Monitoring vinegar acetic fermentation using a colorimetric sensor array." In: *Sensors & Actuators: B. Chemical* 183 (2013), pp. 608 –616. ISSN: 0925-4005.

[48] N. Boden, R. J. Bushby, J. Clements, and B. Movaghar. "Device applications of charge transport in discotic liquid crystals." In: *Journal of Materials Chemistry* 9.9 (1999), p. 2081. ISSN: 09599428.

[49] S. M. Scott, D. James, and Z. Ali. "Data analysis for electronic nose systems." In: *Microchimica Acta* 156.3/4 (2007), pp. 183 –207. ISSN: 00263672.

[50] M. Ghasemi-Varnamkhasti, S. S. Mohtasebi, M. Siadat, H. Ahmadi, and S. H. Razavi. "Research paper: From simple classification methods to machine learning for the binary discrimination of beers using electronic nose data." In: *Engineering in Agriculture, Environment and Food* 8 (2015), pp. 44 –51. ISSN: 1881-8366.

[51] E. Ordukaya and B. Karlik. "Quality Control of Olive Oils Using Machine Learning and Electronic Nose." In: *Journal of Food Quality, Vol 2017 (2017)* (2017). ISSN: 0146-9428.

[52] E. Phaisangittisagul, H. T. Nagle, and V. Areekul. "Intelligent method for sensor subset selection for machine olfaction." In: *Sensors Actuators: B. Chemical* 145 (2010), pp. 507 –515. ISSN: 0925-4005.

[53] H. Zhang, M. Chang, J. Wang, and S. Ye. "Evaluation of peach quality indices using an electronic nose by MLR, QPST and BP network." In: *Sensors & Actuators: B. Chemical* 134 (2008), pp. 332 –338. ISSN: 0925-4005.

[54] N. E. Barbri, J. Mirhisse, R. Ionescu, N. E. Bari, X. Correig, B. Bouchikhi, and E. Llobet. "An electronic nose system based on a micro-machined gas sensor array to assess the freshness of sardines." In: *Sensors & Actuators: B. Chemical* 141 (2009), pp. 538 –543. ISSN: 0925-4005.

[55] L. Xu, J. He, S. Duan, X. Wu, and Q. Wang. "Comparison of machine learning algorithms for concentration detection and prediction of formaldehyde based on electronic nose." In: *Sensor Review* 36.2 (2016), p. 207. ISSN: 02602288.

[56] A. Uçar and R. Özalp. "Efficient android electronic nose design for recognition and perception of fruit odors using Kernel Extreme Learning Machines." In: *Chemometrics and Intelligent Laboratory Systems* 166 (2017), pp. 69 –80. ISSN: 0169-7439.

[57] I. Polaka, E. Gašenko, O. Barash, H. Haick, and M. Leja. "Constructing Interpretable Classifiers to Diagnose Gastric Cancer Based on Breath Tests." In: *Procedia Computer Science* 104.ICTE 2016, Riga Technical University, Latvia (2017), pp. 279 –285. ISSN: 1877-0509.

[58] *Sensigent: Intelligent sensing solutions*. Access date: October 2018. URL: www.sensigent.com/products/cyranose.html.

[59] *Alpha MOS : sensory analysis solutions*. Access date: October 2018. URL: www.alpha-mos.com/new-heracles-neo-electronic-nose.

[60] *Sacmi: Artificial olfactory sensors and systems*. Access date: October 2018. URL: www.sacmi.com/.

[61] *AIRSENSE Analytics: we sense the hazard*. Access date: October 2018. URL: www.airsense.com.

[62] *NASA JPL Electronic Nose*. Access date: October 2018. URL: www.nasa.gov/mission_pages/station/research/experiments/32.html.

[63] *CYBERNOSE biosensor - CSIRO*. Access date: October 2018. URL: www.csiro.au/en/Research/BF/Areas/Protecting-Australias-agricultural-industries/Bio-inspired-products/CYBERNOSE-biosensor.

[64] *The eNose company*. Access date: October 2018. URL: www.enose.nl.

[65] *Breathtec Biomedical Inc*. Access date: October 2018. URL: www.breathtecbiomedical.com.

[66] *FOODsniffer - a smart kitchen tool to enjoy meals safely*. Access date: October 2018. URL: www.myfoodsniffer.com/.

[67] M. Hooren, N. Leunis, D. Brandsma, A.-M. Dingemans, B. Kremer, and K. Kross. "Differentiating head and neck carcinoma from lung carcinoma with an electronic nose: a proof of concept study." In: *European Archives of Oto-Rhino-Laryngology* 273.11 (2016), p. 3897. ISSN: 09374477.

[68] *The Scientist: Exploring life, inspiring innovation. e-Nose Sniffs Out Cancer, and More.* September 2005. URL: www.the-scientist.com/tools-and-technology/e-nose-sniffs-out-cancer-and-more-48392.

[69] R. M. G. E. van de Goor, N. Leunis, M. R. A. van Hooren, E. Francisca, A. Masclee, B. Kremer, and K. W. Kross. "Feasibility of electronic nose technology for discriminating between head and neck, bladder, and colon carcinomas." In: *European Archives of Oto-Rhino-Laryngology* 274.2 (2017), pp. 1053–1060. ISSN: 1434-4726.

[70] H. Shafiek, F. Fiorentino, J. L. Merino, C. López, A. Oliver, J. Segura, I. de Paul, O. Sibila, A. Agustí, and B. G. Cosío. "Using the Electronic Nose to Identify Airway Infection during COPD Exacerbations." In: *PLoS ONE* 10.9 (2015), pp. 1 –16. ISSN: 19326203.

[71] D. K. Chan, L. Zakko, K. H. Visrodia, C. L. Leggett, L. S. Lutzke, M. A. Clemens, J. D. Allen, M. A. Anderson, and K. K. Wang. "Breath Testing for Barrett's Esophagus Using Exhaled Volatile Organic Compound Profiling With an Electronic Nose Device." In: *Gastroenterology (00165085)* 152.1 (2017), p. 24. ISSN: 00165085.

[72] O. Burfeind, M. Bruins, A. Bos, I. Sannmann, R. Voigtsberger, and W. Heuwieser. "Diagnosis of acute puerperal metritis by electronic nose device analysis of vaginal discharge in dairy cows." In: *Theriogenology* 82.1 (2014), pp. 64 –70. ISSN: 0093691X.

[73] C. G. Waltman, T. A. Marcelissen, and J. G. van Roermund. "Prostate Cancer: Exhaled-breath Testing for Prostate Cancer Based on Volatile Organic Compound Profiling Using an Electronic Nose Device (Aeonose™): A Preliminary Report." In: *European Urology Focus* (2018). ISSN: 2405-4569.

[74] G. Wouter H van, B. Marcel, and K. Huib A M. "Diagnosing viral and bacterial respiratory infections in acute COPD exacerbations by an electronic nose: a pilot study." In: *Journal of Breath Research* 10.3 (2016), p. 1. ISSN: 17527155.

[75] *Air Quality Sensors - ams*. Access date: October 2018. URL: www.ams.com/air-quality-sensors.

[76] *Figaro USA, Inc*. Access date: October 2018. URL: www.figarosensor.com.

[77] *RoboScientific*. Access date: October 2018. URL: www.roboscientific.com.

[78] *Alphasense*. Access date: October 2018. URL: www.alphasense.com/.

[79] *Environics*. Access date: October 2018. URL: www.environics.fi.

[80] *ClairAir*. Access date: October 2018. URL: www.clairair.co.uk.

[81] *Draeger*. Access date: October 2018. URL: www.draeger.com.

[82] *Foedisch*. Access date: October 2018. URL: www.foedisch.org.

[83] *Platypus Chemical SensorsTM*. Access date: October 2018. URL: www.platypustech.com/sensors.

[84] *MOCON*. October 2018. URL: www.mocon.com/instruments/greenlight-930.html.

[85] *Honeywell Analytics Neotox XL Oxygen Analyser*. Access date: October 2018. URL: www.keison.co.uk/honeywell_analytics_neotoxxl.shtml.

[86] *Figaro USA, Inc.* Access date: October 2018. URL: www.figarosensor.com/products/sensor/target-gas/co/.

[87] *Electronic Sensor Technology - Portable zNose Model 4200*. Access date: October 2018. URL: www.estcal.com/product/portable-znoser.

[88] A. Hussain, A. T. S. Semeano, S. I. C. J. Palma, A. S. Pina, J. Almeida, B. F. Medrado, A. C. C. S. Pádua, A. L. Carvalho, M. Dionísio, R. W. C. Li, H. Gamboa, R. V. Ulijn, J. Gruber, and A. C. A. Roque. "Liquid Crystals: Tunable Gas Sensing Gels by Cooperative Assembly (Adv. Funct. Mater. 27/2017)." In: *Advanced Functional Materials* 27.27 (2017), n/a. ISSN: 1616301X.

[89] T. Carvalho, V. Augusto, A. Rocha, N. M. T. Lourenco, N. T. Correia, S. Barreiros, P. Vidinha, E. J. Cabrita, and M. Dionisio. "Ion Jelly Conductive Properties Using Dicyanamide-Based Ionic Liquids." In: *JOURNAL OF PHYSICAL CHEMISTRY B* 118.31 (2014), pp. 9445 –9459. ISSN: 15206106.

[90] H. Eimura, D. S. Miller, X. Wang, N. L. Abbott, and T. Kato. "Self-Assembly of Bioconjugated Amphiphilic Mesogens Having Specific Binding Moieties at Aqueous-Liquid Crystal Interfaces." In: *CHEMISTRY OF MATERIALS* 28.4 (2016), pp. 1170 –1178. ISSN: 08974756.

[91] S. P. V., W. M., M. J., T. A., and H.-J. J. "Rebirth of Liquid Crystals for Sensoric Applications: Environmental and Gas Sensors." In: *Advances in Condensed Matter Physics, Vol 2015 (2015)* (2015). ISSN: 1687-8108.

[92] P. Shibaev, J. Madsen, and A. Genack. "Lasing and Narrowing of Spontaneous Emission from Responsive Cholesteric Films." In: *Chemistry of Materials* 16.8 (2004), pp. 1397–1399. ISSN: 08974756.

[93] A. C. Pádua, S. Palma, J. Gruber, H. Gamboa, and A. C. Roque. "Design and Evolution of an Opto-electronic Device for VOCs Detection." In: *Proceedings of the 11th International Joint Conference on Biomedical Engineering Systems and Technologies - Volume 1: BIODEVICES*, INSTICC. SciTePress, 2018, pp. 48–55. ISBN: 978-989-758-277-6. DOI: 10.5220/0006558100480055.

[94] S. I. C. J. Palma, A. P. Traguedo, A. R. Porteira, M. J. Frias, H. Gamboa, and A. C. A. Roque. "Machine learning for the meta-analyses of microbial pathogens' volatile signatures." In: *Scientific Reports* 8.1 (Feb. 2018), p. 3360. DOI: 10.1038/s41598-018-21544-1. URL: https://doi.org/10.1038/s41598-018-21544-1.

[95] A. C. Pádua., J. Gruber., H. Gamboa., and A. C. Roque. "Impact of Sensing Film's Production Method on Classification Accuracy by Electronic Nose." In: *Proceedings of the 12th International Joint Conference on Biomedical Engineering Systems and Technologies - Volume 1: BIODEVICES*, INSTICC. SciTePress, 2019, pp. 56–64. ISBN: 978-989-758-353-7. DOI: 10.5220/0007401900560064.

[96] S. Deshmukh, A. Jana, N. Bhattacharyya, R. Bandyopadhyay, and R. Pandey. "Quantitative determination of pulp and paper industry emissions and associated odor intensity in methyl mercaptan equivalent using electronic nose." In: *Atmospheric Environment* 82 (2014), pp. 401 –409. ISSN: 1352-2310.

[97] I. A. M. Frías, K. Y. P. S. Avelino, R. R. Silva, C. A. S. Andrade, and M. D. L. Oliveira. "Trends in Biosensors for HPV: Identification and Diagnosis." In: *Journal of Sensors* 2015 (2015), p. 1. ISSN: 1687725X.

[98] C. Baldacchini, M. A. Herrero Chamorro, M. Prato, and S. Cannistraro. "Highly Conductive Redox Protein–Carbon Nanotube Complex for Biosensing Applications." In: *Advanced Functional Materials* 21.1 (2011), p. 153. ISSN: 1616301X.

[99] B. Hivert, M. Hoummady, P. Mielle, G. Mauvais, J. Henrioud, and D. Hauden. "Electronic nose: A fast and reproducible method for gas sensor screening to flavour compounds." In: *Sensors Actuators: B. Chemical* 27.Eurosensors VIII (1995), pp. 242 –245. ISSN: 0925-4005.

[100] O. Hotel, J.-P. Poli, C. Mer-Calfati, E. Scorsone, and S. Saada. "A review of algorithms for SAW sensors e-nose based volatile compound identification." In: *Sensors & Actuators: B. Chemical* 255.Part 3 (2018), pp. 2472 –2482. ISSN: 0925-4005.

[101] J. H. Cho and P. U. Kurup. "Decision tree approach for classification and dimensionality reduction of electronic nose data." In: *Sensors & Actuators: B. Chemical* 160 (2011), pp. 542 –548. ISSN: 0925-4005.

[102] E. Siavash, W. Alfian, M. Ella, A. Ramesh P., and C. James A. "Non-Invasive Diagnosis of Diabetes by Volatile Organic Compounds in Urine Using FAIMS and Fox4000 Electronic Nose." In: *Biosensors, Vol 8, Iss 4, p 121 (2018)* 4 (2018), p. 121. ISSN: 2079-6374.

[103] R. T. d. Rocha and I. G. Gutz. "A low-cost and high-performance conductivity meter." In: *Journal of Chemical Education* 74.5 (1997), p. 572. ISSN: 00219584.

[104] G. Santos., C. Alves., A. C. Pádua., S. Palma., H. Gamboa., and A. C. Roque. "An Optimized E-nose for Efficient Volatile Sensing and Discrimination." In: *Proceedings of the 12th International Joint Conference on Biomedical Engineering Systems and Technologies - Volume 1: BIODEVICES*, INSTICC. SciTePress, 2019, pp. 36–46. ISBN: 978-989-758-353-7. DOI: 10.5220/0007390700360046.

[105] A. Pádua, D. Osório, J. Rodrigues, G. Santos, A. Porteira, S. Palma, A. C. Roque, and H. Gamboa. "Scalable and Easy-to-use System Architecture for Electronic Noses." In: *Proceedings of the 11th International Joint Conference on Biomedical Engineering Systems and Technologies - Volume 1: BIODEVICES*, INSTICC. SciTePress, 2018, pp. 179–186. ISBN: 978-989-758-277-6. DOI: 10.5220/0006597101790186.

[106] C. Esteves, G. M. Santos, C. Alves, S. I. Palma, A. R. Porteira, J. Filho, H. M. Costa, V. D. Alves, B. M. M. Faustino, I. Ferreira, H. Gamboa, and A. C. Roque. "Effect of film thickness in gelatin hybrid gels for artificial olfaction." In: *Materials Today Bio* 1 (2019), p. 100002. ISSN: 2590-0064. DOI: https://doi.org/10.1016/j.mtbio.2019.100002. URL: http://www.sciencedirect.com/science/article/pii/S2590006418300401.

[107] V. Nuno I. P., R. Alisa, O. João A. B. P., G. Elvira M. M., and G. M. Teresa S. R. "Cheeses Made from Raw and Pasteurized Cow's Milk Analysed by an Electronic Nose and an Electronic Tongue." In: *Sensors, Vol 18, Iss 8, p 2415 (2018)* 8 (2018), p. 2415. ISSN: 1424-8220.

[108] B. Szulczyński, J. Namieśnik, and J. Gębicki. "Determination of Odour Interactions of Three-Component Gas Mixtures Using an Electronic Nose." In: *Sensors (14248220)* 17.10 (2017), p. 2380. ISSN: 14248220.

[109] A. Lichtenstein, E. Havivi, R. Shacham, E. Hahamy, R. Leibovich, A. Pevzner, V. Krivitsky, G. Davivi, I. Presman, R. Elnathan, Y. Engel, E. Flaxer, and F. Patolsky. "Supersensitive fingerprinting of explosives by chemically modified nanosensors arrays." In: *Nature Communications* 5.6 (2014), p. 4195. ISSN: 20411723.

[110] J. M. Azzarelli, K. A. Mirica, J. B. Ravnsbæk, and T. M. Swager. "Wireless gas detection with a smartphone via rf communication." In: *Proceedings of the National Academy of Sciences* 111.51 (2014), pp. 18162–18166. ISSN: 0027-8424.

[111] B. Esser, J. M. Schnorr, and T. M. Swager. "Selective Detection of Ethylene Gas Using Carbon Nanotube-based Devices: Utility in Determination of Fruit Ripeness." In: *Angewandte Chemie International Edition* 51.23 (2012), p. 5752. ISSN: 14337851.

Appendix 1

Table A.1: Instructions to insert information in the sensing film's database table

Column	Mandatory?	Description
ID	Yes	Sensor identifier (incremental number)
Label	Yes	Sensor label (also written on the glass slide)
Production date	Yes	Date of film production (e.g. 2017-07-20)
IL	Yes	Ionic liquid used (e.g. [BMIM][DCA], [BMIM][Cl]
IL quantity (μL)	Yes	Quantity of ionic liquid used (e.g. 150.00)
LC	Yes	Liquid crystal type selected (e.g. 5 CB)
LC quantity (μL)	Yes	Quantity of liquid crystal (e.g. 5.00)
Polymer(s)	Yes	Polymer(s) name (if multiple, separate by ",")
Polymer(s) quantity	Yes	Quantity of polymer(s) used (if multiple, separate by ",")
Water quantity (μL)	Yes	Quantity of MilliQ water used (e.g. 150.00)
Cross-linking	Yes	Select one of the options (e.g. none, glutaraldehyde)
Spreading technique	Yes	Select one of the options (film coating or spin coating)
Quantity deposited (μL)	Yes	Drop quantity deposited on the glass slide
Thickness (μm)	Only for FC	Thickness of films
SC parameters	Only for SC	e.g. (v:1000, a:700, t:20)

Table A.2: Instructions to fill the interface parameters that will be stored in the experiments' database

Column	Field type	Description
ID	Automatic	Experiment identifier (incremental number)
Data and hour	Automatic	Date and hour when experiment starts
E-nose ID	Automatic	Last three digits of RasPi's IP
ID sensor i i = 1,2,3,4,5,6	Mandatory	Incremental number (check sensing films database) int number
Sample type (text)	Mandatory	Type of sample inside the sample chamber or VOC name (e.g. ethanol, lettuce, coffee)
Sample day (dd/mm/yyyy)	Optional	Days when the sample was placed inside the sample chamber
Sample quantity (mL or g)	Mandatory	Quantity of sample inside the flask Use mL for liquid samples Use mg for solid samples
Sample temperature (°C)	Mandatory	Temperature of sample bath
Atmospheric pressure (hPa)	Optional	At the day and time of experiment
Exposure and recovery times (s)	Mandatory	Periods of exposure and recovery defined (e.g. 15 or 15.0 are valid)
Duration (min)	Mandatory	Total duration of experiment (e.g. 30 or 30.0 are valid)
Sampling rate (Hz)	Mandatory	Acquisition rate Max. RasPi 2B (e-nose v1/v2): 50 Hz Max. RasPi 3: 90 Hz
Researcher ID (text)	Optional	Name of the person(s) responsible for the experiment Use you FCT e-mail initials (e.g. ACPADUA)
Goal (text)	Optional	Brief description of the experiment goal
Time T&H sensor (min)	Optional	Periods for acquisition from the T&H sensors (e.g. 5 or 5.0 are valid)

Table A.3: Instructions to insert information in the database with the sensing films images

Column	Mandatory?	Description
Image of sensing film i before experiment i = 1,2,3,4,5,6	Yes	Insert image
Image of sensing film i after experiment i = 1,2,3,4,5,6	Yes	Insert image
Light intensity (V)	Yes	Applied to take the image
Objective	Yes	Select (e.g. 5X, 10X, 20X)
Adjustments	No	Changes applied to histogram (min/max/gamma)
Nr droplets before	No	Total number of droplets in the image before
Average droplets diameter before	No	Insert value
Average droplets perimeter before	No	Insert value
Nr droplets after	No	Total number of droplets in the image after
Average droplets diameter after	No	Insert value
Average droplets perimeter after	No	Insert value

APPENDIX B

APPENDIX 2

Table B.1: Comparative table of different e-nose versions

E-nose Version		**V0**	**V1**	**V2**	**V3**
Transduction system	Sampling rate	10 Hz	50 Hz	90 Hz	90 Hz
	Elements	NI myDAQ + PC	Arduino Uno + RaspPi2	Arduino Due + RasPi2	Arduino Due + RaspPi3
Detection chamber	Detectors	photoresistors	photoresistors	photoresistors	photodiodes
	Nr. sensors	4	4	6	6
	Stability*	1	2	3	4
	Volume	2 L	1.2 L	28 mL	28 mL
Delivery system	Analysis	0.37 cycles/min	1 cycle/min	2 cycles/min	3 cycles/min

*

Stability and scaling scale:
1: Open and close the chamber was not practical. Chamber with flow losses.
2: Robust and more easy-to-use chamber. Difficult to change sensing films between experiments. Flow losses verified.
3: Easy to change sensing films. Hermetic. PCBs with through-hole technology. components.
4: Easy to change sensing films. Hermetic.. PCBs with surface-mount technology components. Has slots to insert the PCBs and support for sensing films. Has light guiders for LEDs.

Appendix

C

Appendix 3

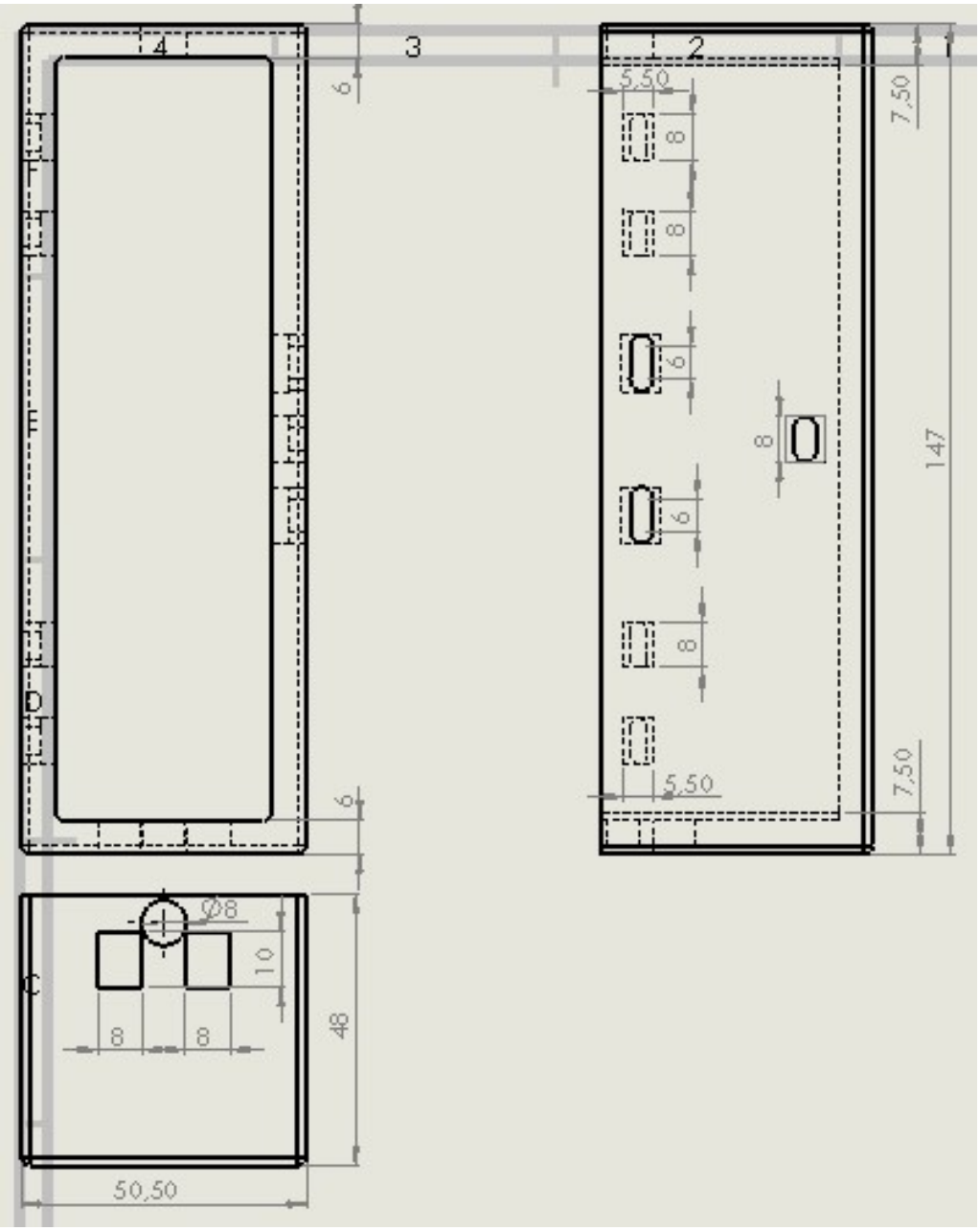

Figure C.1: Technical drawing of the external detection chamber of e-nose v3.

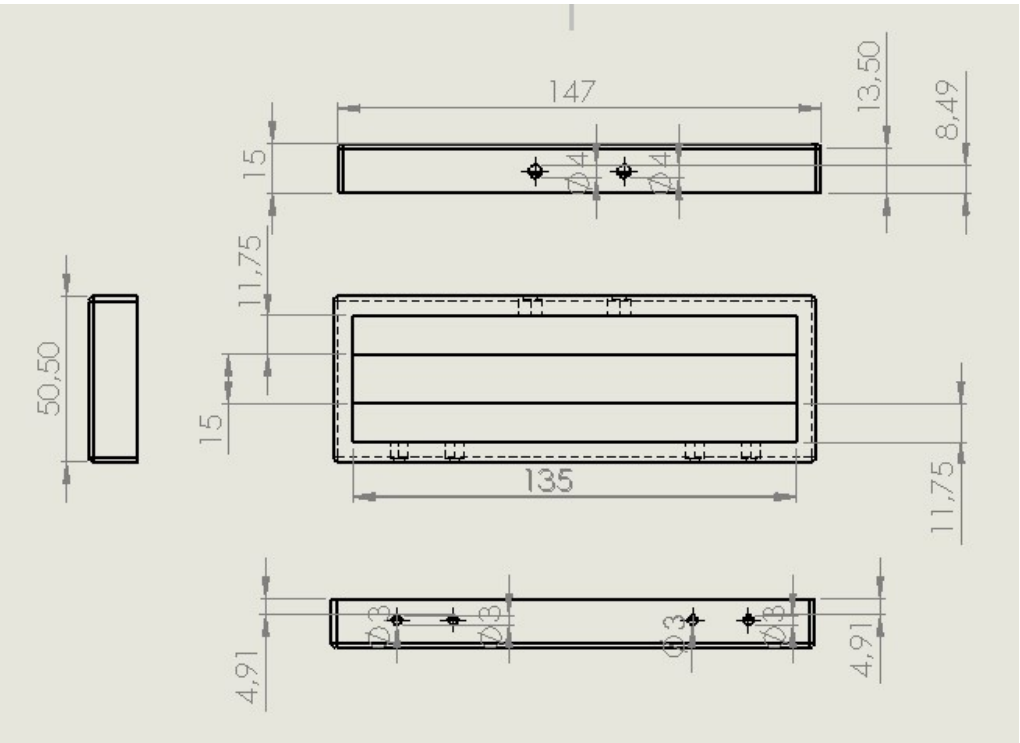

Figure C.2: Technical drawing of the external detection chamber's lid of e-nose v3.

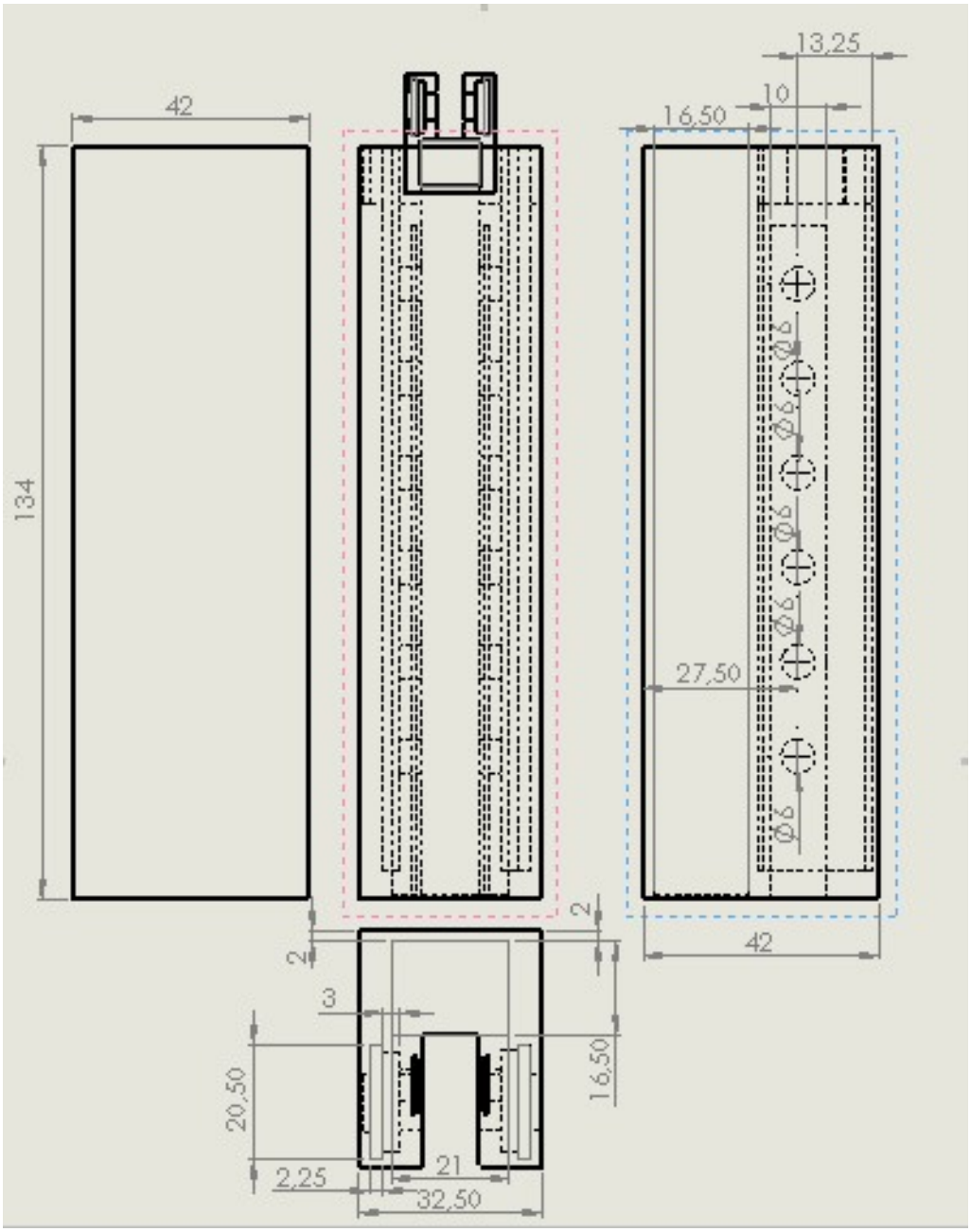

Figure C.3: Technical drawing of the internal structure of e-nose v3.

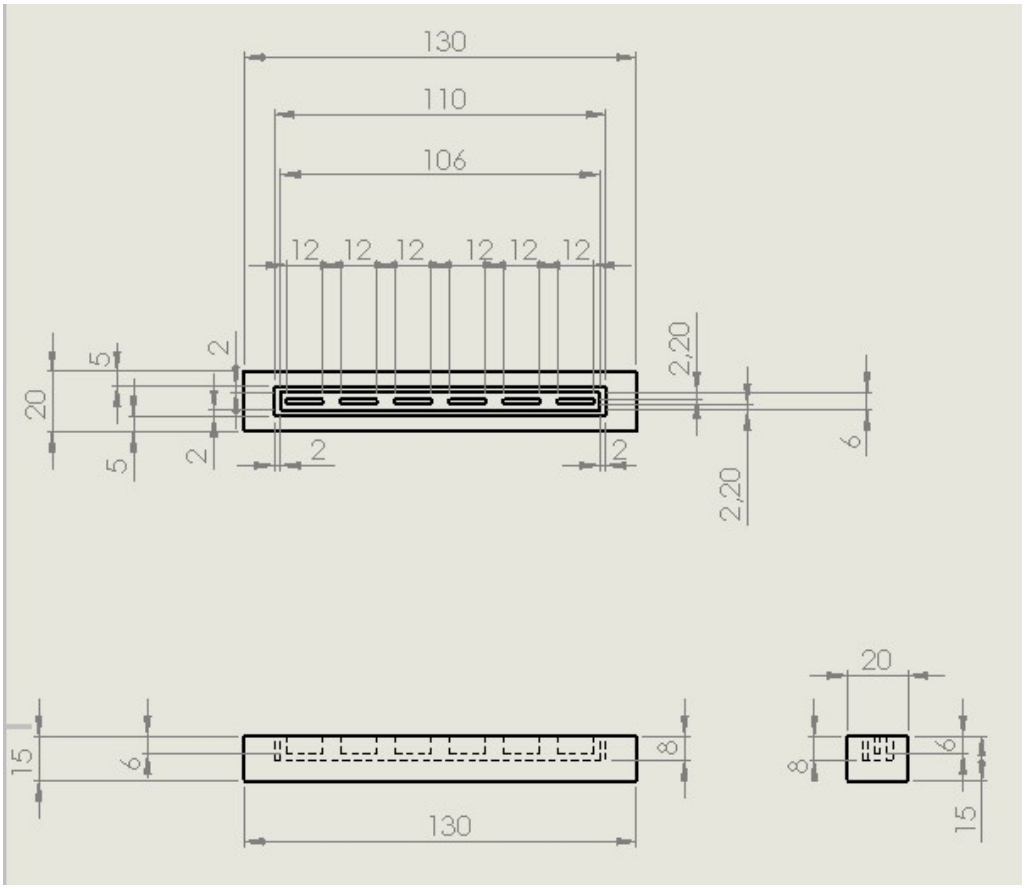

Figure C.4: Technical drawing of the internal support of e-nose v2 and v3.